Norwegian Meteorological Institute
met.no

met.no report

no. 1/2005
Climate

Climate change impacts on water balance in Norway

Torill Engen-Skaugen, Lars A. Roald, Stein Beldring, Eirik J. Førland, Ole Einar Tveito, Kolbjørn Engeland and Rasmus Benestad

Norwegian Meteorological Institute
met.no

report

Title	**Date**
Climate change impacts on water balance in Norway	12.01.2005
Section	**Report no.**
Climate	No. 1/2005
Author(s)	**Classification**
Torill Engen-Skaugen[1], Lars A. Roald[2], Stein Beldring[2], Erik J. Førland[1], Ole Einar Tveito[1], Kolbjørn Engeland[1] and Rasmus Benestad[1]	☒ Free ☐ Restricted
	ISSN 1503-8025
[1] Norwegian Metorological Institute, [2] Norwegian Water Resources and Energy Directorate	**e-ISSN** 1503-8025
Client(s)	**Client's reference**
'Climate Change and Energy Production Potential' funded by EBL kompetanse AS	M1.1.01_01

Abstract

Adjusted climate scenarios for Norway dynamically downscaled with HIRHAM are analysed and used as input in the Gridded Water Balance (GWB) model to obtain scenarios of streamflow at selected catchments in Norway. The scenarios show especially a large increase in streamflow during winter and large decrease during summer. Trend analyses and analyses of the projected change in the flood regime are discussed in the report. The study is ongoing and will be fully reported in 2005 (Roald et al., 2005).
A discussion of uncertainty is performed in the report. A summary of a work comparing evapotranspiration estimates from HIRHAM and from GWB model at different locations in Norway are given. The conclution is that the difference in representation of evapotranspiration in the two models is larger than the projected change in evapotranspiration in a future climate.
A study of the change in heating season at selected Nordic sites is summarised. The conclusion is that the temperature scenarios indicate substantially higher winter temperatures than observed in the 20th century, thus leading to a reduction in heating-degree days.
A study on the relations between long-term variations in runoff and large scale atmospheric circulation pattern is being studied (Tveito and Roald, 2005), a summary of the work is presented in the present report. It is found that atmospheric circulation can describe runoff variations on a seasonal scale. For some regions in some seasons however the relations are weak.

Keywords

Climate change, HIRHAM, GWB, water balance, evapotranspiration, heating season, extreme precipitation, circulation pattern, uncertainty.

	Responsible signature
	_____
	Eirik J. Førland

Postal address	Office	Telephone	Telefax	e-mail: met@met.no	Bank account	Swift code
P.O.Box 43, Blindern	Niels Henrik Abelsvei 40	+47 22 96 30 00	+47 22 96 30 50	Internet: met.no	7694 05 00628	DNBANOKK
NO-0313 OSLO						
Norway						

Postal address	Office	Telephone	Telefax	e-mail: met@met.no	Bank account	Swift code
P.O.Box 43, Blindern	Niels Henrik Abelsvei 40	+47 22 96 30 00	+47 22 96 30 50	Internet: met.no	7694 05 00628	DNBANOKK
NO-0313 OSLO						
Norway						

1. INTRODUCTION

Global warming of the surface temperature with approximately 0.6 °C has been observed during the last 100 years. Different emission scenarios project a further increase of global temperature between 1 °C to 5 °C (Cubash et al., 2001). Globally averaged water vapour concentrations, evaporation and precipitation are projected to increase. At regional scale both increases and decreases in precipitation are projected. The projections of the development of precipitation, however, are even more uncertain than for temperature (Benestad, 2002).

Climate scenarios are produced by Atmospheric-Ocean General Circulation Models (AOGCMs). The spatial resolution of AOGCMs is quite coarse, typically about 3° or 4° in latitude and from 4° to 10° in longitude. The regional and local details of the climate at that scale are lost. As stated by Wood et al (2004); "A minimum standard of any useful downscaling method for hydrological applications needs the historic (observed) conditions to be reproducible". Different downscaling methods are developed to overcome this problem, dynamically, empirically or these two techniques in combination (e.g. Giorgi et al., 2001), to obtain higher resolution for regions or at site locations.

The focus in impact assessments due to climate change is increasing. A regional pattern with focus on a shift in the future climate compared to present may be satisfactory for some assessments. When studying the hydrological cycle, however, these difficulties are huge (Bronstert, 2004; Wood et al., 2004). The limitations of the AOGCMs rainfall estimates is well known, and different methods have been used to omit the problem; the delta change, or perturbation method has been widely used (Middelkoop et al., 2001; Reynard et al, 2001**,** Lettenmaier et al., 1999). Because of the uncertainty connected to the scenarios, especially to precipitation estimates, the focus in climate-change impact studies on water resources in Scandinavia has mainly been on the mean changes on a national or regional level (Roald, et.al, 2003; Sælthun et al., 1998). In the present study, analyses have been performed on hydrological scenarios with focus on shift in hydrological regime and droughts versus extremes. To be able to do so, an empirical adjustment method has been used to tailor the climate scenarios to station level (Engen-Skaugen, 2004).

The study areas and the data used are presented in section 2. Daily time series of precipitation and temperature is interpolated from HIRHAM to weather stations and adjusted to be representative locally. A study of changes in precipitation extremes is summarised in section 3. A study of uncertainty of precipitation and temperature are summarised in section 4. The study is obtained with respect on ensemble scenarios of precipitation and temperature and is based on the studies of Benestad (2000, 2001b, 2003, 2004**).** As stated by Bronsert (2004); "The uncertainty involved in this type of climate-change impact assessment limits the value of the results". To be able to give a reliable estimate on uncertainty, the need for analysis of ensemble runs is crucial both with respect on different emissions, but also different parameterization approaches for regional climate physics. Downscaled scenarios from two regional climate models are used in this study. A comparison of the results from HIRHAM with the Rossby centre regional climate model (Rummukainen et al., 2004), however, is a topic in the Climate and Energy project (CE) (www.os.is/ce).

A study is performed to compare evapotranspiration estimates from HIRHAM and from GWB. The aim of the study was to detect differences to be able to reach a level of consistency of the runoff estimates with the HIRHAM model (Engeland et al., 2004). A summary of the study is given in section 5.

A summary of a study of the impacts of climate change on the water balance in Norway is presented in section 6. The study is to be fully reported in Roald et al. (2005). Heating season and heating degree days have been analysed for some selected cities in Fennoscandia, Iceland, Greenland and Svalbard (Førland et al., 2004), the study is summarised in section 7.

A study on relations between long-term variations in runoff and large scale atmospheric circulation will be described in Tveito and Roald (2005). A summary of the study is given in section 8. A summary of the topics given in the report are presented in section 9.

2. STUDY AREA AND DATA

2.1 Climate and discharge in Norway

The Norwegian climate is characterised by the northern location of the country, the long distance from northern parts to southern parts of the country, the long ice free coastline and the large variation in topography. The continental parts of Norway are characterised by mean monthly winter temperatures below -15 °C. Mean monthly summer temperature normally reach 6 to 8 °C in the high mountain areas in the south while the mean monthly summer temperature in south-eastern parts of northern Norway normally is around 10-12 °C. The temperature decreases with longitude and altitude in summer. Mean monthly summer temperature reach 14-16 °C in the coastal south-eastern parts of the country (Tveito et al. 2000). Mean annual precipitation is largest (>3000 mm/year) in western parts of Norway where the humid Atlantic low pressure air masses reaches hilly land areas. The precipitation amounts decreases further east depending on both distance from coast and topography. The driest areas in Norway is the leeward side of the mountain area in the south (<350 mm/year) and the eastern parts of Northern Norway (300-450 mm/year) (Tveito et al. 1997). Precipitation in south western parts is largest during autumn and winter, while the precipitation is at its maximum during summer and autumn in the eastern parts of the country.

Differences in precipitation and temperature regimes of Norway are reflected in the mean annual and seasonal runoff of the country. Coastal areas have largest discharge during winter and autumn. October is the typical flooding month in southern and south-eastern areas while November and December is the dominant flood period in western areas. Inland areas are dominated with melting floods in spring (April-June) and typically low discharge during winter, the discharge is high in autumn (August/September – October). The mountain areas are characterised by dominant melting floods during summer (July – August) and low discharge in winter (Gottschalk et al. 1979; Beldring et al. 2002)

2.2 Observations

Data from 20 catchments in the station network of the Hydrology Department, Norwegian Water Resources and Energy Directorate were used, situated between 58˚30' and 69˚30' northern latitude (Fig. 2.1, Table 2.1). The catchments represent different landscape types, including mountains and alpine terrain, subalpine and boreal forests, non-forested areas below

the tree line, lakes, bogs and glaciers. The catchments areas range from 23 to 5693 km^2, and cover elevations between 11 and 2362 m a.s.l. 57 precipitation and temperature stations were used in the simulations (Fig. 2.1). The climate varies from maritime to continental, and several runoff regimes classified according to seasonal variations of runoff are found (Gottschalk et al., 1979). Some of the catchments are located in a mountain type regime with dominant spring and summer high flows caused by snowmelt and winter low flows, others are located in a coastal type regime with dominant autumn and winter high flows caused by rain and summer low flows. There are also many transitional regime catchments with varying degrees of dominance of spring snowmelt and autumn rain high flows. In addition to these 20 catchments with runoff observations, the area used by the Lyse power production company in south-western Norway was studied. There are no stream flow series available for the Lyse catchment either for calibration or verification of the simulated series.

The stream flow time series were subject to double mass analysis (Alexandersson, 1986) and Pettit-test (Pettit, 1979) to ascertain their consistency and quality. Although discharge determined from stage measurements and rating curves for natural conditions has an inherent uncertainty, the stream flow data used in this study are considered the most reliable in Norway. The uncertainty is largest during winter conditions, when ice in river cross sections and at lake outlets invalidates the rating curves that have been established for ice-free conditions. Observed water levels must be corrected by comparison with nearby stations not affected by ice before the rating curves can be applied. Since stream flow is low during periods with air temperatures below the freezing point, this uncertainty has negligible effect on the annual water balance. The regulated series, especially the series from Rathe and Kobbvatn, have been corrected for the effect of regulations prior to the use in calibration and the comparison between observed runoff and the simulated runoff in the control period. The corrected data series are more affected by noise than series from natural catchments.

Observations of evaporation at 3 locations in Sweden and Finland are used (Fig. 2.1). 6 locations of evapotranspiration in Norway are presented in the figure as well. These are, however, not observations but locations were evapotranspiration is simulated and studied (Chapter 5).

Temperature stations in Fennoscandia, Iceland, Svalbard and Greenland is used to estimate the heating season at the locations (Chapter 6). An overview of the locations is given in Figure 2.2.

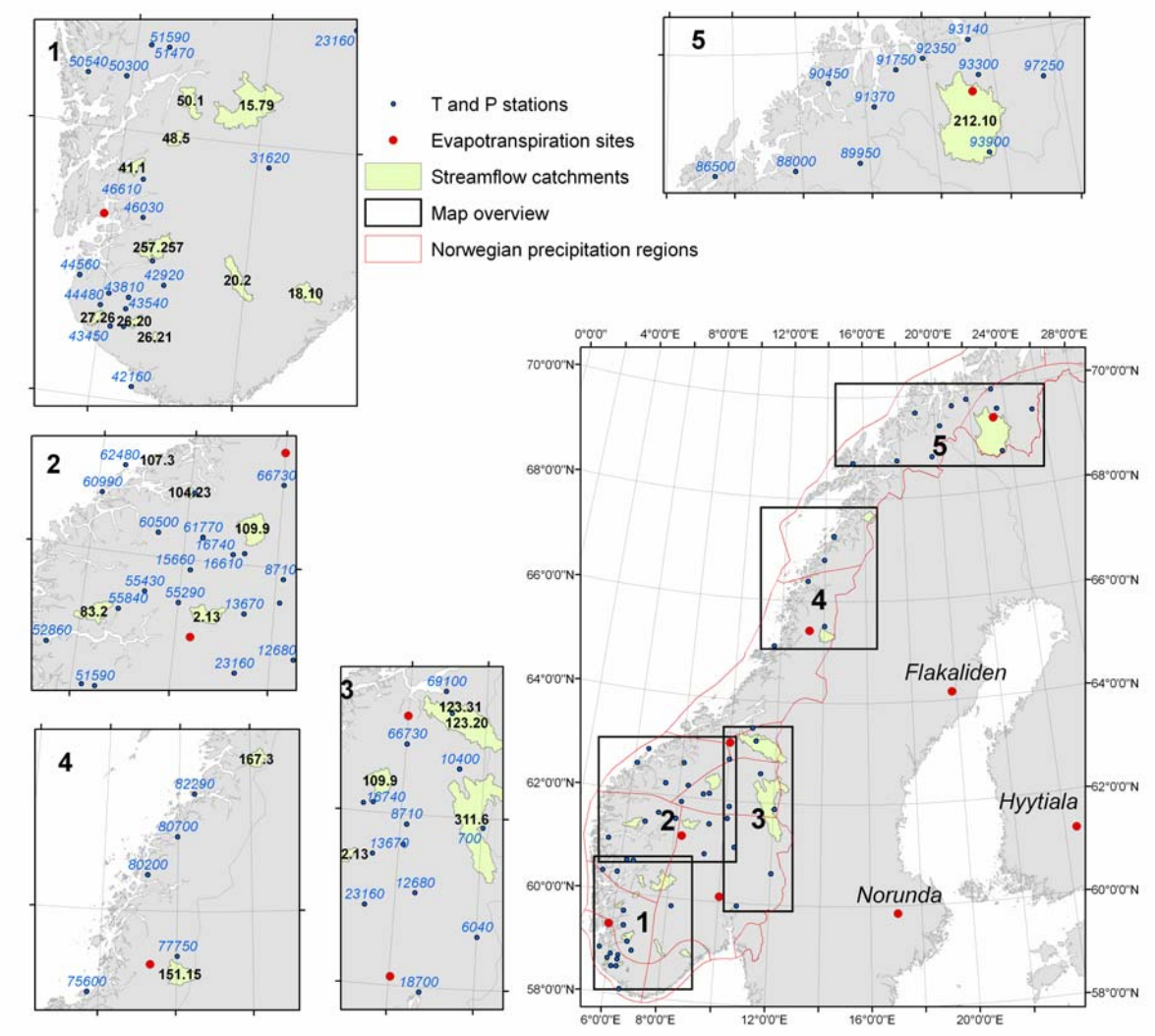

Figure 2.1 An overview of selected catchments, precipitation and temperature stations, and evapotranspiration sites used.

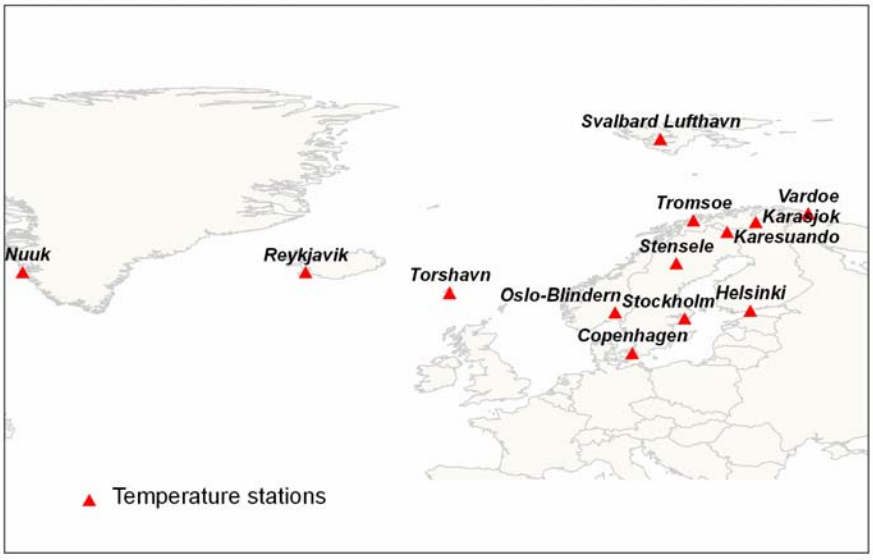

Figure 2.2 An overview of the location of the temperature stations used in the heating season study (section 7).

Table 2.1. Catchments used for hydrological modelling

Catchment no.	Name	Area	Mean annual runoff	Min. altitude	Max. altitude
311.6	Nybergsund	4410	484	350	1755
2.13	Sjodalsvatn	480	1314	940	2362
15.79	Orsjoren	1178	839	951	1539
18.10	Gjerstad	237	935	49	658
20.2	Austenå	277	1138	228	1146
26.20	Årdal	76	2124	105	750
26.21	Sandvatn	27.5	1961	306	572
27.26	Hetland	69.5	1840	23	555
41.1	Stordalsvatn	127	3251	51	1294
48.5	Reinsnosvatn	121	2357	595	1637
50.1	Hølen	229	1649	130	1681
83.2	Viksvatn	507	2663	145	1636
104.23	Vistdal	66.4	1811	47	1525
107.3	Farstad	23.5	1408	11	764
109.9	Risefoss	744	681	556	2284
123.20	Rathe	3053	983	14	1752
123.31	Kjelstad	142	1239	200	1166
151.15	Nervoll	650	1340	345	1682
167.3	Kobbvatn	389	2012	8	1512
212.10	Masi	5693	484	272	1089
257.257	Lyse	309	2951	635	1290

2.3 Climate models and downscaling

Two different AOGCMs are used in the study; the ECHAM4/OPYC3 model developed at the Max Planck institute (MPI) in Hamburg with the GSDIO integration (Roeckner et al., 1999) and HadAm3 model developed at the Hadley centre in UK (Gordon et al., 2000). The spatial resolution of AOGCMs is typically ~300 * 300 km^2. Thus, to obtain reliable estimates of the climate at specific regions in Norway, downscaling is necessary. Results from AOGCMs are dynamically downscaled with the regional climate model HIRHAM (Bjørge et al., 2000). HIRHAM is similar to the model used at MPI and the Danish Meteorological Institute (DMI) and is based on the dynamics of the weather forecast model HIRLAM which is operationally used at the Norwegian Meteorological Institute (met.no) and the physics of ECHAM4. HIRHAM has a spatial resolution of ~55 *55 km^2. The resulting physical parameters have a 6 hourly time resolution and there is consistency between the parameters.

HIRHAM is run with one control period and one scenario period. The control run is one realisation of today's climate, representing the present climate. The estimated day-to-day variability is thus not comparable with observations, however the mean monthly values and standard deviation based on daily values should be comparable. The models are run with different emission scenarios IS92a, A2 and B2 (Cubash et al., 2001). Up to 2050 IS92a gives slightly lower increase in global temperature than A2 and B2. Up to 2100 IS92a and B2 gives approximately 2.5 °C increase in global temperature while A2 is giving an increase of 3.5 °C. ECHAM4/OPYC3 is run with emission scenario IS92a up to 2049, and the UK model, HadAm3, is run with SRES emission scenarios A2 and B2 up to 2100. The model runs have different control periods and scenario periods (Table 2.2).

Table 2.2 The Atmospheric-Ocean General Circulation Models (AOGCMs) and emission scenarios used with respective control and scenario period.

Model	Emission scenario	Control period	Scenario period
ECHAM4/OPYC3	IS92a	1980-1999	2030-2049
HadAm3	A2	1961-1990	2071-2100
HadAm3	B2	1961-1990	2071-2100

Daily values of at site measurement of temperature and precipitation are traditionally used as input to the hydrological model. Estimates of temperature and precipitation are therefore interpolated from HIRHAM to selected locations. There are large difficulties using temperature and precipitation interpolated from HIRHAM as station data representing the at site location. The station altitude is wrongly represented in the model and the number of rainy days is typically estimated too large (Frei et al., 2003). The dynamically downscaled temperature and precipitation data are therefore empirically adjusted to be representative locally. The adjustment procedure is described in Engen-Skaugen (2004).

2.4 Climate scenarios

Temperature

To be able to use the scenarios locally, daily temperature values from HIRHAM are interpolated to sites where observations of temperature and precipitation are available (Fig. 2.1). The estimates of mean monthly temperature and mean monthly standard deviation based on daily values however, show large differences. The interpolated daily data therefore had to be adjusted to be representative locally (Engen-Skaugen, 2004). The adjusted temperature data is found to be satisfactorily adjusted both with respect to the mean monthly values and monthly standard deviation values based on daily data. An example showing the adjusted temperature data for the two control periods (1961-1990 and 1980-1999) at station 55840 Fjærland-Skarestad is given in Figure 2.3. The modelled and observed curves show rather well agreement. The second control period (1980-1999) show similar seasonal cumulative distribution curve as for the first control period (1961-1990). A small increase however, can be observed for the latest period in wintertime. Past variations in temperature in Norway are described in Hanssen-Bauer and Nordli (1998) and Førland et al. (2000).

Dynamically downscaling of the ECHAM4/OPYC3 AOGCM with emission scenario IS92a to Norwegian regions projects that the largest temperature increase in 50 years will occur in Northern parts especially in wintertime (2-3 °C, or ~0.4-0.6°C/dec). At the south-western, eastern and middle regions of the country the mean annual temperature increase is projected to ~1.1°C in 50 years, with the largest increase in autumn and winter (~1.0-~1.4°C in 50 years, or ~ 0.2-0.28°C/dec) (Hanssen-Bauer et al., 2003; Førland et al., 2000). The projected increase in adjusted temperature data at the selected temperature and precipitation stations (Fig. 2.1) for the ECHAM4/OPYC3 GSDIO model run with the IS92a scenario is presented in Appendix 1. The same regional pattern as described by Hanssen-Bauer et al. (2003) and Førland et al. (2000) can be recognised; the largest increase in temperature is projected in the north during winter.

Mean temperature change obtained by dynamical downscaling of the HadAm3 model with emission scenario B2 is presented in Appendix 3. The time window studied (2071-2100) goes further in to the future compared to the ECHAM4/OPYC3 model run (2030-2049) projecting

a larger total warming (11 decades compared to 5 decades). The temperature increase per decade, however, is rather similar for spring and autumn. Some differences can be seen in summer where the temperature increase is highest along the coast and lower further inland. The increase in winter and summer is lower per decade compared to the ECHAM4/OPYC3 IS92a scenario.

Dynamically downscaling of the HadAm3 model with emission scenario A2 shows the same temperature change pattern as obtained with the B2 emission scenario. The temperature increase is stronger though in all seasons (Appendix 2).

The projected mean seasonal temperature change is discussed above. The adjustment method developed by Engen-Skaugen (2004) makes it possible to analyse the at site scenarios in more details. Even though the adjustment is found satisfactory there are still uncertainties associated to the scenario estimates (see Section 3). However, three stations are selected to be discussed in more details; these are 700 Drevsjø (Fig. 2.4), 55840 Fjærland-Skarestad (Fig. 2.5) and 82290 Bodø (Fig. 2.6) (see Fig. 2.1 for the locations of the stations). Observations are used instead of the control run in the Figs.

Fig. 2.4 shows that during spring, summer and autumn a shift in the cumulative distribution curve of daily temperature values towards higher values is projected for the whole range of temperature values in the curve. The cumulative distribution of daily temperature values in winter, however, show small increase in the warmest days, and larger temperature increase in the coldest days, which indicates a different temperature distribution during winter season in the future. As can be seen by the cumulative distribution curve of observations for the two control periods, a shift towards a warming of the coldest winter days has already occurred. The HadAm3 estimates, which is run for the period 2071-2100, lead to the largest temperature change (HadAm3 A2 projects a larger temperature increase compared to the emission scenario B2). Similar pattern can be seen for the stations 55840 Fjærland-Skarestad and 82290 Bodø (Figs. 2.5 and 2.6).

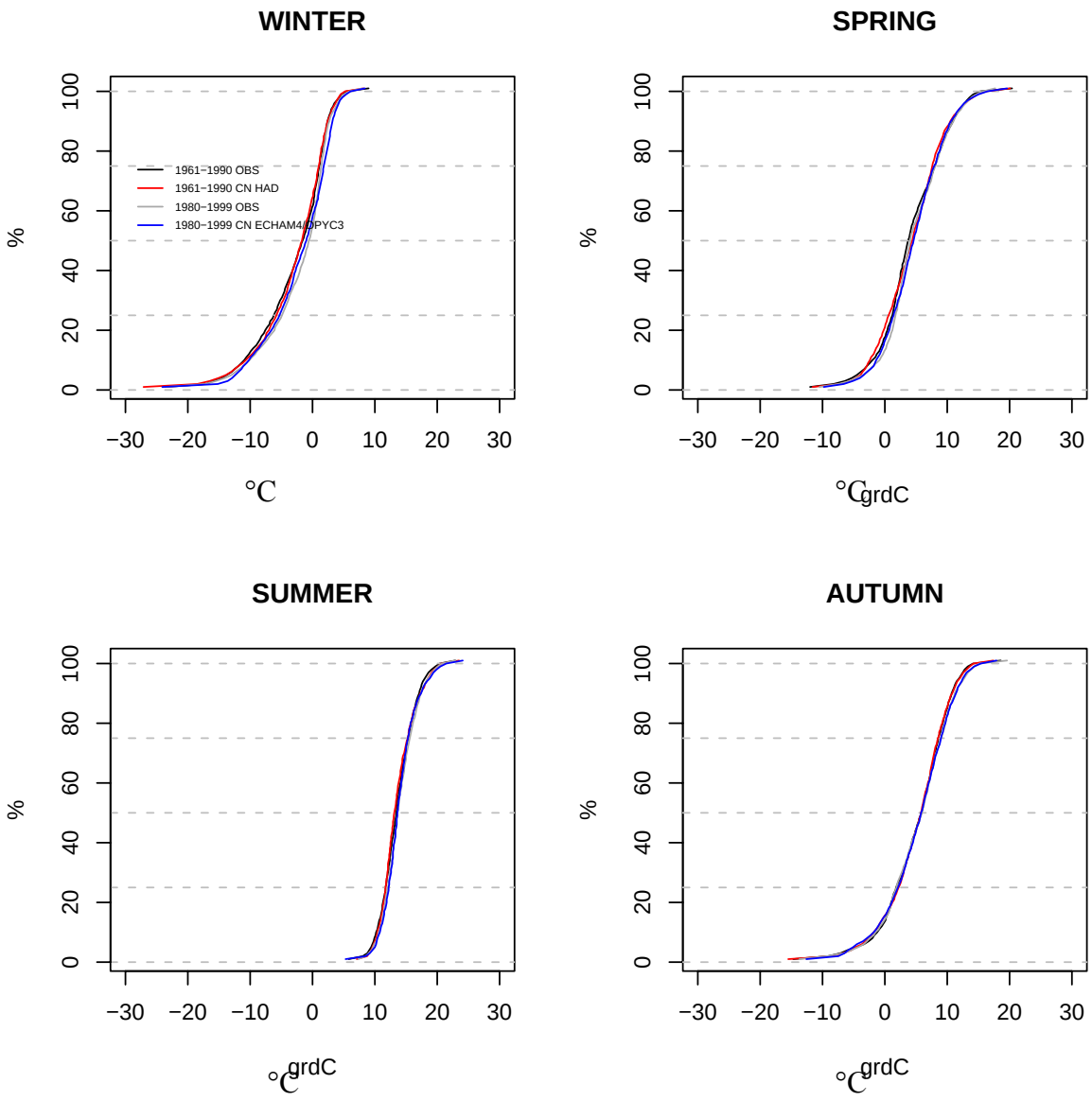

Figure 2.3. Seasonal cumulative distribution curves of observed daily temperature values for the period 1961-1990 (black) and 1980-1999 (grey) at station 55840 Fjærland-Skarestad together with adjusted daily temperature values of the control period of the HadAm3 model (1961-1990) (red) and ECHAM4/OPYC3 model (1980-1999) (blue).

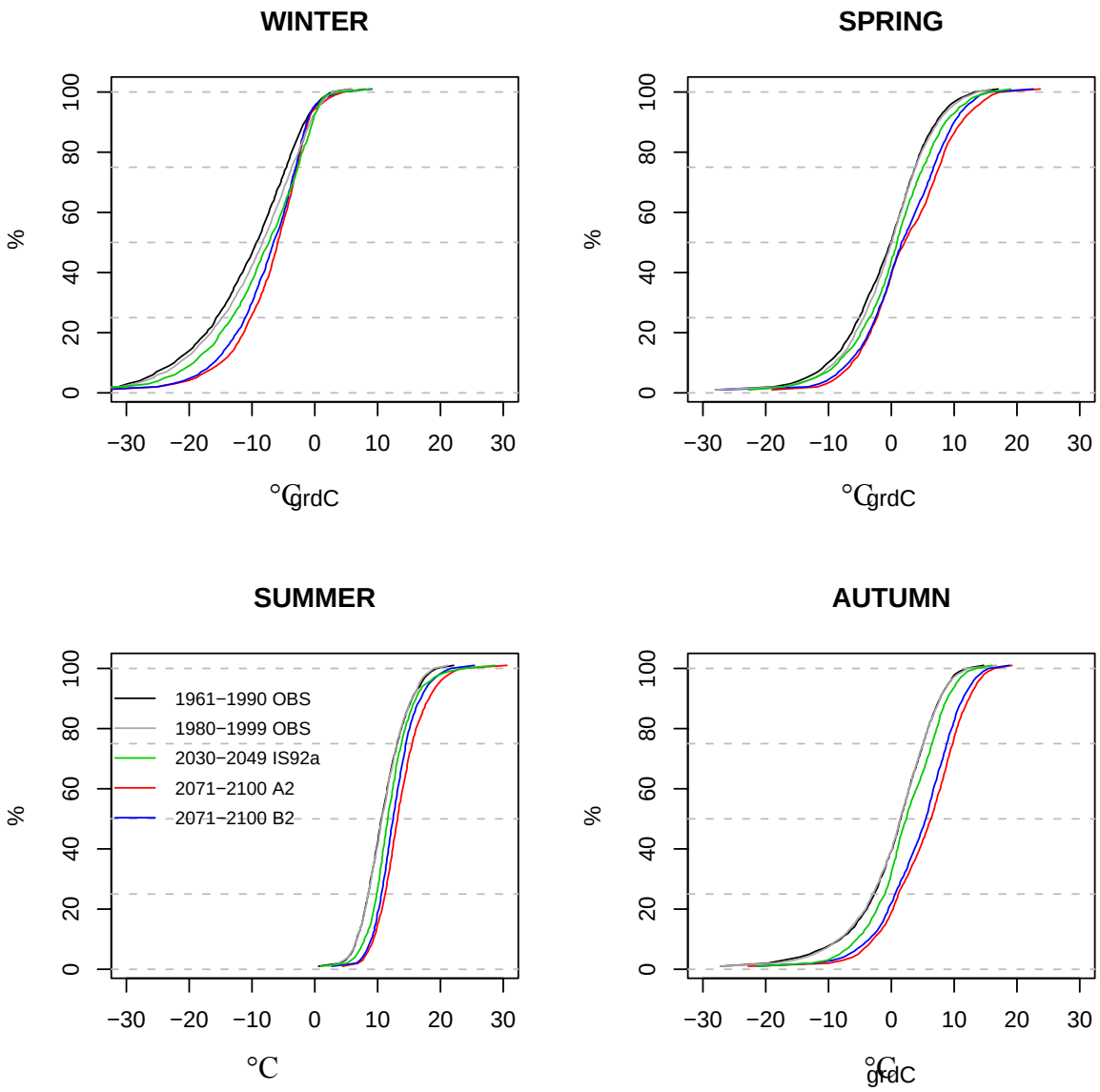

Figure 2.4 Cumulative distribution curves of daily temperature values based on observations for the periods 1961-1990 (black) and 1980-1999 (grey) at station 700 Drevsjø together with three different scenarios; ECHAM4/OPYC3 with the IS92a emission scenario representing the period 2030-2049 (green), HadAm3 with the A2 (red) and B2 (blue) emission scenario representing the period 2071-2100.

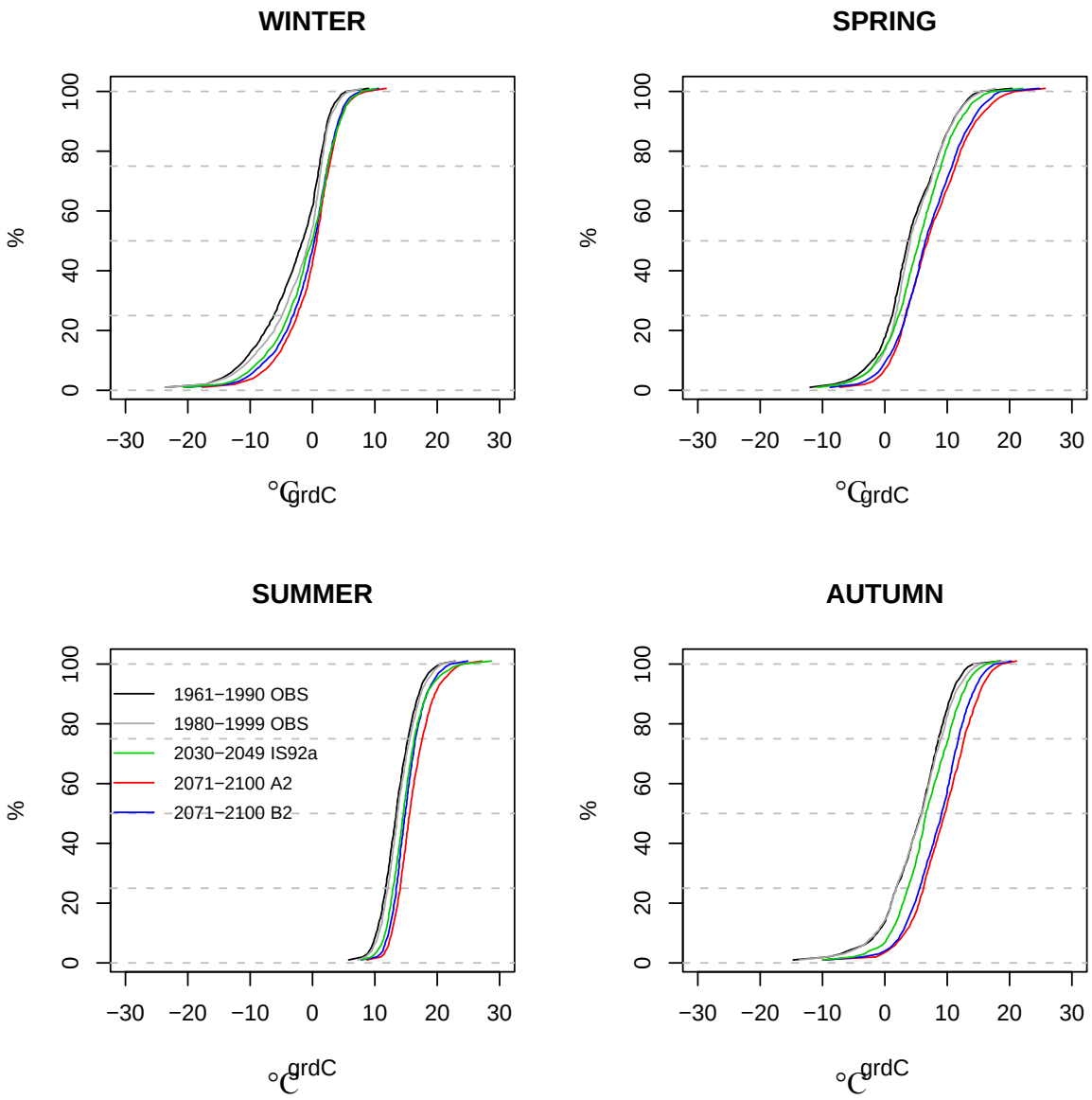

Figure 2.5 Cumulative distribution curves of daily temperature values based on observations for the periods 1961-1990 (black) and 1980-1999 (grey) at station 55840 Fjærland-Skarestad together with three different scenarios; ECHAM4/OPYC3 with the IS92a emission scenario representing the period 2030-2049 (green), HadAm3 with the A2 (red) and B2 (blue) emission scenario representing the period 2071-2100.

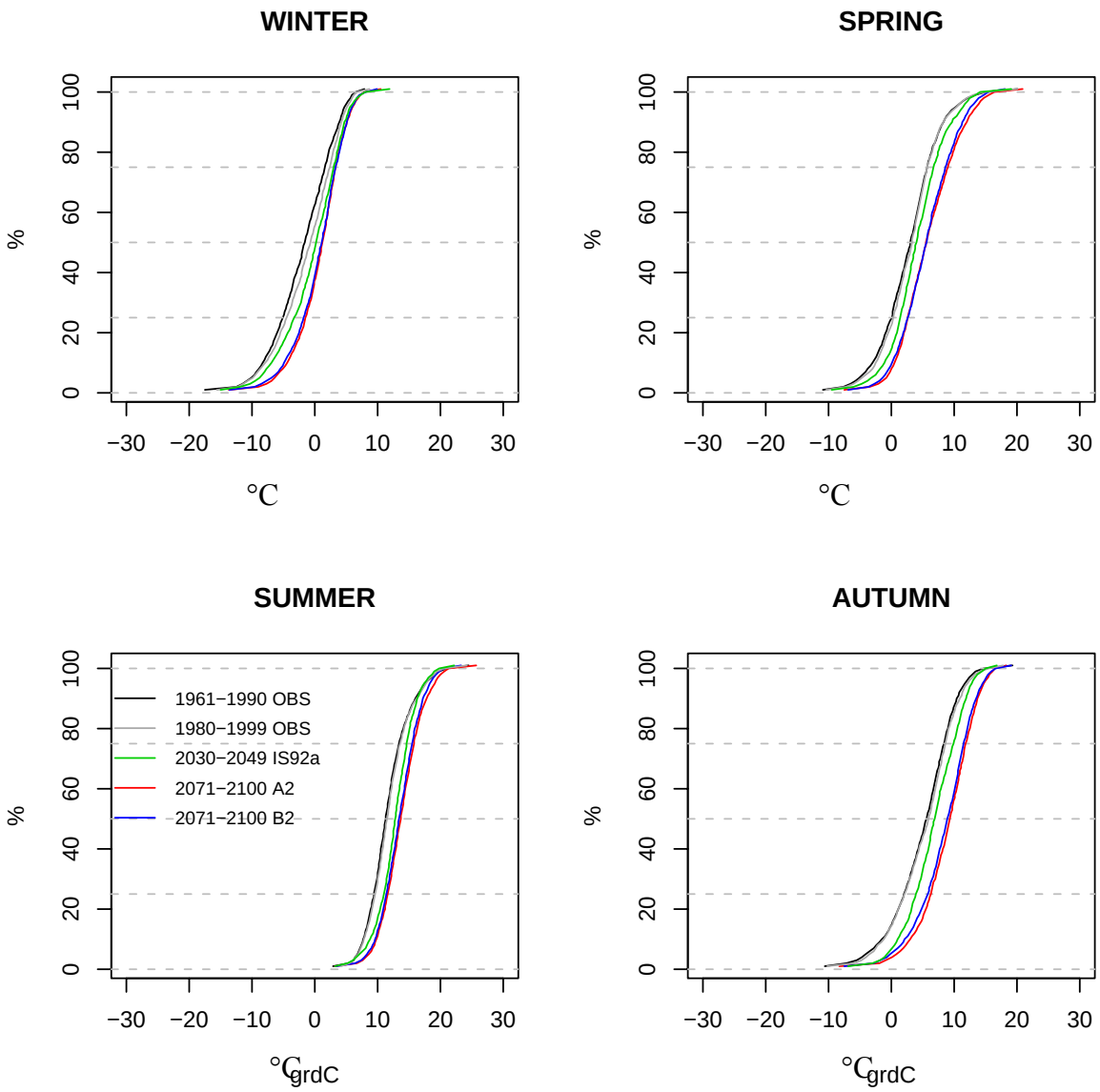

Figure 2.6 Cumulative distribution curves of daily temperature values based on observations for the periods 1961-1990 (black) and 1980-1999 (grey) at station 82290 Bodø together with three different scenarios; ECHAM4/OPYC3 with the IS92a emission scenario representing the period 2030-2049 (green), HadAm3 with the A2 (red) and B2 (blue) emission scenario representing the period 2071-2100.

Precipitation

Daily precipitation values have been interpolated from HIRHAM to be representative at the stations locations. As for temperature, mean monthly statistics for the control run should be comparable with mean monthly statistics based on daily precipitation observations. However, the statistics show rather different estimates, therefore daily at site estimates both for the control period and the scenario period had to be adjusted to be representative locally (Engen-Skaugen, 2004).

An example of the frequency distribution curve of adjusted precipitation data for the two control periods (1961-1990 and 1980-1999) together with the frequency distribution curve of precipitation observations for the respective periods are presented for daily values and monthly values in Figs 2.7 and 2.8 respectively for station 55840 Fjærland-Skarestad. The

cumulative distribution curves of the two control runs fits rather satisfactory to the observed both for daily and monthly values. There has been an increase in precipitation at the western coast region in winter and spring. A reduction in precipitation is observed in the autumn for the same region and no marked differences during summer (Førland et al., 2000). The same pattern can be recognised in Figs 2.7 and 2.8. Further descriptions of past variation in precipitation are given in Førland et al. (2000).

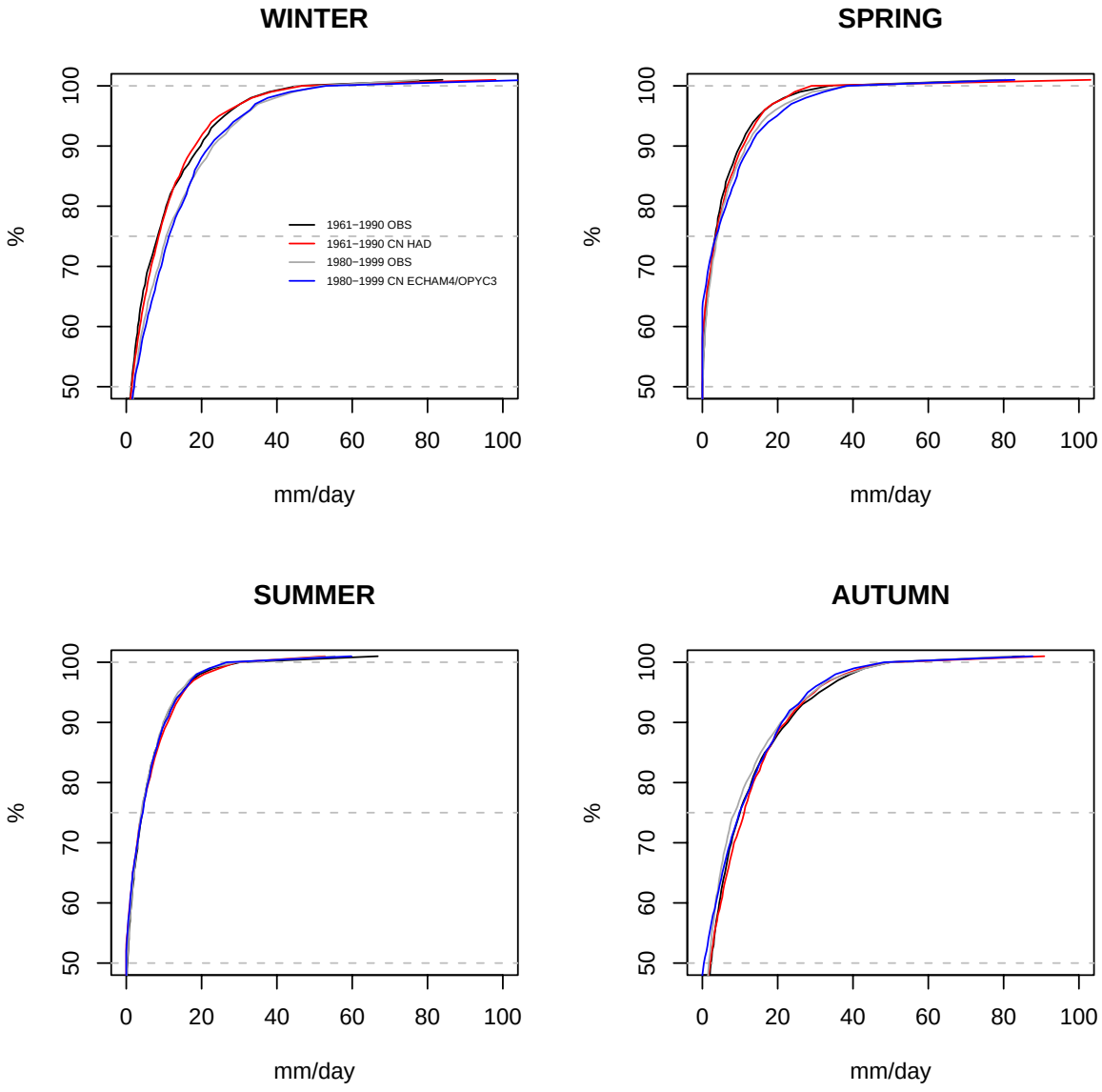

Figure 2.7 Seasonal cumulative distribution curves of observed daily precipitation values for the period 1961-1990 (black) and 1980-1999 (grey) at station 55840 Fjærland-Skarestad together with adjusted daily temperature values of the control period of the HadAm3 model (1961-1990) (red) and ECHAM4/OPYC3 model (1980-1999) (blue).

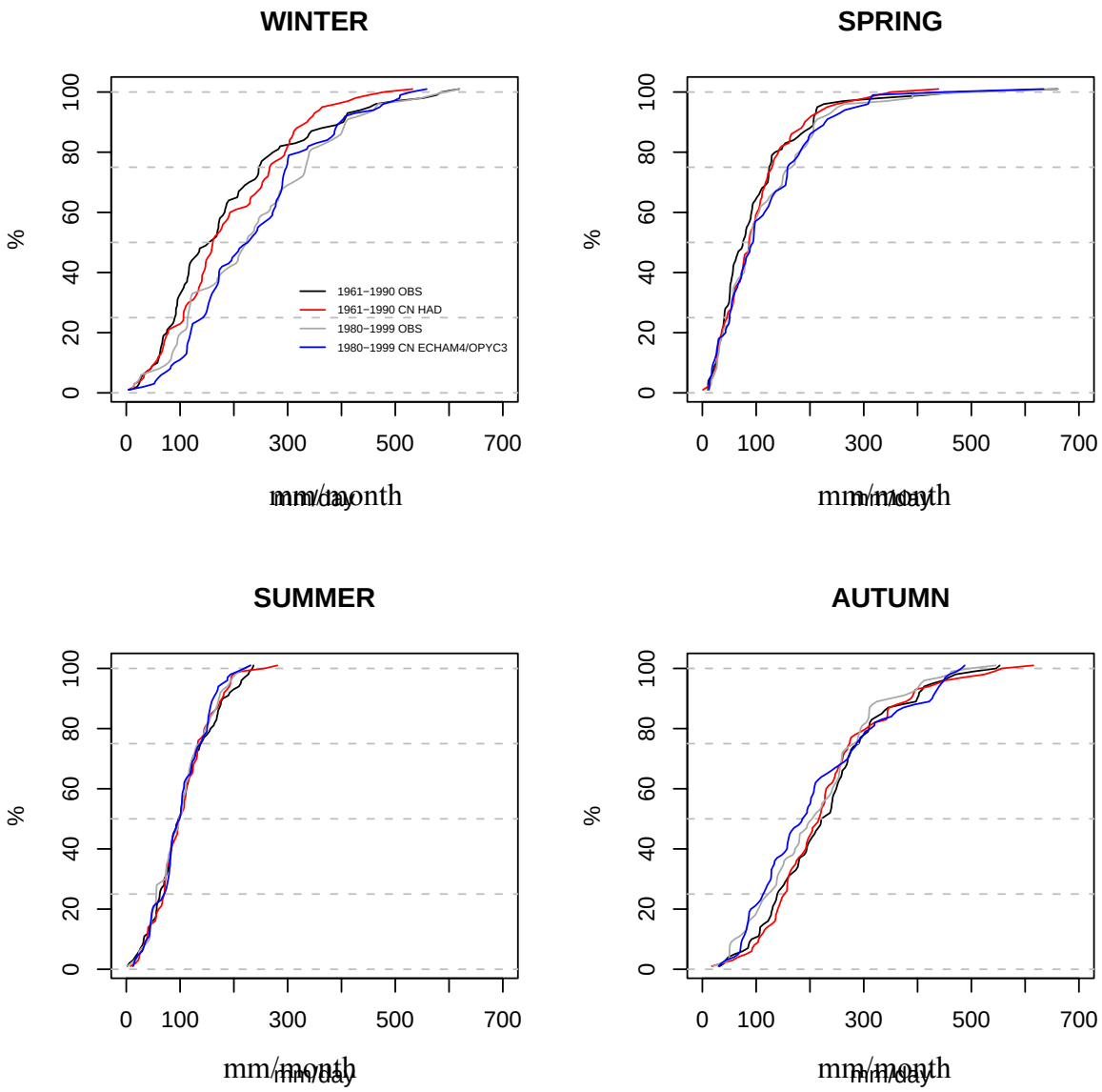

Figure 2.8 Seasonal cumulative distribution curves of observed monthly precipitation values for the period 1961-1990 (black) and 1980-1999 (grey) at station 55840 Fjærland-Skarestad together with adjusted daily temperature values of the control period of the HadAm3 model (1961-1990) (red) and ECHAM4/OPYC3 model (1980-1999) (blue).

The largest annual increase in precipitation projected with the ECHAM4/OPYC3 model with the IS92a emission scenario in 50 years is projected to occur in western parts of the country (Hanssen-Bauer et al. 2003; Førland et al., 2000). For western Norway as a whole, an increase in annual precipitation of ~10-25 % (or 2-5% per decade) is projected. The largest increase in precipitation is projected to occur in western parts during summer and autumn (~15-30 % or 3-6 % per decade). Precipitation in south-eastern parts of Norway is projected to decrease in summer and spring (~0- -10 % or 0- -2 % per decade) (Førland et al, 2000). The same relative change pattern of mean seasonal precipitation as described by Førland et al (2000) and Hanssen-Bauer et al. (2003) can be recognized in the adjusted HIRHAM estimates for the selected stations (Appendix 4).

The HadAm3 model and emission scenario A2 in winter projects a larger increase in precipitation in southern regions (3-4.5 % per decade) compared to the ECHAM4/OPYC3 IS92a (2-3% per decade) and HadAm3 B2 estimates (2-3 % per decade) (Appendix 5 and 6). In autumn the precipitation increase is largest in the south-eastern parts with the HadAm3 model with the B2 emission scenario (~ 1-2.7 % per decade) compared to the HadAm3 model and A2 scenario (~ -1.4-1.4 % per decade) and ECHAM4/OPYC3 and IS92a scenario (~0-2 % per decade). In western areas however, the increase is projected to be largest with the ECHAM4/OPYC3 model (IS92a) (~1-5% per decade). A decrease in precipitation is projected in the western and northern areas during spring with the HadAm3 scenario with B2 and in the northern parts with the A2 scenario. The largest differences between the two AOGCMs are found in summer, where a decrease in precipitation in southern areas is projected with the HadAm3 model both with the A2 emission scenario and B2 emission scenario (~ 0 - -1.4 % per decade) compared to an increase in the ECHAM4/OPYC3 model (~ 0-6 % per decade). The opposite is the occasion in northern parts (increase in HadAm3 model decrease in ECHAM4/OPYC3). The differences are explained by differences in the projected change of the large scale circulation pattern in the AOGCM and the different time windows (Haugen and Ødegaard, 2003).

Some examples of the cumulative distribution curves of observed daily and monthly precipitation data both for observations within the two control periods and the three model runs are presented for station 700 Drevsjø (Figs 2.9-2.14). The ECHAM4/OPYC3 model represent the period 2030-2049 (20 years) while the HadAm3 model represents the period 2071-2100 (30 years). The figures show the regional pattern in the change in precipitation as described above. In southeastern parts the HadAm3 model with A2 emission scenario projects largest increase during winter while the B2 scenario projects largest relative increase in autumn. The HadAm3 B2 scenario is driest during summer (Figs. 2.9 and 2.10). In northern areas, the HadAm3 B2 projects the largest increase in precipitation during summer, while ECHAM4/OPYC3 projects the largest increase in spring where HadAm3 A2 and HadAm3 B2 project a drier climate at this station. Autumn show an increase in all models, the ECHAM4/OPYC3 model however projects the largest increase. In winter, the two models project opposite change in precipitation, the ECHAM4/OPYC3 model projects an increase in precipitation while the HadAm3 model projects a decrease in precipitation (Figures 2.11 and 2.12). In the western parts of the country, there are no changes in precipitation during summer projected with the HadAm3 model both with the A2 and B2 emission scenario while the ECHAM4/OPYC3 model projects an increase in precipitation. The HadAm3 B2 scenario projects largest increase in autumn, HadAm3 A2 projects no change here. The ECHAM4/OPYC3 model IS92a projects the largest increase in precipitation both in winter and spring in the western part of the country (Figs. 2.13-2.14).

The change in the 99 percent percentile of seasonal daily precipitation is discussed in Chapter 3.

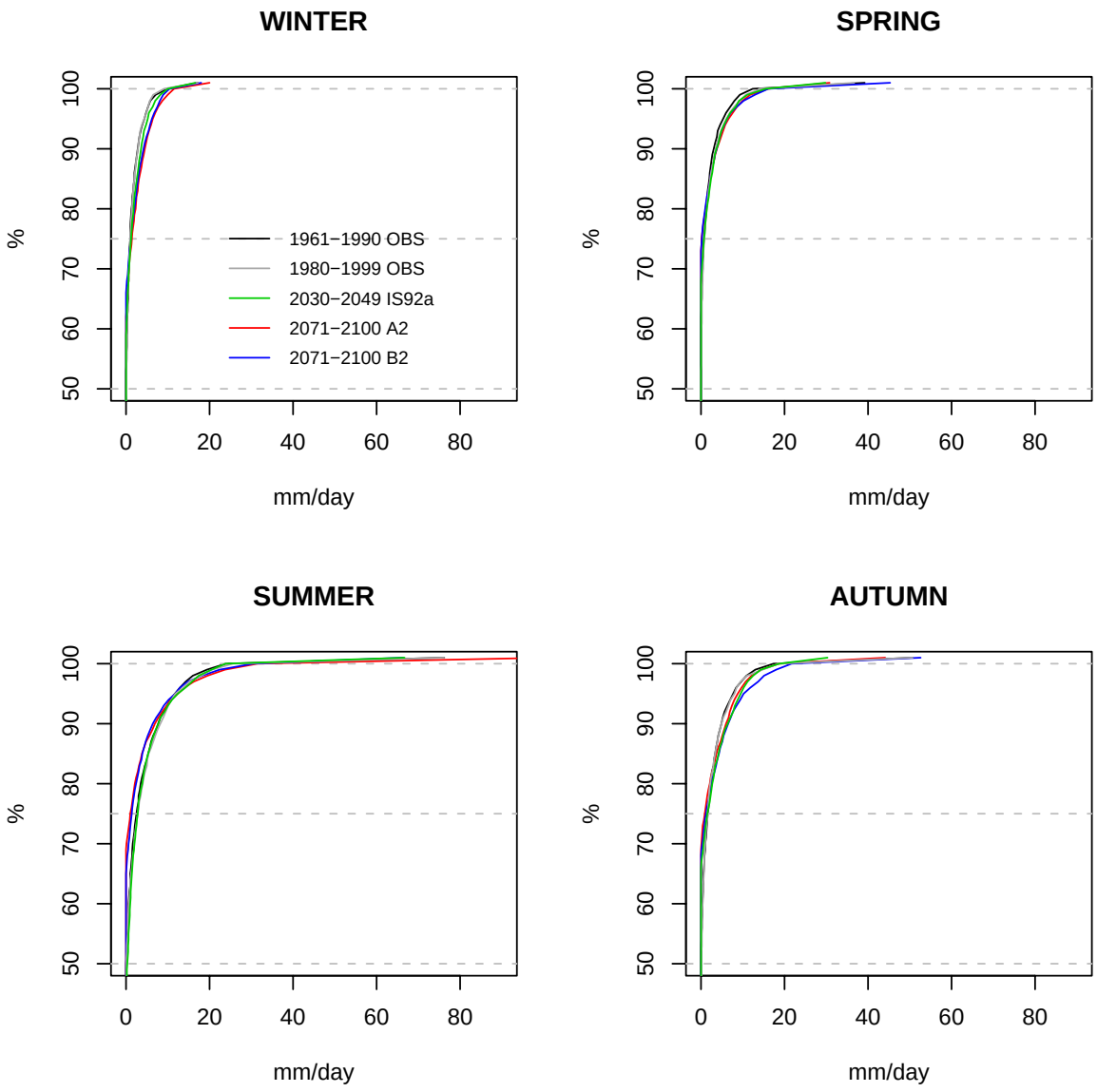

Figure 2.9 Cumulative distribution curves of daily precipitation values based on observations for the periods 1961-1990 (black) and 1980-1999 (grey) at station 700 Drevsjø together with three different scenarios; ECHAM4/OPYC3 with the IS92a emission scenario representing the period 2030-2049 (green), HadAm3 with the A2 (red) and B2 (blue) emission scenario representing the period 2071-2100.

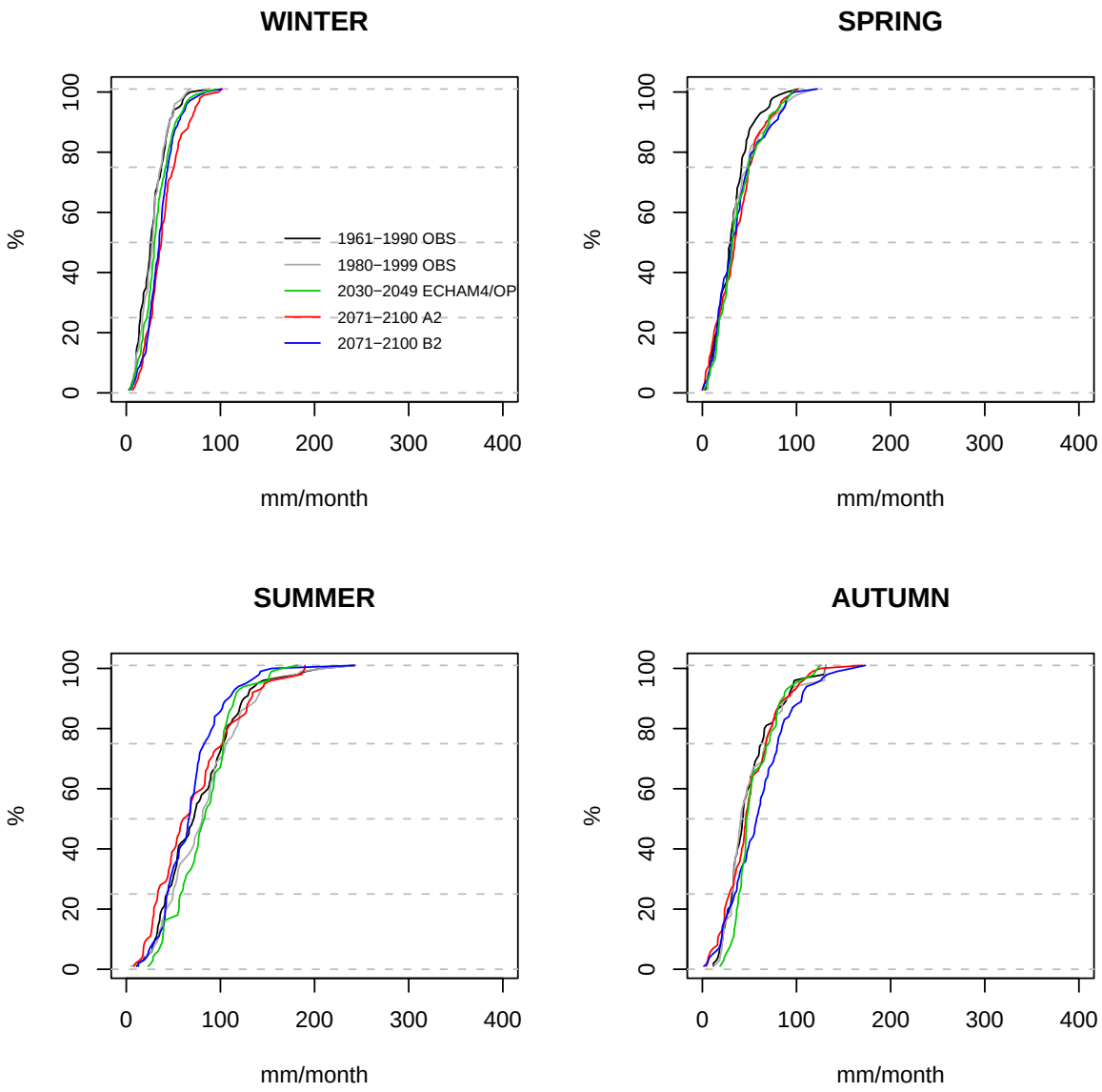

Figure 2.10 Cumulative distribution curves of monthly precipitation values based on observations for the periods 1961-1990 (black) and 1980-1999 (grey) at station 700 Drevsjø together with three different scenarios; ECHAM4/OPYC3 with the IS92a emission scenario representing the period 2030-2049 (green), HadAm3 with the A2 (red) and B2 (blue) emission scenario representing the period 2071-2100.

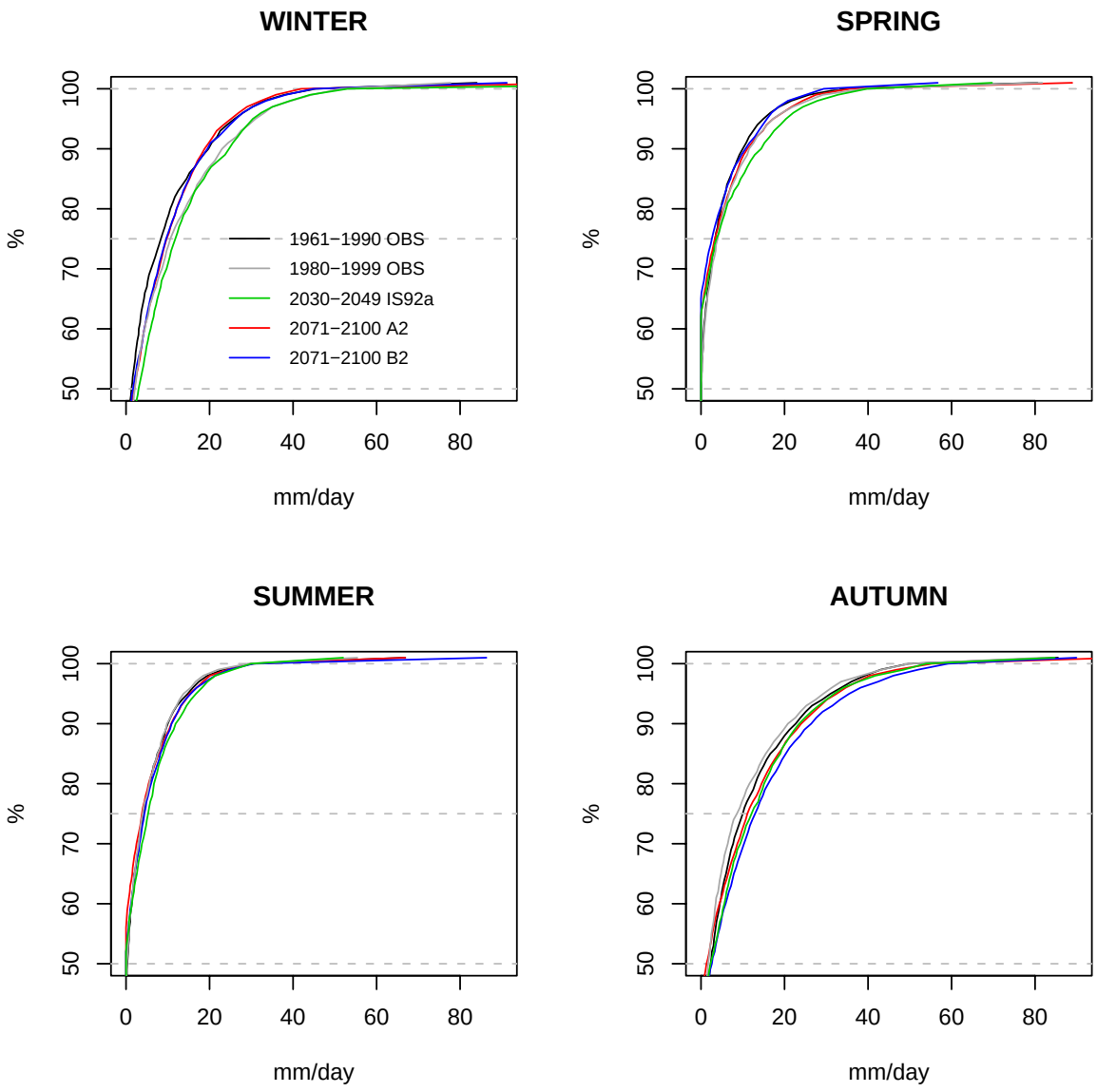

Figure 2.11 Cumulative distribution curves of daily precipitation values based on observations for the periods 1961-1990 (black) and 1980-1999 (grey) at station 55840 Fjærland-Skarestad together with three different scenarios; ECHAM4/OPYC3 with the IS92a emission scenario representing the period 2030-2049 (green), HadAm3 with the A2 (red) and B2 (blue) emission scenario representing the period 2071-2100.

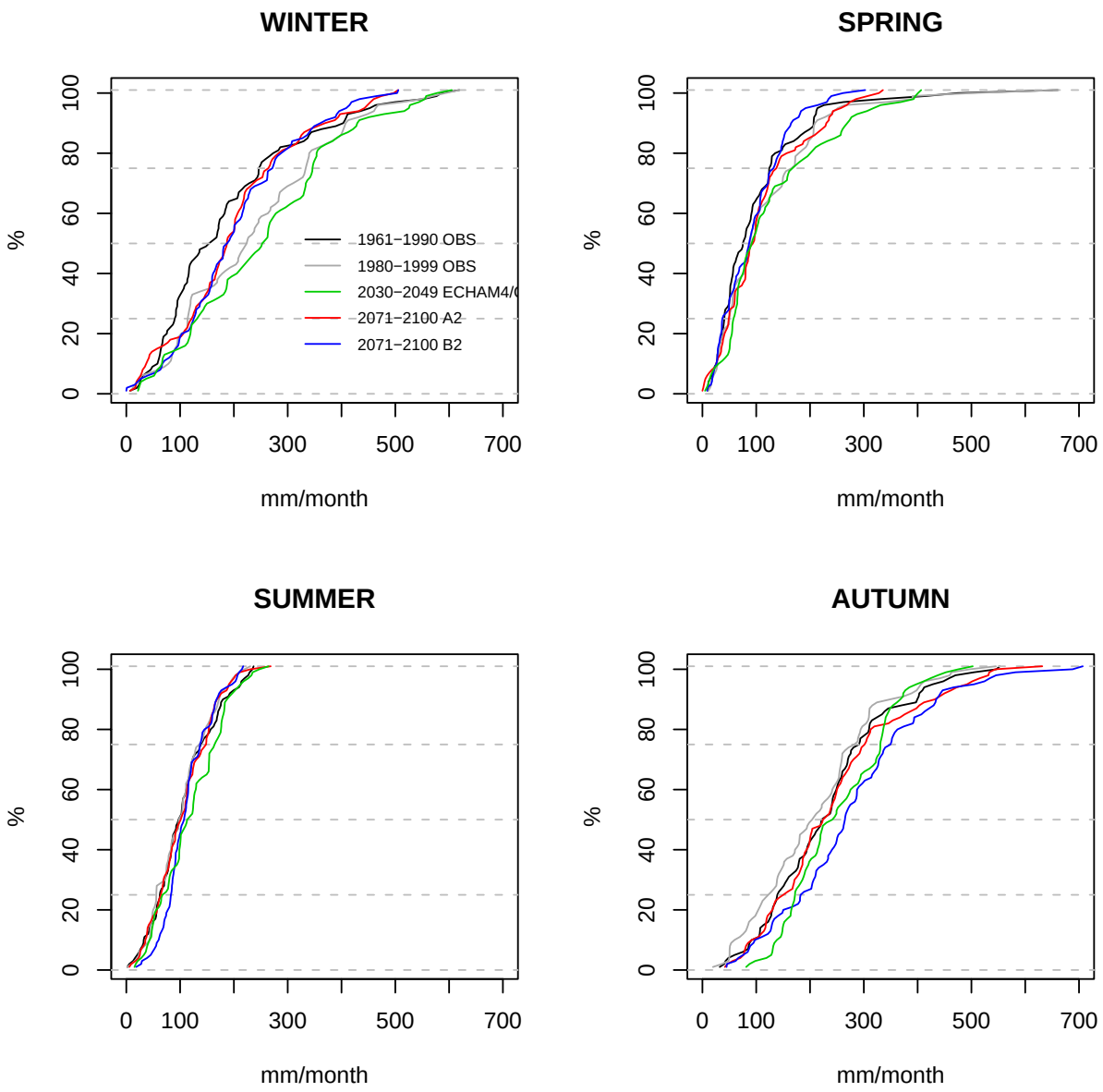

Figure 2.12 Cumulative distribution curves of monthly precipitation values based on observations for the periods 1961-1990 (black) and 1980-1999 (grey) at station 55840 Fjærland-Skarestad together with three different scenarios; ECHAM4/OPYC3 with the IS92a emission scenario representing the period 2030-2049 (green), HadAm3 with the A2 (red) and B2 (blue) emission scenario epresenting the period 2071-2100.

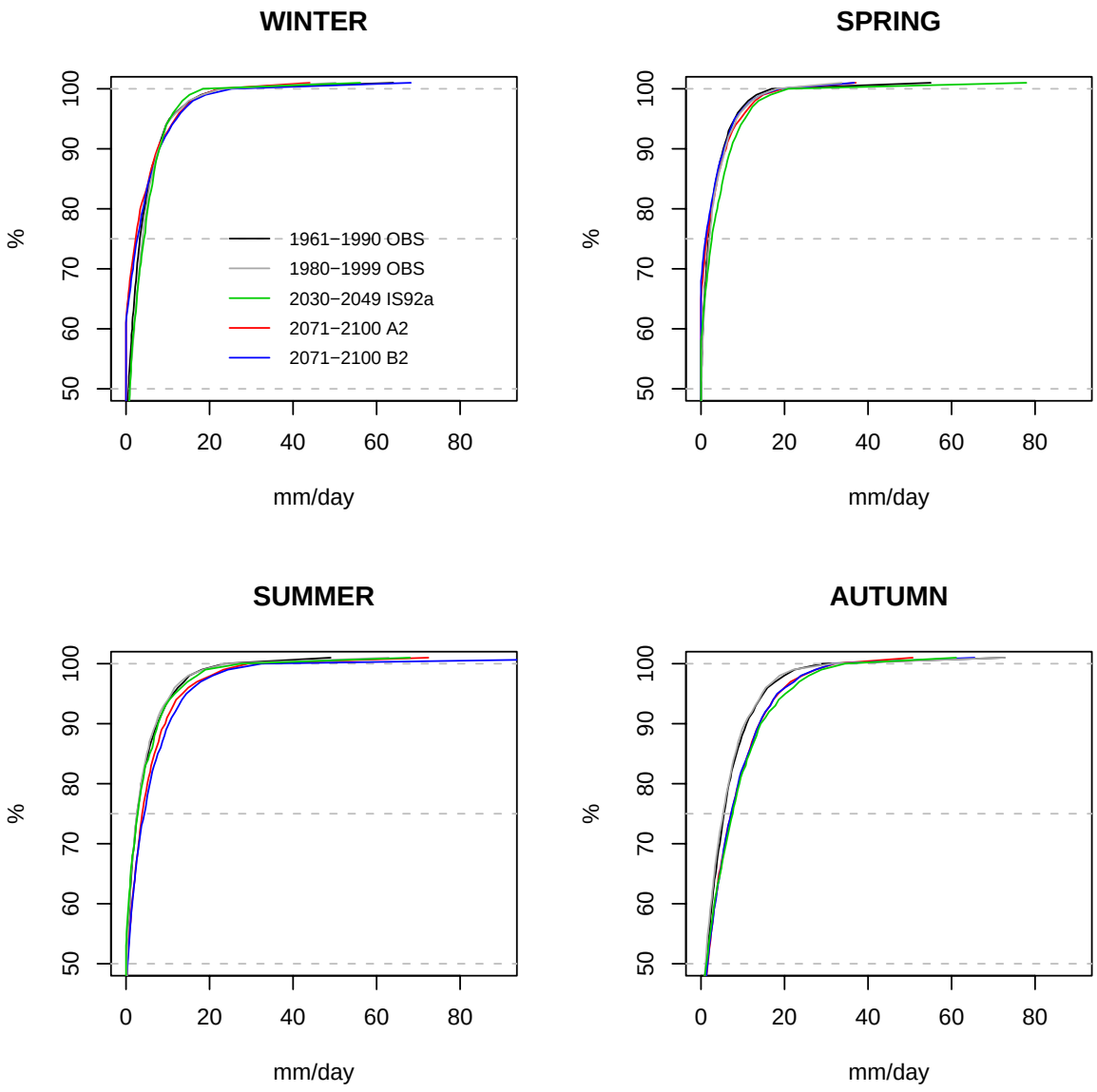

Figure 2.13 Cumulative distribution curves of daily precipitation values based on observations for the periods 1961-1990 (black) and 1980-1999 (grey) at station 82290 Bodø together with three different scenarios; ECHAM4/OPYC3 with the IS92a emission scenario representing the period 2030-2049 (green), HadAm3 with the A2 (red) and B2 (blue) emission scenario representing the period 2071-2100

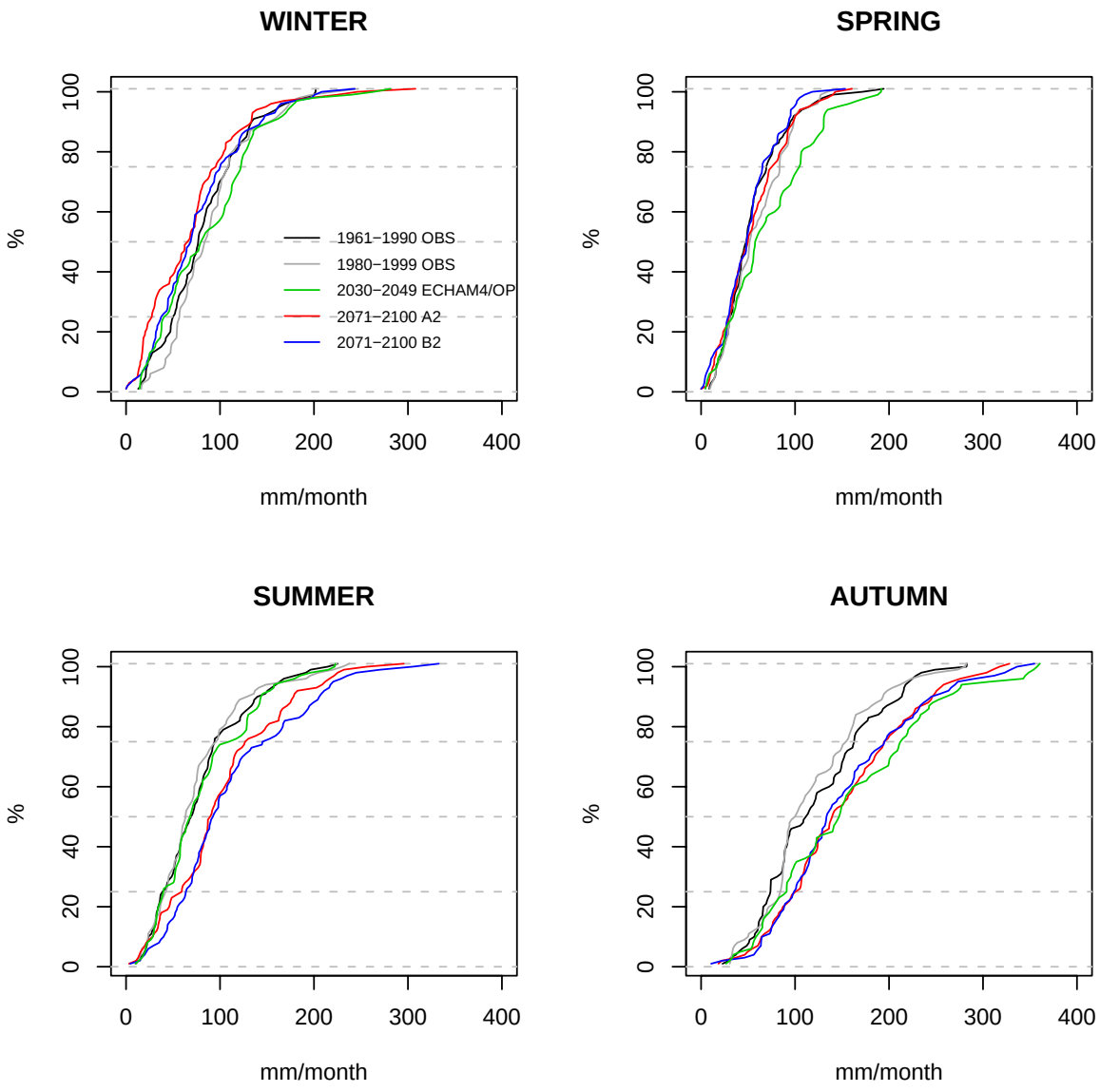

Figure 2.14 Cumulative distribution curves of monthly precipitation values based on observations for the periods 1961-1990 (black) and 1980-1999 (grey) at station 82290 Bodø together with three different scenarios; ECHAM4/OPYC3 with the IS92a emission scenario representing the period 2030-2049 (green), HadAm3 with the A2 (red) and B2 (blue) emission scenario representing the period 2071-2100

3. CHANGES IN EXTREME PRECIPITATION EVENTS

A study of how extreme daily precipitation will change in three different simulations of a future climate (Sections 2.3 and 2.4) at some selected stations is presented in this section. To obtain reliable estimates of extremes with large return periods, long time series of precipitation is required. Different time periods with lengths of 20 and 30 years are available in the present study (Section 2.3), which is too short to analyse extreme events with large return intervals. Extreme precipitation is therefore in this study defined as the 99 percentile of daily precipitation, which is the threshold value where daily precipitation has been observed equal to or larger than this value only 1 % of all the observing days.

Cumulative distribution curves of daily precipitation for both observed and for three scenario periods are presented in Section 2.4 for three selected stations (700 Drevsjø, 55840 Fjærland-Skarestad, 82290 Bodø), in addition a southern station is included (43500 Ualand). See Fig. 2.1 for the locations of the stations. The seasonal 99 percentile value of daily precipitation observations and daily precipitation estimates obtained with the HadAm3 for the control period, 1961-1990, for the four selected stations is presented in Table 3.1 together with the seasonal 99 percentile of the HadAm3 run with the A2 and B2 emission scenario respectively. The seasonal 99 percentile of daily observed precipitation and daily precipitation data estimated with the ECHAM4/OPYC3 model with the IS92a emission scenario for the period 1980-1999 is presented in the table as well together with the scenario 2030-2049. The results for station 700 Drevsjø and 55840 Fjærland Skarestad are visualised in a diagram as well (Figure 3.1).

The study of the seasonal 99 percentile of the three different scenario data requires that the control run is reliably reproduced compared to observations not only on a mean monthly basis, the statistical properties of the 99 percentiles of daily values must be reliably reproduced as well. Table 3.1 shows that for all the stations the extreme values obtained with the HadAm3 and ECHAM4/OPYC3 model for the respective control periods are rather similar to the observed values. There are some differences at some locations, e.g. 43500 Ualand in winter (11% difference with the ECHAM model) and autumn (13% difference with the HadAm3 model) and also 700 Drevsjø in winter (15% difference with the HadAm3 model) and autumn (-11% difference with the ECHAM model). However, as a whole the 99 percentile of precipitation is rather well reproduced for all seasons.

The projected change in the 99 percentile of daily precipitation is in correspondence with the mean change in precipitation projected by ECHAM4/OPYC4 and HadAm3 for southern Norway (Section 2.4). In south-eastern Norway, however, where all three scenarios project a reduction in precipitation during summer, an increase is projected in the 99% percentile for the HadAm3 model both with the A2 and B2 emission scenario. This feature indicates less, but more intense summer rainfall in these areas in the future.

Another interesting question is how often will the seasonal 99 percentile of the present climate occur in a future climate? At 700 Drevsjø, an increase in mean precipitation in all seasons is projected except during summer. In winter a small change in the 99% value, a large increase (>3 times projected with HadAm3 A2) in the number of times the present winter percentile will occur in the future is observed.

At 55840 Fjærland-Skarestad, increased precipitation is projected especially during autumn. And a small increase during spring for the HadAm3 A2 scenario is projected. An increase can be observed in the 99% value (Table 3.1 and Fig. 3.1) and an increase in number of times the present 99% value will occur in the future is observed (double for the HadAm3 B2 and ECHAM4/OPYC3 IS92a scenarios during autumn). Mean annual precipitation is projected to increase the most at 82290 Bodø in summer and spring. The largest increase in the 99 % value is projected to occur during summer. The present 99 % value will occur 2.5 more frequent than to day for the HadAm3 B2 scenario.

Fig. 3.2 shows that even though the mean seasonal change in precipitation is projected to decrease, the intensity of the present 99 percentile may happen more frequently in the future (700 Drevsjø in summer). It can also be seen that even though the mean precipitation is projected to increase in winter, there is a reduction in the 99 percentile (Fig. 3.1), and the present 99 percentile value will appear less frequently (55840 Fjærland-Skarestad).

Skaugen et al. (2003) used the weather generator Randomised Bartlett-Lewis Rectangular Pulse model (RBLRPM) (Onof and Wheater, 1993; Onof 2000) on unadjusted daily

precipitation from the ECHAM4/OPYC3 model with the IS92a emission scenario to analyse change in extreme precipitation of duration 1 and 5 days. Precipitation data were interpolated from HIRHAM to 16 stations in Norway. Skaugen et al. (2003) found that the change in extreme values in the scenario period show tendencies towards increased extreme values and seasonal shifts. The regional variability, however, is large. The present study is based on only four stations. A marked seasonal shift can not be observed. Large seasonal variations in the 99 percentile value for three projections of a future climate, however, have been recognised.

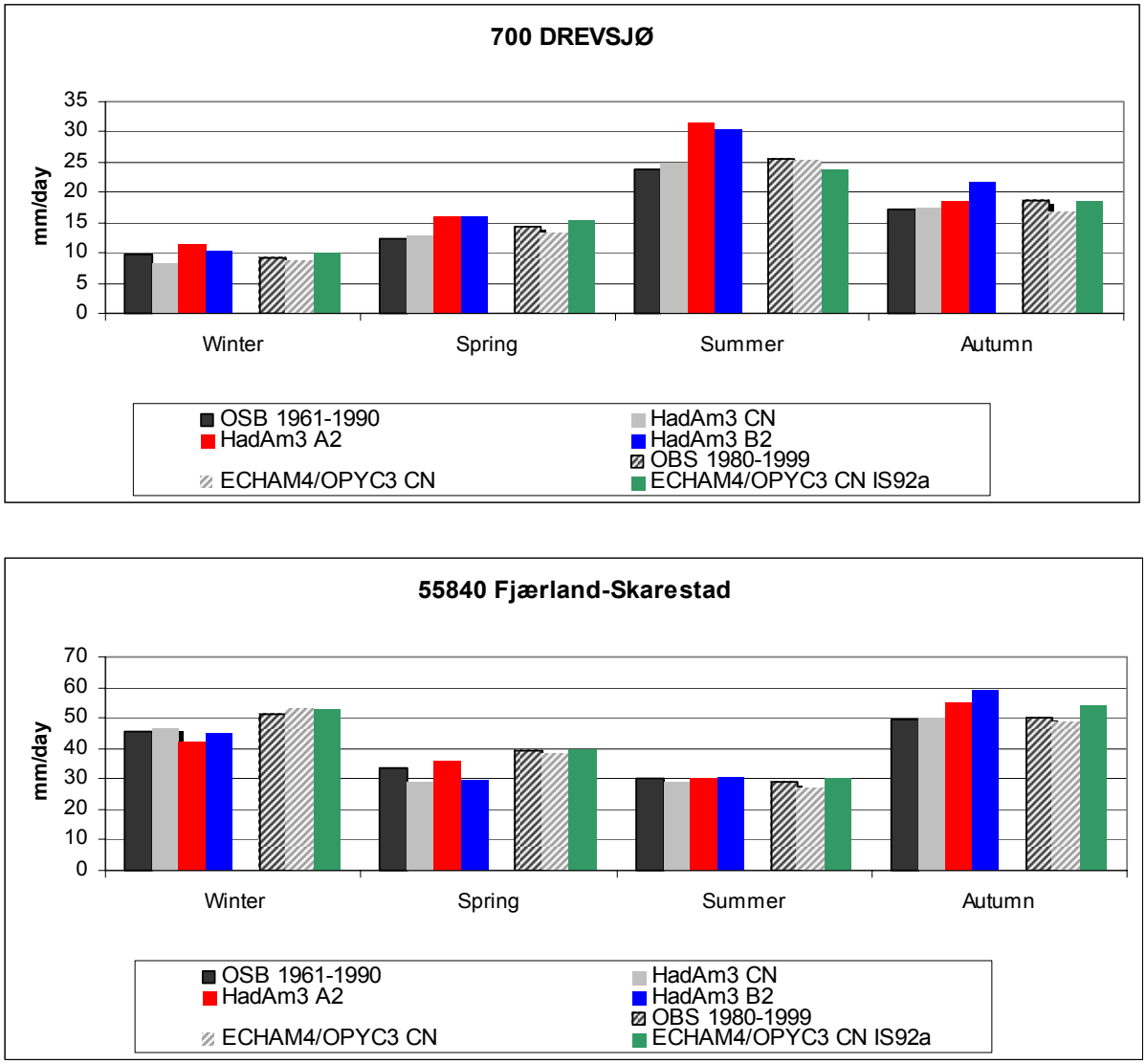

Figure 3.1 The 99 percentile of observed and modelled daily precipitation at stations 700 Drevsjø and 55840 Fjærland-Skarestad.

Table 3.1 The 99 percentile of seasonal daily precipitation value [mm/day] at 4 stations in Norway (Fig. 2.1) for two different control runs (1961-1990 and 1980-1999) and observations for the two periods. The 99 percentile is presented for the three scenarios as well.

	Winter	Spring	Summer	Autumn
Station 43500 Ualand				
OBS 1961-1990	50	38	41	55
HadAm3 CN 1961-1990	54	40	43	62
HadAm3 A2 2071-2100	72	43	45	72
HadAm3 B2 2071-2100	65	44	45	75
OBS 1980-1999	54	42	40	58
ECHAM4/OPYC3 CN 1980-1999	60	39	40	61
ECHAM4/OPYC3 CN IS92a 2030-2049	76	34	43	65
Station 55840 Fjærland Skarestad				
OBS 1961-1990	46	34	30	50
HadAm3 CN 1961-1990	47	29	29	50
HadAm3 A2 2071-2100	42	36	30	55
HadAm3 B2 2071-2100	45	29	31	59
OBS 1980-1999	51	39	29	50
ECHAM4/OPYC3 CN 1980-1999	53	38	27	48
ECHAM4/OPYC3 CN IS92a 2030-2049	53	40	30	54
Station 82290 Bodø				
OBS 1961-1990	22	17	24	29
HadAm3 CN 1961-1990	21	17	22	27
HadAm3 A2 2071-2100	22	20	29	32
HadAm3 B2 2071-2100	25	19	32	32
OBS 1980-1999	23	18	24	31
ECHAM4/OPYC3 CN 1980-1999	20	18	23	29
ECHAM4/OPYC3 CN IS92a 2030-2049	18	21	27	34
Station 700 Drevsjø				
OBS 1961-1990	10	12	24	17
HadAm3 CN 1961-1990	8	13	25	18
HadAm3 A2 2071-2100	11	16	31	19
HadAm3 B2 2071-2100	10	16	30	22
OBS 1980-1999	9	14	26	19
ECHAM4/OPYC3 CN 1980-1999	9	13	25	17
ECHAM4/OPYC3 CN IS92a 2030-2049	10	15	24	19

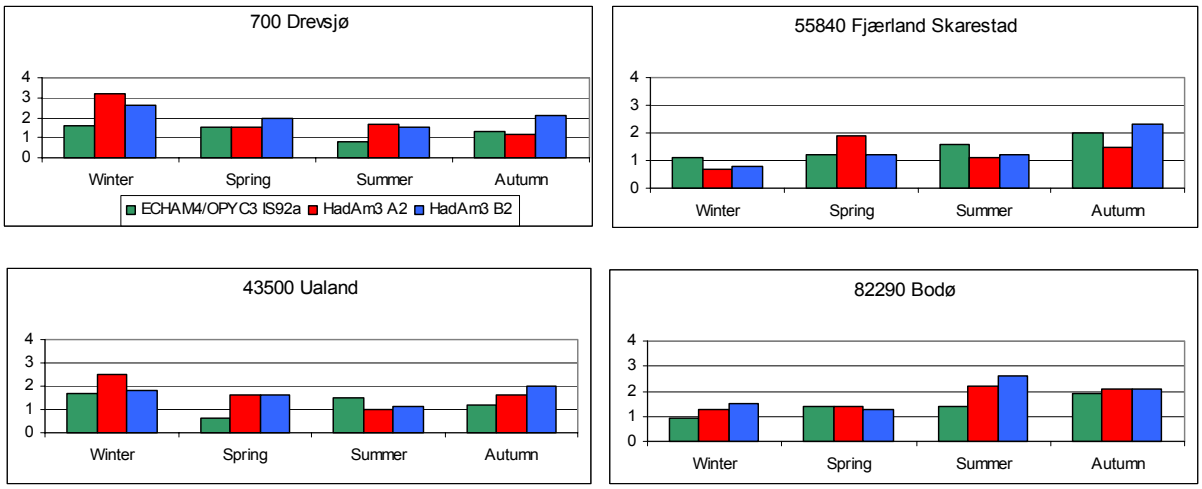

Figure 3.2 How often will the present 99 percentile value of daily precipitation at four selected stations appear in a future climate (ECHAM4/OPYC3 (IS92a), HadAm3 (A2, B2)).

4. UNCERTAINTY

4.1 Uncertainties in climate modelling

The modelling of climate involves a number of uncertainties as the understanding of the entire climate system with all relevant processes is incomplete. Furthermore, climate models cannot possibly account for every process at the very smallest scales explicitly. Hence, AOGCMs must approximate descriptions of a large number of processes that take place on a spatial scale unresolved by the model grid boxes. For instance, the description of cloud processes, ocean currents, and vapour/energy exchange between the atmosphere and the surface may vary with the location and can only be described by a general approximation. A variety of climate models exist and it has been shown that each model can give a different picture of the climate evolution (Cubash et al, 2001). An example is given of 16 different model projections to different sites in Norway for the period 2000-2050 in October (Fig. 4.1). Even when a climate model is perfect there may be uncertainties associated with a simulated climate change. Benestad (2000) noted that the climate model spin-up process is important for the description of the local climatic evolution, and that there were regional differences between four simulations done with the HadCM2 model for different initial conditions. These differences were regarded as a result of the non-linear chaotic behaviour of climate, and hence part of the unpredictable natural variability (Benestad, 2001b). It is also evident that these natural fluctuations contaminate the climate change analysis such as for 30-year long time slices. Benestad (2003) argued that part of the natural variations are 'externally forced', by for instance volcanoes, solar activity or landscape changes, and will therefore not be captured by climate models only prescribed with emission data.

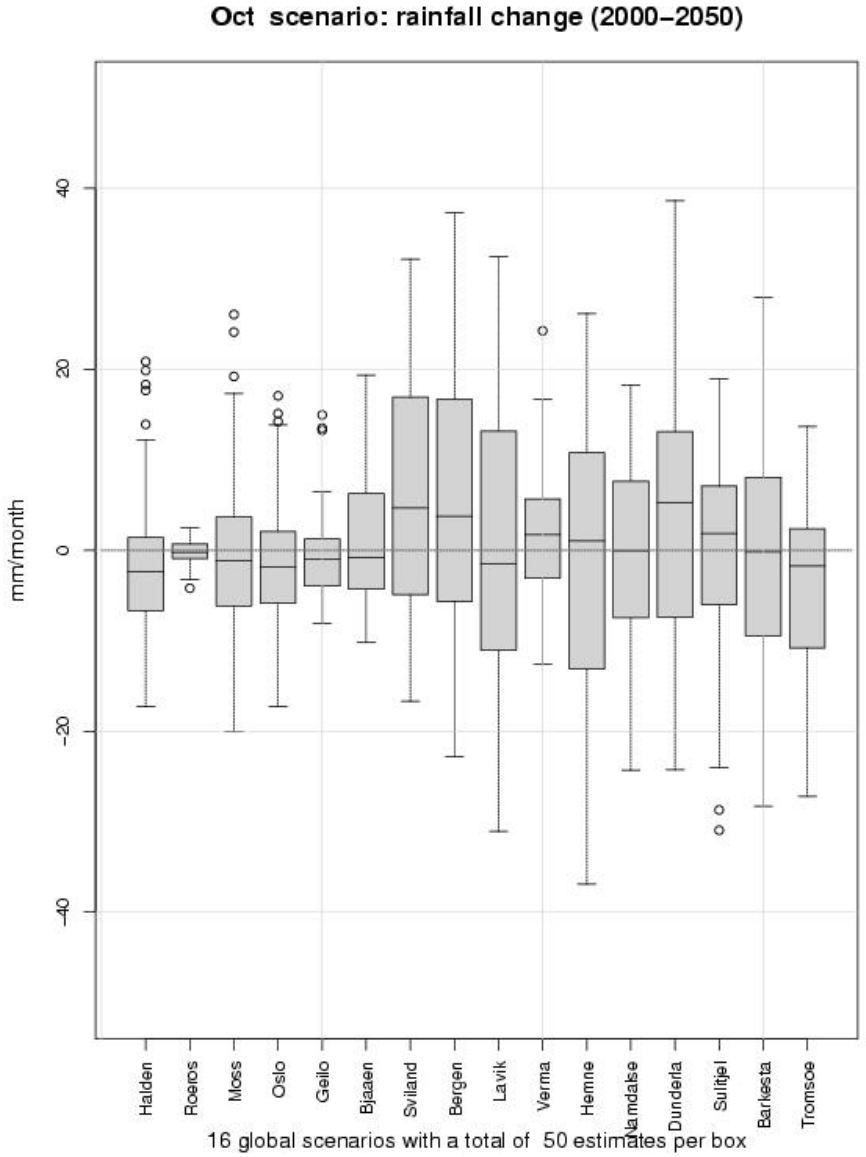

Figure 4.1 Projected mean monthly precipitation trend for October based on 16 different global scenarios for the period 2000-2050. The box shows the interquantile range (20-75 percentiles), the horizontal line gives the median value and the whiskers extend to the most extreme data points which is no more than |1.5| the interquartile range from the box (Benestad, 2002)

4.2 Uncertainties in dynamical downscaling

Regional climate models (RCMs) are promising tools to derive climate change scenarios on spatial scales that are represented too coarse by the AOGCMs. RCM simulations are frequently used as input data for climate impact studies (Wood et al. 2004; Bronstert, 2004) which require the representations of the present climate to be realistically reproduced by the RCM especially with respect to the variability, change and impacts on extreme events. The statistics of precipitation estimates, (mean, wet-day frequency, precipitation intensity and quantiles of the frequency distribution) based on five different RCMs are analysed by Frei et al (2003). They found considerable biases when comparing the statistics.

The time resolution of archived output from dynamically downscaled scenarios is typically on a 6 hourly basis. The spatial resolution (typically 50 x 50 km^2), however, is too coarse to be representative locally. The terrain in the regional climate models is smoothened, the sites elevation is thus wrongly represented, and the frequency of days with precipitation is overestimated (Charles et al., 1999). Observed climate of specific sites, especially in areas with complex topography, is therefore not well reproduced. The AOGCM is initially developed to capture the overall regional weather pattern of an area. Interpolation of temperature and precipitation data from RCMs to at site locations therefore requires special attention.

It is also important to note that the representation of a parameter in RCM may be either a point value or a mean value for a given grid box volume, and which of these representations are used in the model formulation may not always be obvious when bringing together a large variety of different models describing a range of processes over different scales.

4.3 Uncertainties in trend analysis

By adopting best-fit linear trend scenarios for sufficiently long time intervals (at least 60 years), the mean rate of change for the given period can be estimated and systematic biases between control integration and transient run can be ignored. The uncertainty in the trend estimate can easily be calculated. The length of time interval influences the sensitivity to natural variability of interannual and decadal time scales. The linear trend method is valid, even if the slow changes are non-linear, as long as we only want a measure for the mean climate change over a given time period. It may also be useful to use a polynomial trend model for cases where the evolution clearly is not linear (Benestad, 2003). This approach should not, however, be used for extrapolating outside the given time interval. It is important to stress the importance of evaluating the past climatic trends before making scenarios for the future, because there are no reason to believe that the GCMs will be able to provide a reliable prediction for the future if they cannot predict the past (Benestad, 2004, 2003, 2002).

5. EVAPOTRANSPIRATION

Evaporation is an important part of the land surface water balance and the energy balance at the boundary between the land surface and the atmosphere. Evaporation processes are therefore important parts of both hydrological models that solve the water balance, and meteorological models that essentially solve the vertical energy balance. In Norway the regional meteorological model HIRHAM (Christensen et al., 1996; Björge et al., 2000) and the regional hydrological model GWB (Beldring et al., 2002, 2003) have been used for assessing the changes in evaporation for climate change scenarios (Section 2.3 and 2.4). The aim of this section is to compare the evaporation estimated by the GWB and HIRHAM models for present climate and the estimated changes in evaporation for the climate change scenarios obtained with the AOGCM called HadAm3 (Gordon et al., 2000) and the emission scenario A2 and B2 (Cubash et al., 2001). The study is fully reported in Engeland et al. (2004).

5.1 Comparison of the models

The GWB model applies an empirical equation with temperature as forcing variable for calculating the total evaporation, whereas the HIRHAM model has a more physically based equation where the forcing variables are air vapor deficit and wind. Both models let the parameters depend on land cover types, and then reduce the evaporation due to water deficit in the soil moisture zone. A big difference in the modelling of evaporation from snow covered surfaces is found. The GWB model set snow evaporation to zero whereas the HIRHAM model calculates an evaporation from the snow as it is interception storage. It should also be noted that the calculated evaporation in HIRHAM is a part of the model dynamics whereas the GWB model is purely hydrologic and the calculated evaporation act as a sink. In the HIRHAM model the model points are connected by the dynamics, whereas for the GWB model the calculations are performed independently for each grid cell. For both models the evaporation is an 'internal flux' that has not been explicitly validated. The aim of GWB model has been to obtain good simulation of runoff whereas for the HIRHAM model the aim has been to obtain good simulations of climate in general. The evaporation estimates from the two models are therefore not directly comparable.

The model simulations were compared to three point measurements located in Sweden and Finland, then the two models were compared at six HIRHAM points located all over Norway as shown in Fig. 2.1. The points were selected to cover most of the climatic variability in Norway. In order to compare only the evaporation algorithms, we chose to use the temperature and precipitation fields from the HIRHAM model directly as climatic forcing input in the GWB model. The model data is neither adjusted nor interpolated them.

5.2 Results

To get an impression of how well the models describe the evaporation processes, we first compared the evaporation estimated by the GWB and HIRHAM models for the control period to evaporation observations in Fig. 5.1. The simulated evaporation is based on meteorological variables calculated from the HIRHAM model and not on observed values. The day-to-day variation is therefore not identical, statistical measures should, however, be comparable.

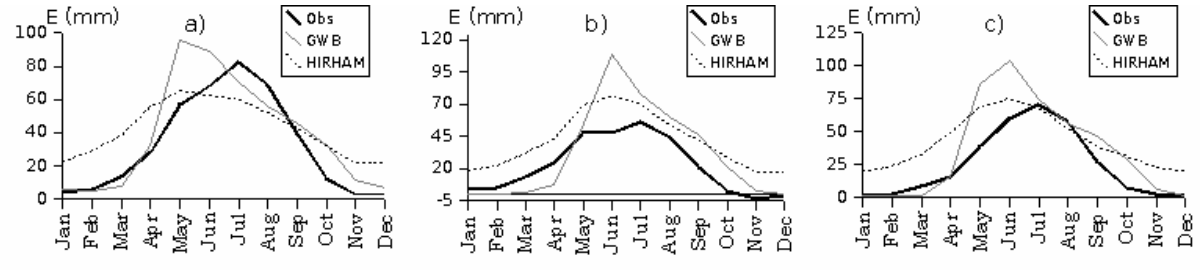

Figure 5.1 Observed and simulated average monthly evaporation for a) Norunda (Sweden) b) Flakliden (Sweden) and c) Hyytiala (Finland).

The HIRHAM model overestimates the winter evaporation (October – April) at all sites. The winter-evaporation from the HIRHAM model would probably improve with a new parameterisation of evaporation from snow cover where specific surface parameters for snow-

cover are included. The GWB model underestimates the winter evaporation, especially in the months January – March. The reason is that the calculated evaporation from snow covered surfaces is zero. The GWB model requires a more explicit parameterisation of winter evaporation in order to improve the results. In the spring, after the snow cover has melted, and in late autumn the GWB model overestimates the evaporation.

Fig. 5.2 shows the seasonal variation in calculated evaporation, whereas Fig. 5.3 shows the average annual evaporation. Both figures show results in the six selected HIRHAM points for the control period and the scenarios A2 and B2. The results presented in the figures are related to the altitude of the HIRHAM points and further adjustments are necessary to obtain representative values at locations with a different altitude. We recognize the same differences between the two models as seen in Fig. 5.1, and much of these differences can be explained by the parameterisation of the winter evaporation and the climate variables driving the evaporation.

When comparing evaporation from the two climate change scenarios, larger differences between the two models than the differences between the scenarios are detected, in terms of both absolute and relative changes in evaporation. However, some qualitative similarities between the two models can be observed. Both indicate the highest increase in evaporation in spring and autumn, and the lowest increase or in some cases decreased evaporation during summer. The average annual evaporation increases in both models. But quantitatively the differences are large. The GWB model indicates the highest rice in evaporation, both as percentage and as absolute values. At all locations the evaporation from the GWB model increases significantly in the months that become more snow-free in the scenario periods. This is because the GWB model sets transpiration from vegetation to zero for snow-covered areas. In most location the HIRHAM model indicates increased evaporation in winter season and less evaporation in the summer season, probably due to water stress whereas the GWB model indicate reduced evaporation during summer season only in eastern Norway.

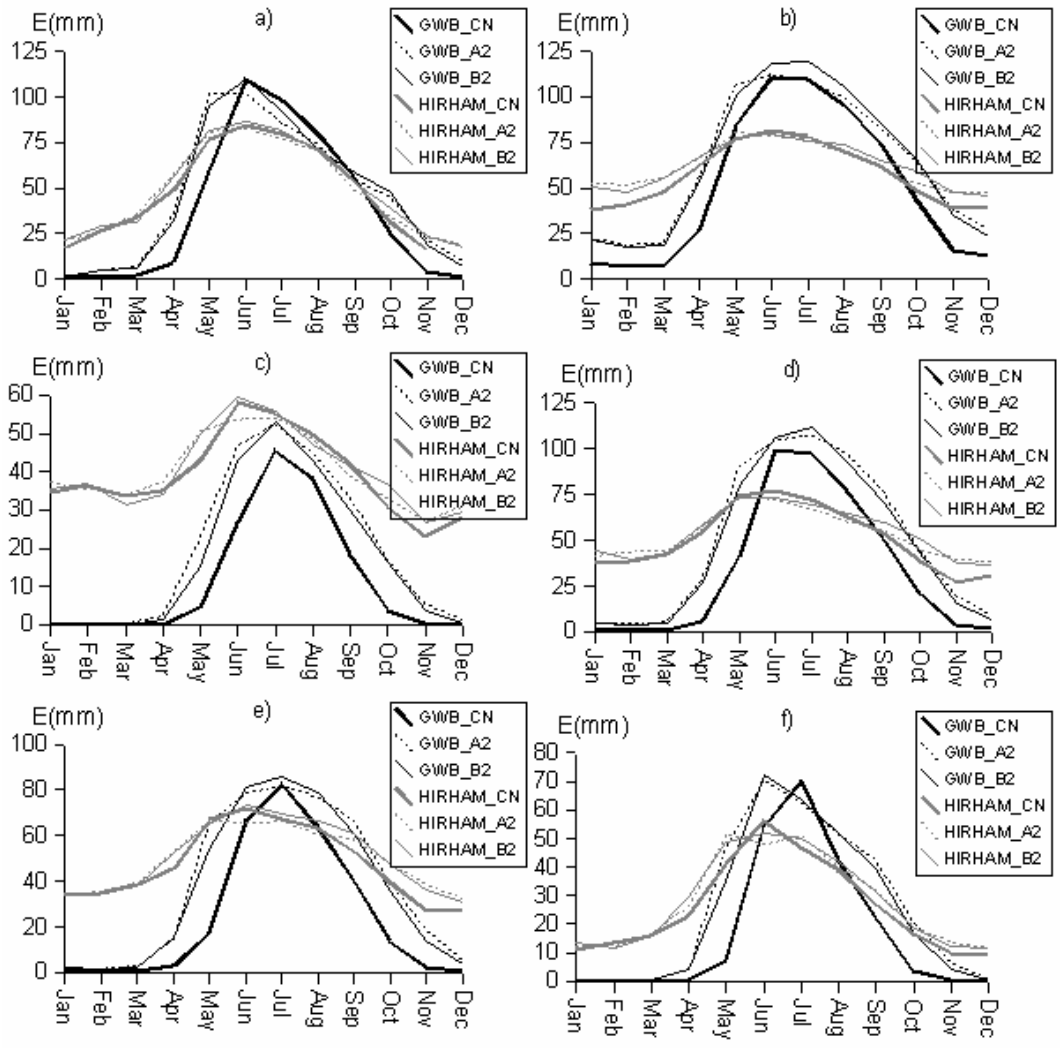

Figure 5.2 Average monthly evaporation in grid-cells in a) Southeastern Norway b) West Norway, c) Mountains, d) Trøndelag, e) Nordland, and f) Finnmark

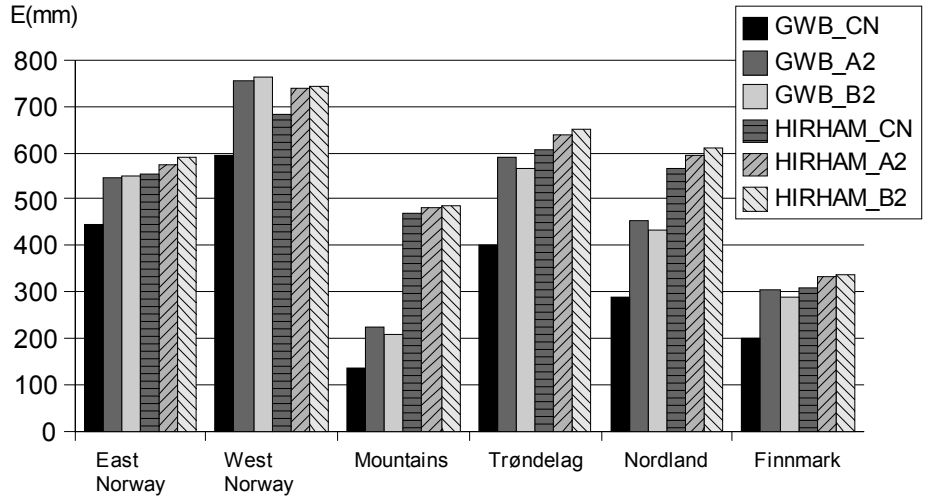

Figure 5.3 Average annual evaporation in grid-cells in Norway.

6. STREAMFLOW

6.1 Modelling changes in streamflow

The Gridded Water Balance model (GWB-model) (Beldring et al. 2003), a spatially distributed version of the HBV-model (Bergström, 1995), was used in this work. The model performs water balance calculations for square grid cell landscape elements characterized by their altitude and land use. Each grid cell may be divided into two land use zones with different vegetations, a lake area and a glacier area. The model is run with daily time steps, using precipitation and air temperature data as input. It has components for accumulation, sub-grid scale distribution and ablation of snow, interception storage, sub-grid scale distribution of soil moisture storage, evapotranspiration, groundwater storage and runoff response, lake evaporation and glacier mass balance. Potential evapotranspiration is a function of air temperature, however, the effects of seasonally varying vegetation characteristics are considered. The algorithms of the model were described by Bergström (1995) and Sælthun (1996). The model is spatially distributed since every model element has unique characteristics that determine its parameters, input data are distributed, water balance computations are performed separately for each model element, and finally, only those parts of the model structure which are necessary are used for each element. When watershed boundaries are defined, runoff from the individual model grid cells is sent to the respective catchment outlets without delay.

A regionally applicable set of parameters was determined by calibrating the model with the restriction that the same parameter values are used for all computational elements of the model that fall into the same class for land surface properties (Beldring et al. 2002). This calibration procedure rests on the hypothesis that model elements with identical landscape characteristics have similar hydrological behaviour, and should consequently be assigned the same parameter values. The model discretization units should represent the significant and systematic variations in the properties of the land surface, and representative (typical) parameter values must be applied for different classes of soil and vegetation types, lakes and glaciers (Gottschalk et al., 2001). The model was calibrated using available information about climate and hydrological processes from all gauged catchments in Norway with reliable observations, and parameter values were transferred to other catchments based on the classification of landscape characteristics. Several automatic calibration procedures, which use an optimization algorithm to find those values of model parameters that minimize or maximize, as appropriate, an objective function or statistic of the residuals between model simulated output and observed watershed output, have been developed. The nonlinear parameter estimation method PEST (Doherty et al., 1998) was used in this study. PEST adjusts the parameters of a model between specified lower and upper bounds until the sum of squares of residuals between selected model outputs and a complementary set of observed data are reduced to a minimum. A multi-criteria calibration strategy was applied, where the residuals between model simulated and observed monthly runoff from several catchments located in areas with different runoff regimes and landscape characteristics were considered simultaneously.

The precipitation stations used in this study were classified in five exposure classes with fixed correction factors for rain, snow and mixed type precipitation according to a Nordic study

(Førland et al., 1996). The precipitation data were accordingly given a simplified precipitation type classification. Precipitation and temperature values for the model grid cells were determined by inverse distance interpolation of observations from the three closest precipitation stations and the two closest temperature stations. Differences in precipitation and temperature caused by elevation were corrected by site specific precipitation-altitude gradients and fixed temperature lapse rates for days with and without precipitation, respectively. There is considerable uncertainty with regard to the variation of precipitation with altitude in the mountainous terrain of Norway. Specific precipitation-altitude gradients were therefore determined for each of the 20 catchments, and these values were used for all grid cells within a catchment. Few mountain stations necessitate to use these general gradients. The precipitation-altitude gradients were reduced by 50 % for elevations above 1200 m a.s.l., as drying out of ascending air occurs in high mountain areas due to orographically induced precipitation (Daly et al., 1994). The reduction of 50 % is arbitrarily chosen, however, the height of 1200 metres is not, as this is the approximate altitude of the coastal mountain ranges in western and northern Norway. These mountains ranges release most of the precipitation associated with the eastward-migrating extratropical storm tracks that dominate the weather in Norway. The temperature lapse rates for days with and without precipitation were also determined by calibration, however, the same values were used for all grid cells.

In order to have confidence in a hydrological model, its performance must be validated. Model performance is usually evaluated by considering one or more objective statistics or functions of the residuals between model simulated output and observed watershed output. The objective functions used in this study were the Nash-Sutcliffe and bias statistics of the residuals, which have a low correlation (Węglarczyk, 1998). The Nash-Sutcliffe efficiency criterion ranges from minus infinity to 1.0 with higher values indicating better agreement. It measures the fraction of the variance of observed values explained by the model:

$$NS = 1 - \frac{\sum_{t=1}^{n}\left(q_t^{obs} - q_t^{sim}\right)^2}{\sum_{t=1}^{n}\left(q_t^{obs} - q^{mean}\right)^2}$$

where q_t^{obs} is observed watershed output at discrete times t, q_t^{sim} is the corresponding model simulations, q^{mean} is the mean of the observed values, and n is the number of data points to be matched. Bias (relative volume error) measures the tendency of model simulated values to be larger or smaller than their observed counterpart:

$$BIAS = \frac{\sum_{t=1}^{n}\left(q_t^{sim} - q_t^{obs}\right)}{\sum_{t=1}^{n} q_t^{obs}}$$

Although the Nash-Sutcliffe efficiency criterion is frequently used for evaluating the performance of hydrological models, it favours a good match between observed and modelled high flows, while sacrificing to some extent matching of below-mean flows. It is for this reason that two different measures of model performance were considered. The results from calibrating the model are shown in Table 6.1. If sufficient data were available, a test of model performance in an independent period was also performed.

Table 6.1. Catchments used for hydrological modelling

Catchment no.	Name	Calibration period	Calibration Nash-Sutcliffe	Calibration Bias
311.6	Nybergsund	1961-1990	0.91	0.0
2.13	Sjodalsvatn	1976-1990	0.77	0.0
15.79	Orsjoren	1983-1990	0.86	0.0
18.10	Gjerstad	1981-1990	0.69	0.0
20.2	Austenå	1971-1990	0.76	0.0
26.20	Årdal	1976-1990	0.69	0.0
26.21	Sandvatn	1976-1990	0.77	0.0
27.26	Hetland	1976-1990	0.56	0.0
41.1	Stordalsvatn	1976-1990	0.67	0.0
48.5	Reinsnosvatn	1976-1990	0.82	0.0
50.1	Hølen	1976-1990	0.84	0.0
83.2	Viksvatn	1976-1990	0.79	0.0
104.23	Vistdal	1976-1990	0.55	0.0
107.3	Farstad	1976-1990	0.58	0.0
109.9	Risefoss	1970-1990	0.69	0.0
123.20	Rathe	1970-1990	0.78	0.0
123.31	Kjelstad	1970-1990	0.52	-0.003
151.15	Nervoll	1976-1990	0.80	0.0
167.3	Kobbvatn	1970-1990	0.78	0.0
212.10	Masi	1976-1990	0.84	0.0

6.2 Comparison of observed and simulated runoff in the control period

The GWB-model was used to simulate series of streamflow for a control period, representing the present climate. These series cannot be compared directly to the observed series for the same period, but the statistical properties of the two series should agree fairly well (Section 2.4). The statistical properties of these series have been compared, where the entire control period is covered by observations. The control period covers the years 1980-1999 for the ECHAM4/OPYC3 model and the period 1961-1990 for the HadAm3-model. The number of streamflow series used in the comparison differs between the two control periods because of differences in the length of observations for each series. The annual and seasonal mean values for the two model runs together with observations are shown in Fig. 6.1 and for the standard deviations of the annual and seasonal values in Fig. 6.2. The ratio between annual and seasonal means and standard deviations of streamflow both for observed and for simulated for the control period 1980-99 (ECHAM4/OPYC3 model) are presented in the Tables in Appendix 7-8 respectively. The ratio between annual and seasonal means and standard deviations of streamflow both for observed and simulated for the control period 1961-1990 (HadAm3 model) presented respectively in Appendix 9A and 9B.

The mean value and standard deviations of the annual values agrees well for most of the basins. The errors are larger in the seasonal means and standard deviations for some of the catchments, while others tend to agree fairly well. The differences are in most cases larger in the winter and autumn than in the other seasons.

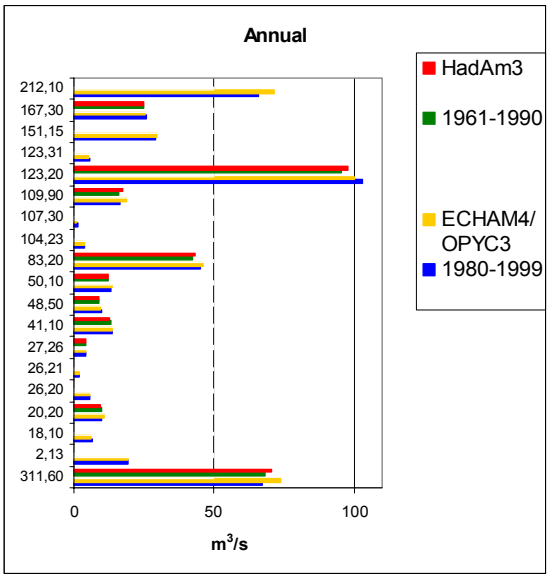

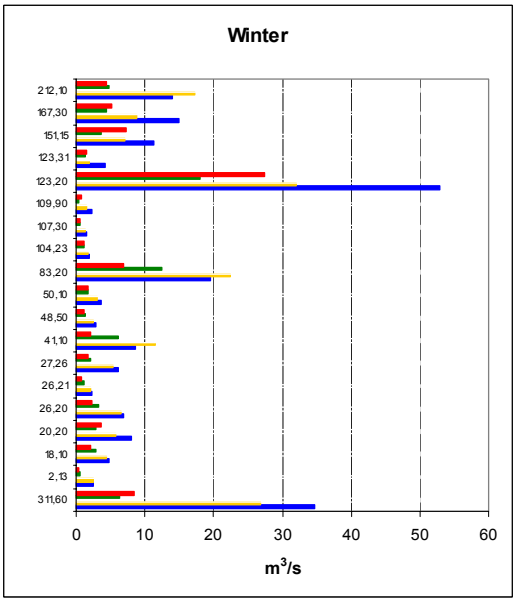

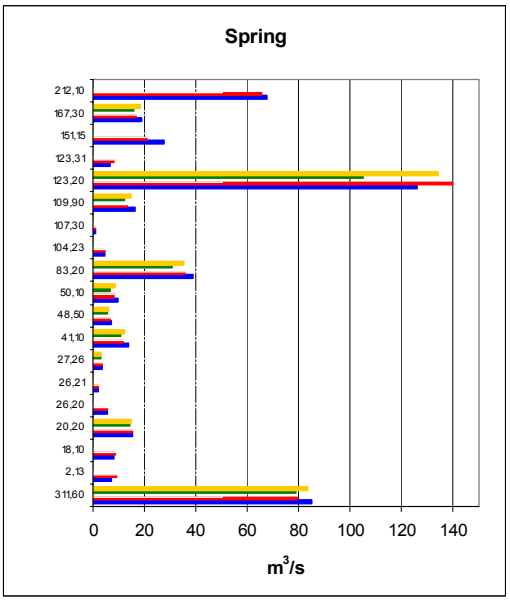

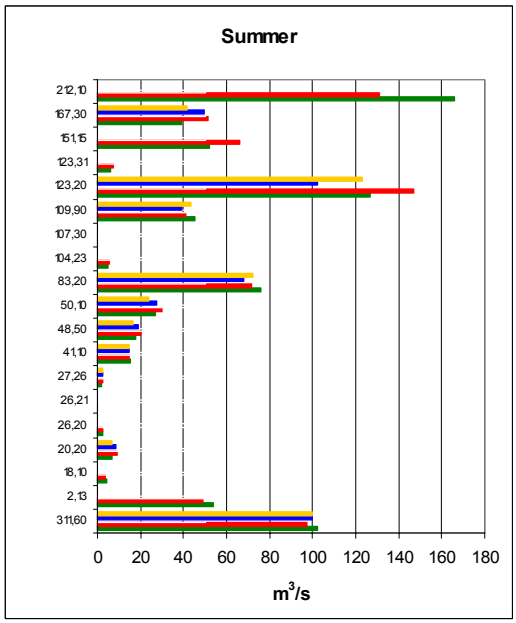

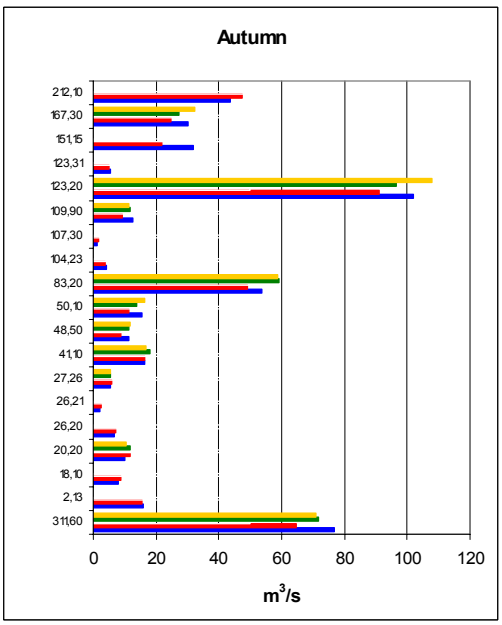

Figure 6.1 Mean annual and seasonal values for the two model runs together with observations

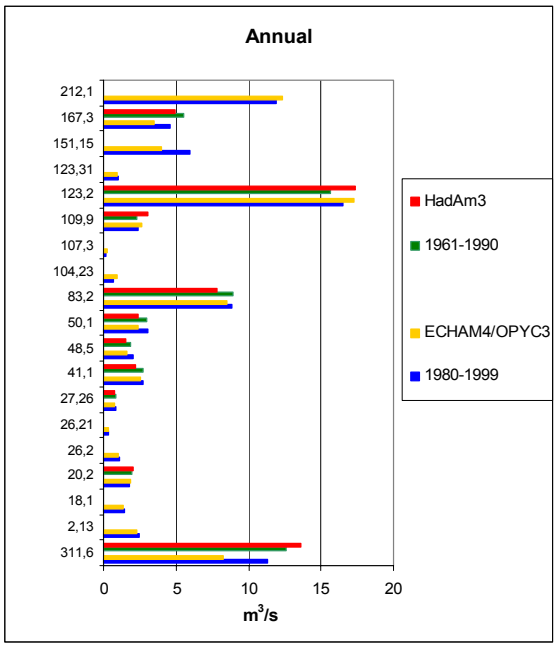

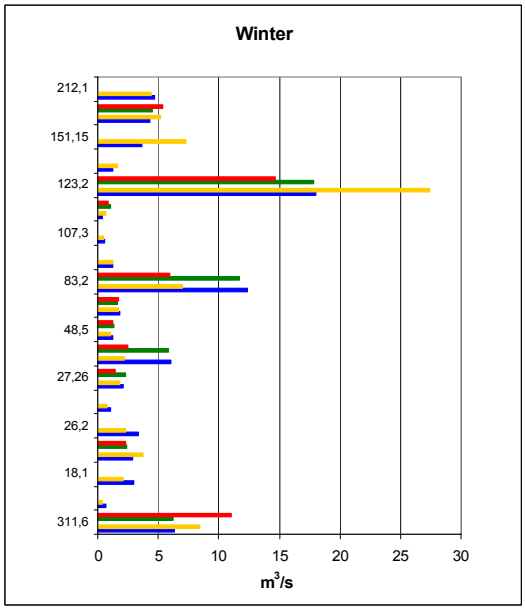

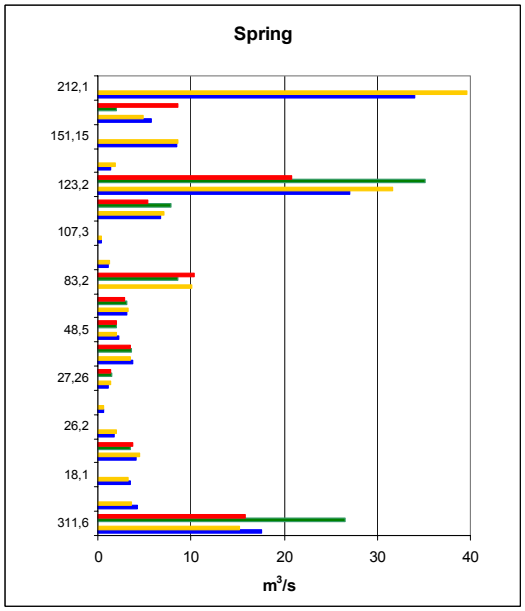

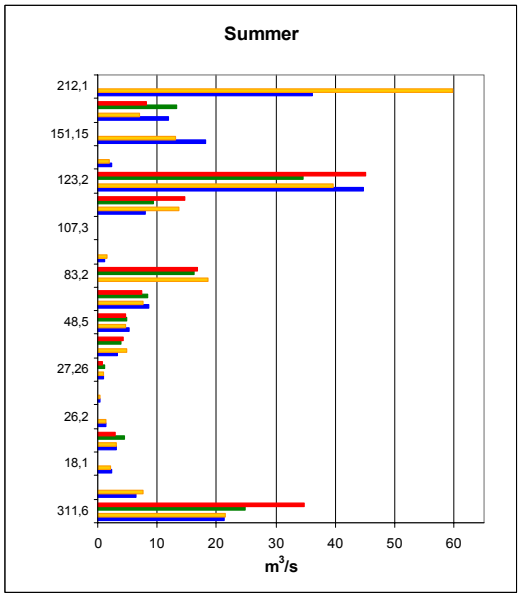

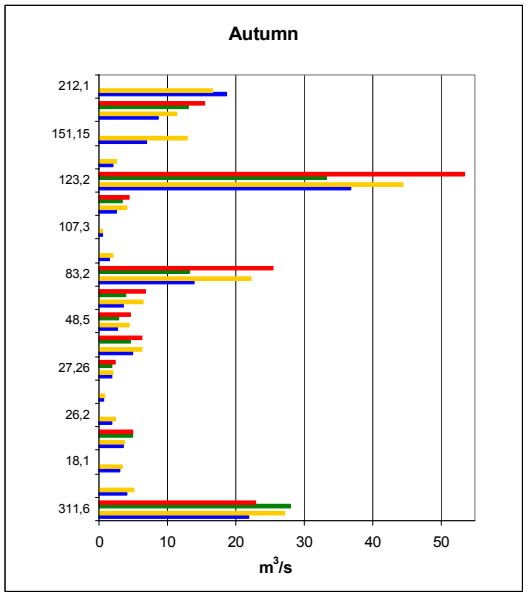

Figure 6.2 Mean annual and seasonal standard deviation for the two model runs together with standard deviation for observations

Simulated and observed mean annual flood and the standard deviation of the annual flood are presented in Fig. 6.3 for the two model runs. Annual and seasonal flood statistics are also shown for two catchments, 83.2 Viksvatn and 311.6 Nybergsund in Fig. 6.4. Statistics of annual flood and annual minimum flow are compared in Appendix 10 for the period 1980-99 (ECHAM4/OPYC3). Annual and seasonal flood statistics for the control period 1961-1990 (HadAm3) are compared in Appendix 11A and 11B. The number of catchments is smaller due to lack of streamflow observations for the entire 1961-1990 period.

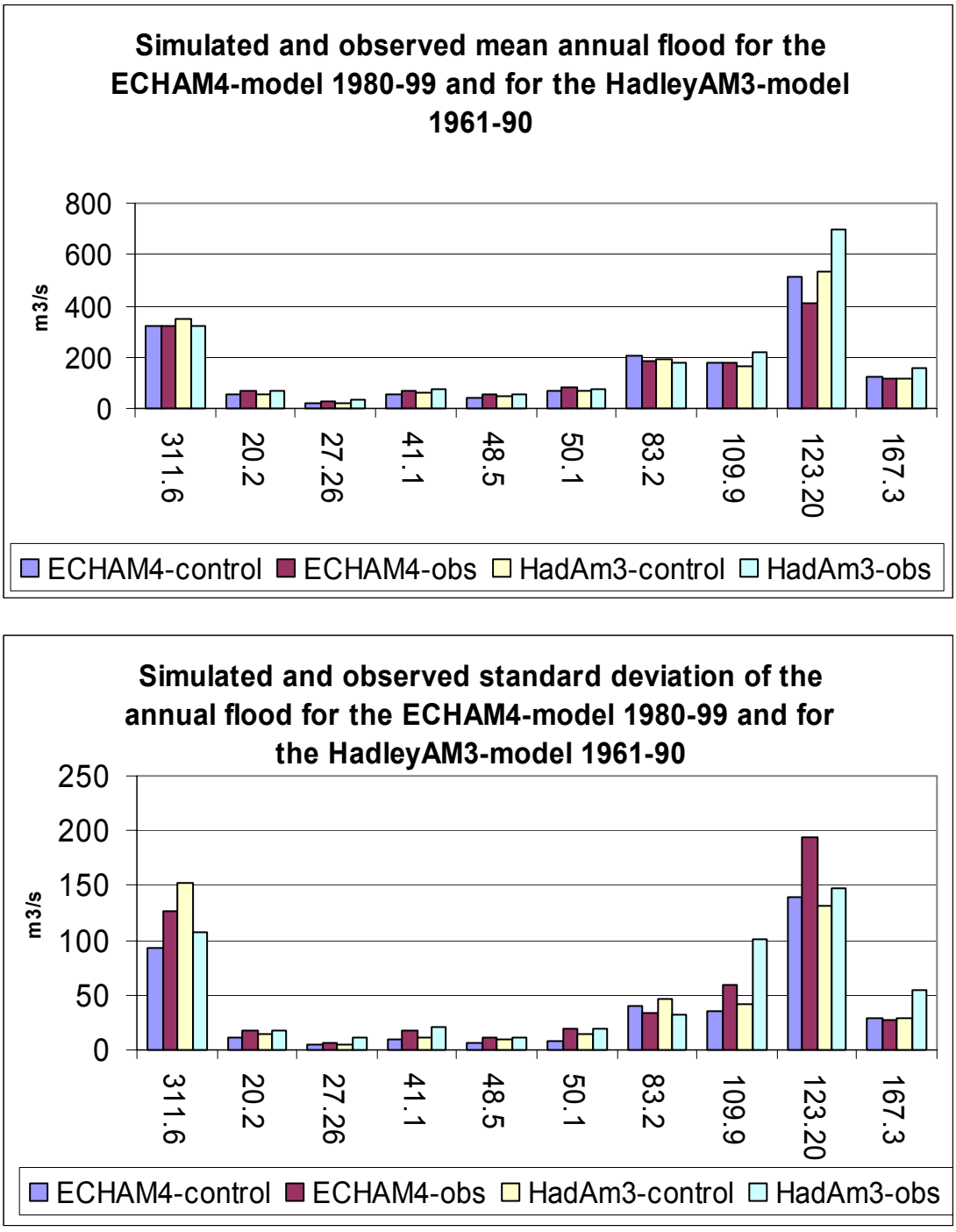

Figure 6.3 Simulated and observed mean flood and standard deviation of the annual flood and seasonal flood statistics for all catchments with observations in the period 1961-99.

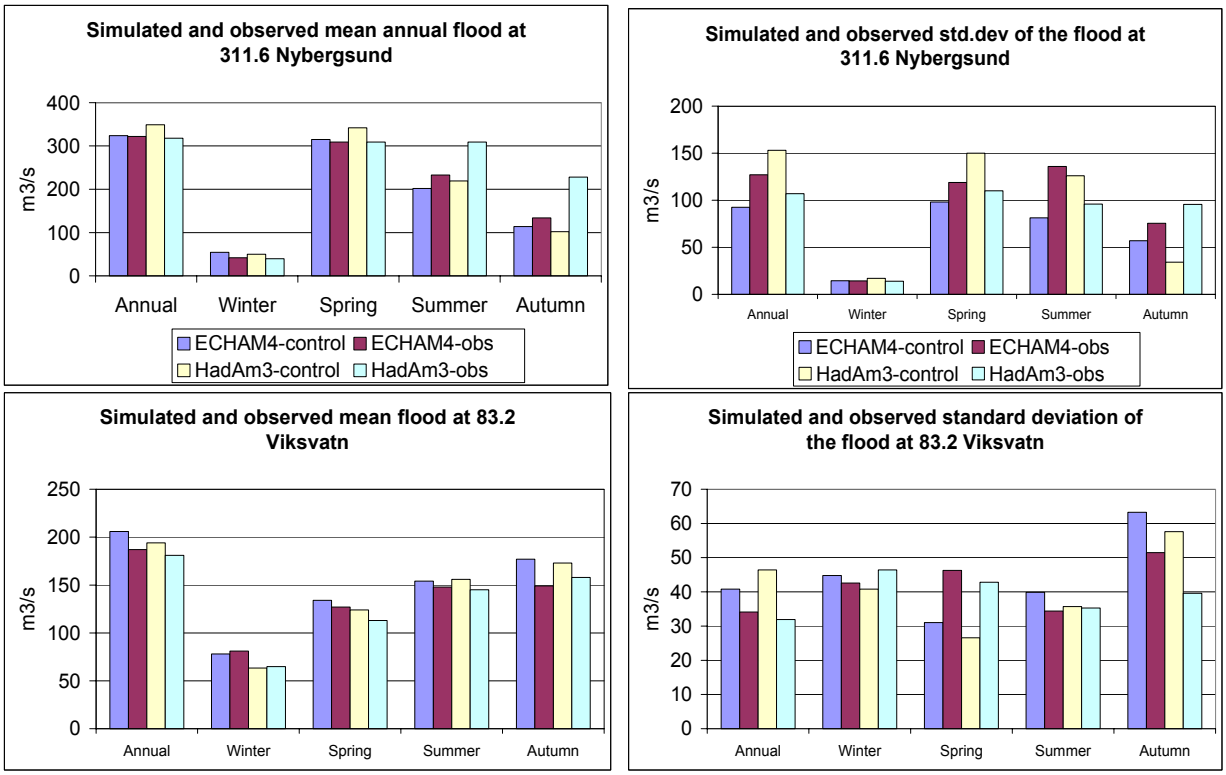

Figure 6.4 Simulated and observed mean flood and standard deviation of the annual flood and seasonal flood statistics for 311.6 Nybergsund and 83.2 Viksvatn

There is a considerable bias in flood and low flow characteristics for most of the catchments, indicating that the results for the extremes are unreliable. The bias does not show any strong regional pattern, and can be both positive and negative. The low flow statistics is based on the lowest flow every year, which may be a corrected value. The "observed" series from 123.20 Rathe and 167.3 Kobbelv are corrected for the effect of regulation. The procedure tends to result in somewhat higher flood values than in a natural catchment and zero runoff on some days in the winter. This is the case at 123.20 Rathe, but the results from 167.3 Kobbelv are quite good as seen in Appendix 10 and 11A and 11B.

6.3 Changes in streamflow

The GWB model was run for the scenarios and control periods described in Section 3.2. Series of daily streamflow were simulated for these periods. Several streamflow characteristics were examined, and are presented in a supplementary report for each catchment (Roald et al 2005).

The percentage change in annual and seasonal mean streamflow both for the ECHAM4/OPYC3 model with the IS92a emission scenario for the period 2030-2049 compared to the control period 1980-1999, and the HadAm3 model with the two emission scenarios A2 and B2 for the scenario period 1961-1990 are presented in Fig. 6.5. The changes are especially large in winter and summer, positive in winter and negative in summer. The change in streamflow in these seasons is presented for winter and summer seasons in Figs. 6.6 and 6.7 respectively. The change in the annual and seasonal mean streamflow for the ECHAM4/OPYC3-model is given in Appendix 12 and for the HadAm3-model in Appendix 13.

The change in the annual and seasonal standard deviations in the scenario and control period is shown in Appendix 14 and 15 for the two models. Each annual series have also been tested for trends based on the Mann-Kendall statistics, as shown in Appendix 16 for the ECHAM4/OPYC3 model with the emission scenario IS92a. The mean annual streamflow, as well as filtered values is presented as time series graphs in Appendix 17A and 17B for two catchments. Similar graphs are included in Roald et al. (2005) for all catchments.

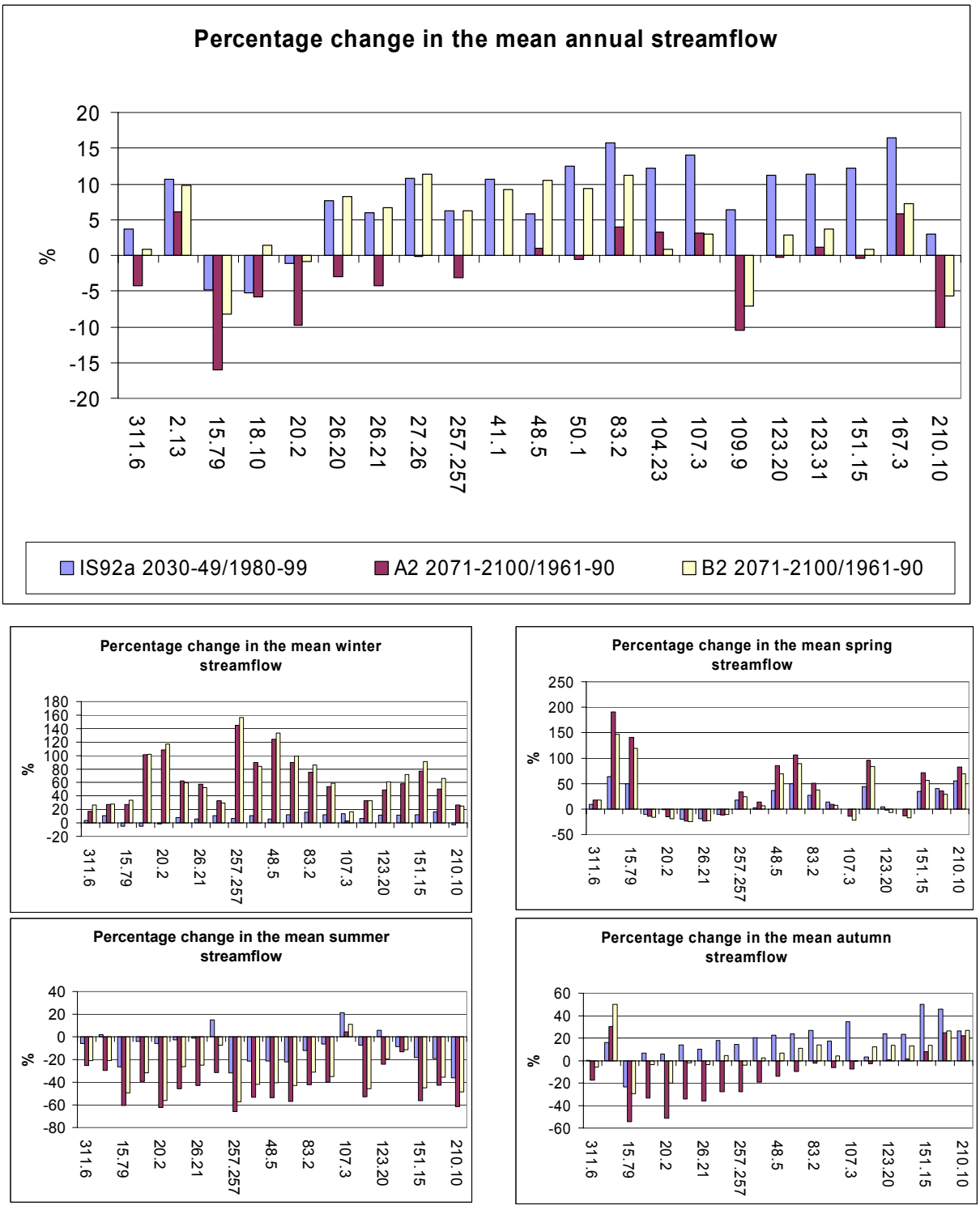

Figure 6.5 Percentage changes in the annual and seasonal mean streamflow simulated with the ECHAM4/OPYC3 model between 1980-99 and 2030-49 with the IS92a emission scenario and with the HadAm3-model between 1961-90 and 2071-2100 with the emission scenarios A2 and B2.

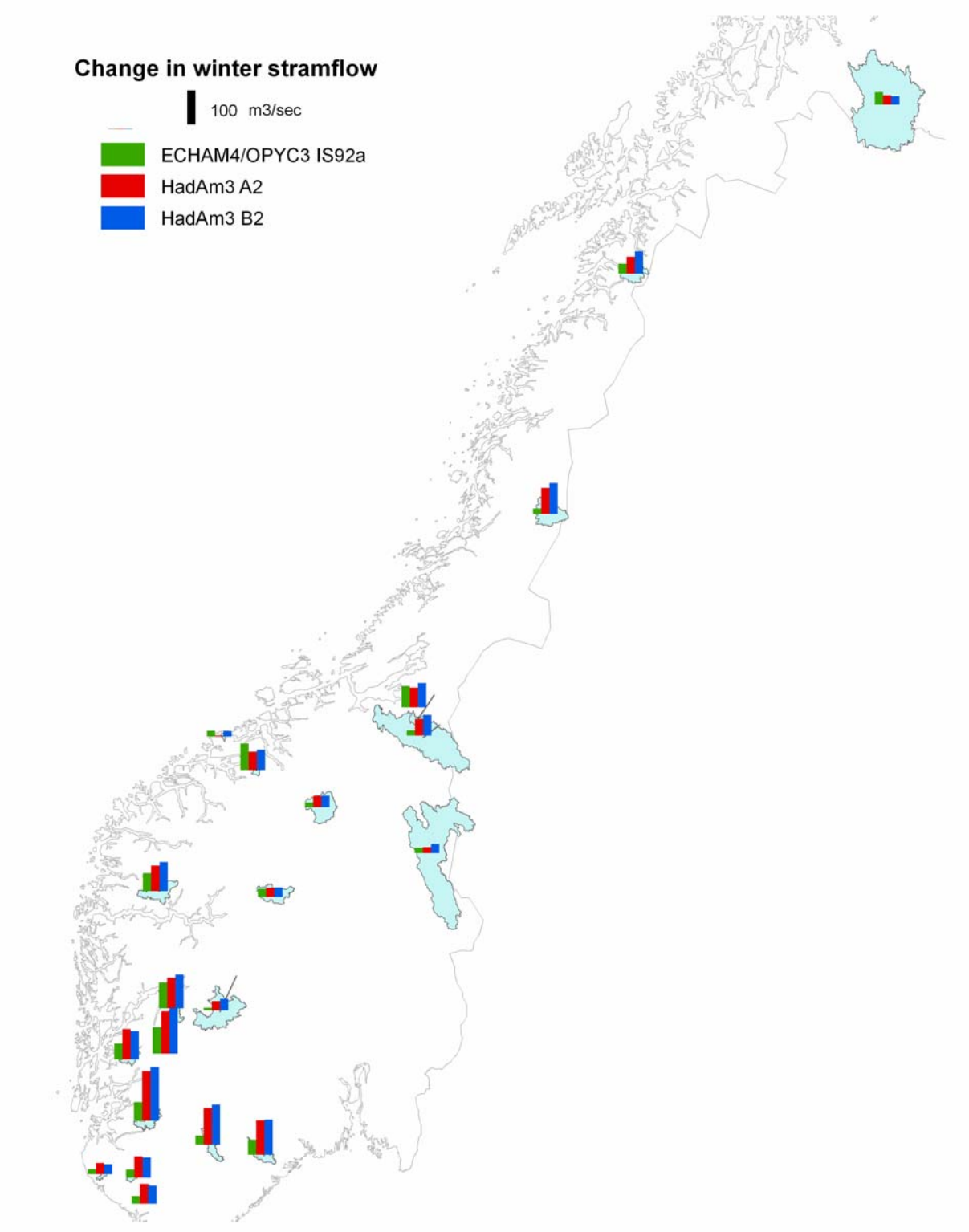

Figure 6.6 Changes in the mean winter streamflow simulated with the ECHAM4/OPYC3 model with the IS92a emission scenario and with the HadAm3-model with the emission scenarios A2 and B2.

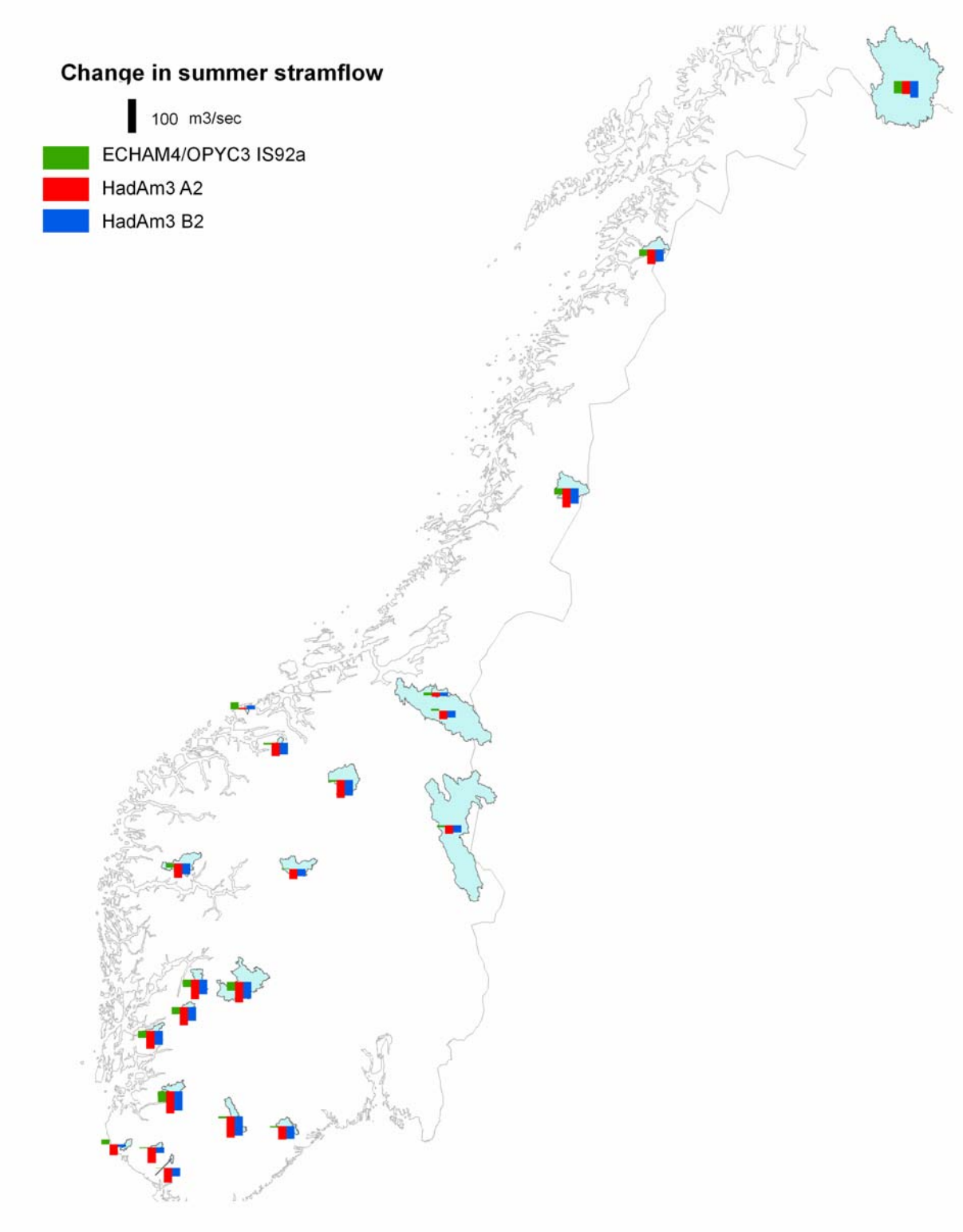

Figure 6.7 Changes in the mean summer streamflow simulated with the ECHAM4/OPYC3 model with the IS92a emission scenario and with the HadyAm3-model with the emission scenarios A2 and B2.

The changes in the annual and seasonal flood statistics were examined for all catchments. The changes in the mean annual flood are shown in Fig. 6.8. Flood frequency analysis were applied for the two time slices of both models. The changes in the mean annual flood, the

standard deviation, and flood of return periods of 5, 10, 20 and 50 years have been shown for four selected catchments in Fig. 6.9.

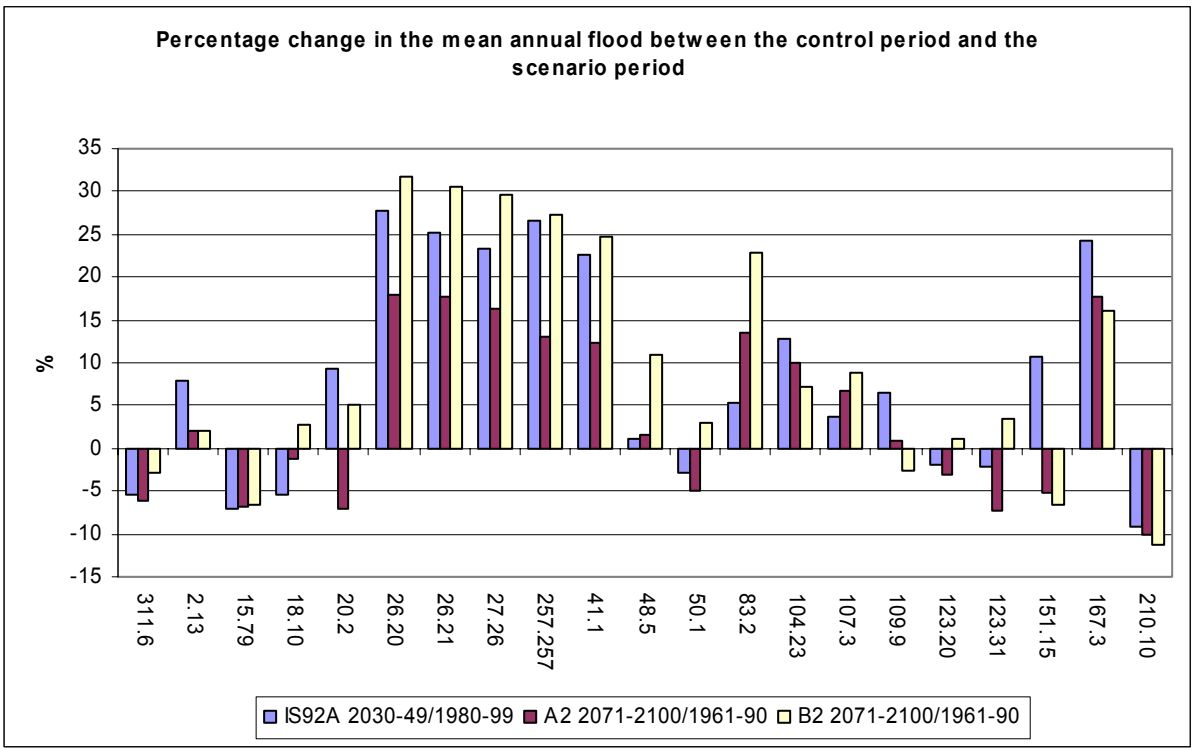

Figure 6.8 Percentage changes in the mean annual flood at all catchments simulated with the ECHAM4/OPYC3-model with emission scenario IS92A and with the HadAm3 model with the emission scenarios A2 and B2.

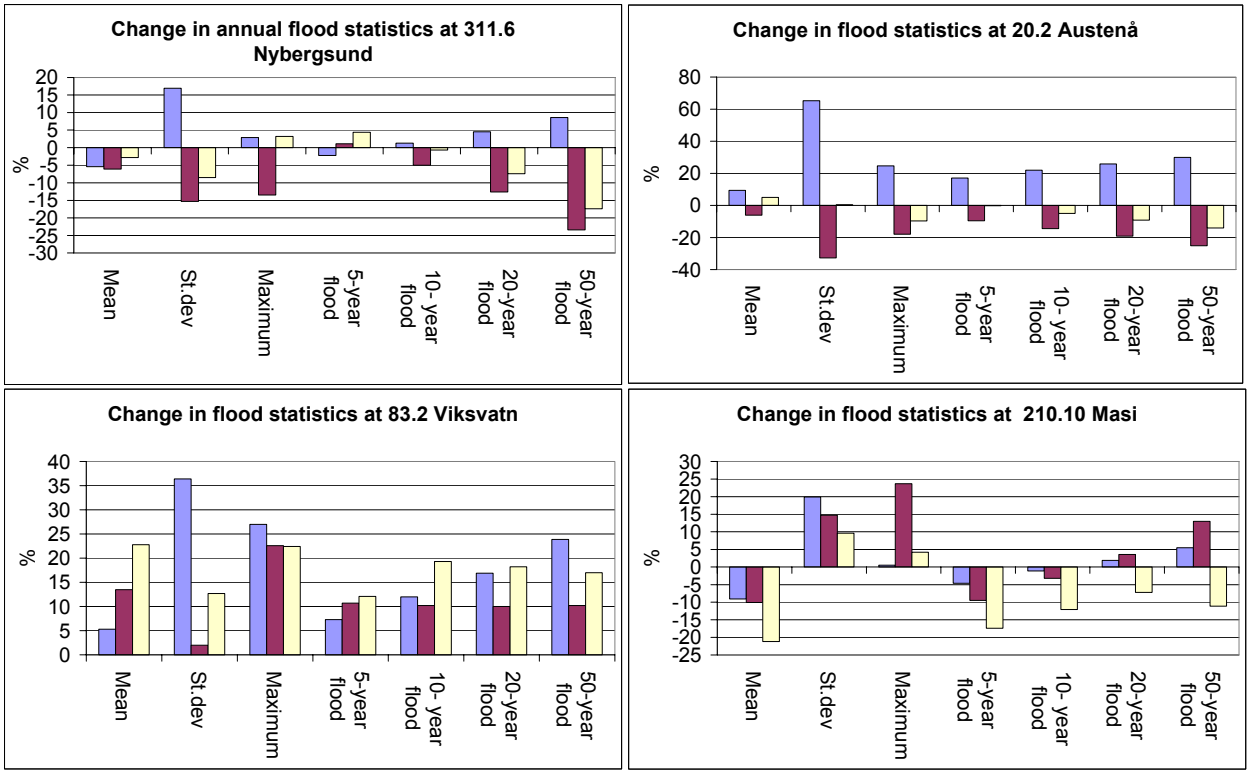

Figure 6.9 Percentage change in selected flood statistics at four catchments.

6.4 Discussion

The results from the ECHAM4/OPYC3 model with the IS92a emission scenario indicates an increase in the mean annual streamflow of 3.7 to 16.5 % or 0.74 to 3.3 % per decade increase except in a region in the inland mountainous and the southernmost part of East Norway, where a decrease of 4.8 to 11.2 % or 0.96 to 2.24 % per decade has been found between 1980-99 and 2030-49. The decrease of 3 % in Alta River in Finnmark agrees with findings in Roald et al. (2003). The winter runoff will increase everywhere, most in the central part of West Norway, where an increase up to 77.5 % has been found. The spring streamflow will decrease in the southernmost part of Norway from 0.8 to 20.1 % or 0.16 to 4.02 % per decade, but it will increase in most other catchments, most in the mountainous areas, caused by an earlier snowmelt. The summer streamflow will decrease in most catchments, but a moderate increase has been found in two coastal catchments. The autumn streamflow will increase everywhere, except in the Orsjoren catchment. The increase ranges from 0.2 to 34.7 % or 0.04 to 6.94 % per decade.

The variability, expressed by the annual and seasonal standard deviations, indicates that the variability will be at least as large as in the present climate. The increase in the standard deviation is especially large in the winter in most of the catchments.

Applying the Mann-Kendall test to each series of annual and seasonal means indicates a region in West Norway with a significant trend in the winter during the transient period 1980-2049 with the ECHAM4/OPYC3 IS92a scenario as shown in Appendix 16. The trend extends into the spring and autumn for most of these series, while a significant negative trend has been found in the summer. The positive trend in the spring and autumn extends also into North Norway as well the significant negative trend in the summer. Hisdal et al. (2004) have examined selected long term runoff series in the Nordic countries for annual and seasonal trends. They found a similar regional pattern of trends as in the transient scenario for the period 1961-2000. Roald et al. (2003) found the largest increase in streamflow on the extreme west coast of Norway. Hisdal et al. (2004) have, however, shown that such trends are not present in the coastal catchments, although the trends appear in the more mountainous fjord and inland catchments.

The mean annual flood tend to decrease in inland catchments draining high mountain areas, unless the catchments are affected by glaciers. The mean annual flood will otherwise increase in South and West Norway and in Nordland. The increase in the south is projected to be up to 27.7 %. The results are, however, quite uncertain considering the bias between the control period and the observations in many catchments.

The streamflow scenarios based on the HadAM3-model refers to the period 2071-2100, which is further into the future than the scenarios based on the ECHAM4/OPYC3-model. The control period is also different and includes the 1960s and 1970s, which were drier than the period 1980-99 used as control period for the ECHAM4/OPYC3-model in some regions in Norway. Results from the HadAm3 model with the emission scenario B2 indicate a increase in the annual streamflow in the annual streamflow in most of the catchments in West and North Norway ranging between 0 to 34.2 % or 0 to 3.1 % per decade. The annual streamflow decrease in most of the cartchments in the eastern and southernmost part of South Norway ranging between 5.5 to 19.7 % or 0.5 to 1.8 % per decade. The same model with the A2 scenario indicates a decrease in most of southern and eastern part of South Norway, and a moderate increase in the west and in the Kobbvatn basin in Nordland. The HadAm3 A2

scenario results generally in lower streamflow than for the HadAm3 B2 scenario for all catchments. The annual streamflow will decrease between 5.7 to 24.6 % or 0.52 to 2.34 % in the eastern and southernmost part of South Norway and between 8.8 to 19.8 % or 0.8 to 1.8 % per decade in Mid- and North Norway. The streamflow will increase in West Norway between 7 to 17.5 % or 0.63 to 1.6 % per decade. The winter is projected to be wetter in both emission scenarios, the spring will be dryer in the south and wetter in the mountains and in most catchments in the west and the north. The summer will be much drier, and the autumn will be drier in a region extending to Trøndelag, with one exception in the Sjodalsvatn catchment with a contribution of glacier meltwater according to the HadAm3 A2 scenario. The winter streamflow will increase dramatically in catchments in the high mountain catchments, especially in the A2 scenario. The changes in these scenarios reflect more rainfall and snowmelt events in the winter, and greater losses because of evapotranspiration in the summer.

The mean annual flood increases in most catchments for the HadAm3 B2 scenario, while a regional pattern appear in the HadAm3 A2 results. There is a decrease in the east and south as well as in Trøndelag and Finnmark, and increase in the west.

7. CHANGES IN HEATING SEASON AND HEATING DEGREE-DAYS

The heating season is the period of the year when buildings need to be heated. The sums of heating degree-days closely correlate to energy consumption for heating, and have numerous other practical implications (Quayle and Diaz, 1980, Guttman and Lehman, 1992). The amount of energy for heating of buildings is also depending on other climatological factors (wind speed, radiation), as well as factors related to demographic changes, living standards, and building instructions (e.g. volume of heated buildings, preferred indoor temperatures, thermal insulation, etc.) (Venäläinen et al., 2004). The heating season is in the present study defined as the period of the year when the smoothed daily mean temperature is below a threshold $\hat{T}$, while heating degree-days (HDD) are the sum of the difference between a base temperature T_{base} and the daily mean temperature T_i (Taylor, 1981):

(2) $$HDD = \sum_{i=1}^{365} (T_i - Tbase), \quad T_i < \hat{T}$$

$HDD = 0, \quad T_i \geq \hat{T}$

In the USA, the base temperature T_{base} is 65F (Groisman et al., 2003) while in

Norway T_{base} =17°C and $\hat{T}$ =10°C (Skaugen and Tveito, 2002). The latter values are used in the present analysis.

Groisman et al. (2003) found a statistically significant decrease in annual heating degree-days during the past 50 years of 6% over the entire Arctic, with a maximum absolute and relative reduction in heating degree-days over Western Canada and Alaska (9% and 8% per 50 years respectively). For Eurasia, significant reductions were found for Russia (6-7% per 50 years), indicating that there have been reduced heating costs in relative terms.

The present study focuses on empirically downscaled monthly mean temperature. Empirical downscaling consists of revealing empirical links between large-scale patterns of climate

elements (e.g. air pressure, sea surface temperature, etc.) and local climate elements (e.g. temperature, precipitation, etc.), and applying them on output from global or regional models (Benestad, 2001a). Hanssen-Bauer et al. (2003) showed that empirical downscaling has the potential for describing spatial climate features that are not resolved by the currently available regional climate models. The empirical downscaling was based on an approach utilising common EOFs as described in Benestad (2001a, 2002), using multiple regression for calibrating the empirical models.

Table 7.1 indicates that the heating season for the period 1961-90 lasted the whole year through at both Nuuk (Greenland), Svalbard Airport as well as in Vardø. In Oslo, Helsinki and Stockholm the heating season started in the end of September and ended in mid-May. In Copenhagen the heating season lasted 1 month less than in the other Fennoscandian capitals. For the scenario period 2021-2050 the heating season will still last the whole year through at Nuuk and Svalbard, while it will be 2-4 weeks shorter in the Nordic capitals.

The highest sum of heating-degree-days (HDD) for the normal period 1961-90 is found for Svalbard Airport (>8500 degrees), while it in e.g. Oslo, Helsinki and Stockholm is ca. 3500-4000, and in Copenhagen ca 2700 degrees. Generally the length of the heating season and the HDD-sum were higher for 1901-30 and lower for 1931-60 than for the present normal period. During the latest years (1990-2002), the HDD-sums have been lower than for the normal period 1961-90. The projected values for the scenario period 2021-2050 indicate a reduction of heating-degrees of 10-20% at most of the stations in Iceland and Fennoscandia. The projected HDD-sum in Tromsø will be at the same level as the 1961-90 value for Helsinki, and the Stockholm value will at the same level as during 1961-90 in Copenhagen. (A more comprehensive survey of long-term variations in heating-degrees is presented by Førland et al., 2004)

Table 7.1. Length of heating season and sum of heating degree-days (HDD) 1901-2050. (The Δ-values are differences between actual period and standard normal period 1961-90)

Station name	1961-90 Start	End	Length (days)	HDD	ΔLength 2021 -2050
Nuuk	-	-	365	6705	0
Reykjavik	18.aug	02.jul	319	4325	-34
Torshavn	28.aug	26.jun	312	3492	-29
Svalbard Ap.	-	-	365	8618	0
Karasjok	20.aug	15.jun	300	6751	-18
Vardø	-	-	365	5707	-53
Tromsø	23.aug	23.jun	305	4933	-26
Stensele	26.aug	04.jun	283	5631	-22
Karesuando	19.aug	13.jun	299	6647	-29
Copenhagen	14 Oct	05 May	204	2708	-26
Oslo-Blindern	19.sep	13 May	237	3794	-18
Helsinki	21.sep	17 May	239	3972	-15
Stockholm	28.sep	13 May	228	3484	-18
	ΔHDD 1901 -1930	1931 -1960	1990 -2002	2021 -2050	ΔHDD (%) 2021 -2050
Nuuk	74	-238	120	-428	-6
Reykjavik	55	-345	-185	-690	-16
Torshavn	195	-217	-140	-514	-15
Svalbard Ap.	-	-460	-573	-1769	-21
Karasjok	-85	-307	-403	-1351	-20
Vardø	89	-100	-342	-1236	-22
Tromsø	148	-120	-102	-978	-20
Stensele	160	-92	-325	-1229	-22
Karesuando	39	-203	-351	-1485	-22
Copenhagen	233	95	-198	-502	-19
Oslo-Blindern	76	-50	-290	-808	-21
Helsinki	187	20	-228	-920	-23
Stockholm	64	-16	-273	-694	-20

8. RELATIONS BETWEEN LONG-TERM VARIATIONS IN RUNOFF AND LARGE SCALE ATMOSPHERIC CIRCULATION PATTERNS

Runoff in Norway shows large inter-annual and inter-regional variations. These variations can to a large extent be related to regional climate anomalies caused by variations in the pressure fields in the North-Atlantic region. Hanssen-Bauer and Førland (2000) showed that long-term variations in temperature and precipitation on decadal scale can be related to mean sea level pressure. The spatial distribution of both precipitation occurrence and amounts in Norway can also be explained by atmospheric circulation (Tveito, 2002). Tveito and Hisdal (1995) found significant relations between empirical orthogonal function of monthly pressure and precipitation observation series in Norway.

One objective in this study has been to identify possible links between large scale atmospheric circulation and runoff anomalies in Norway. A long-term objective is to address future runoff-anomalies based on future changes in atmospheric circulation, and assess climate change impacts on flood- and drought conditions in Norway. In this chapter the study and results are presented in brief. Tveito and Roald (2005) give a more complete presentation of the study and the results.

8.1 Data and methods

The runoff of Norway show regional variations due to different physiographical and climatological characteristics. Studies of long-term runoff series have shown that Norway can be divided into thirteen homogenous runoff regions Førland et al (2000). In this study regional index series for twelve (region 1 through 12) of these regions are applied. For region 13 there are no sufficient homogenous runoff records to establish a high-quality index series. The regions are shown in Fig. 2.1. The series cover different time periods due to the available runoff record. In this paper the period 1901-2000 is analysed. In the three northernmost regions the runoff observation network was established in the beginning of the 20th century, so for the regions 10, 11 and 12 the index series starts in 1908, 1909 and 1912 respectively.

To describe the atmospheric circulations patterns the well known Grid-Point Pressure Data for the Northern Hemisphere (Jones, 1987) provided by the CRU at East Anglia University (http://www.cru.uea.ac.uk) is used. This monthly gridded dataset has a spatial resolution of 5° latitude by 10° longitude. It covers the period 1873 to 2000, but in this analysis only the period 1901-2000 is applied.

The circulation patterns are derived by principal component analysis (PCA). Principal components are established for two different domains (Fig. 8.1). Domain 1 covers the North Atlantic region from 60°W to 40°E and 30-80°N. Domain 2 is extended to the 100 °E. In this chapter only principal components for domain 1 will be discussed.

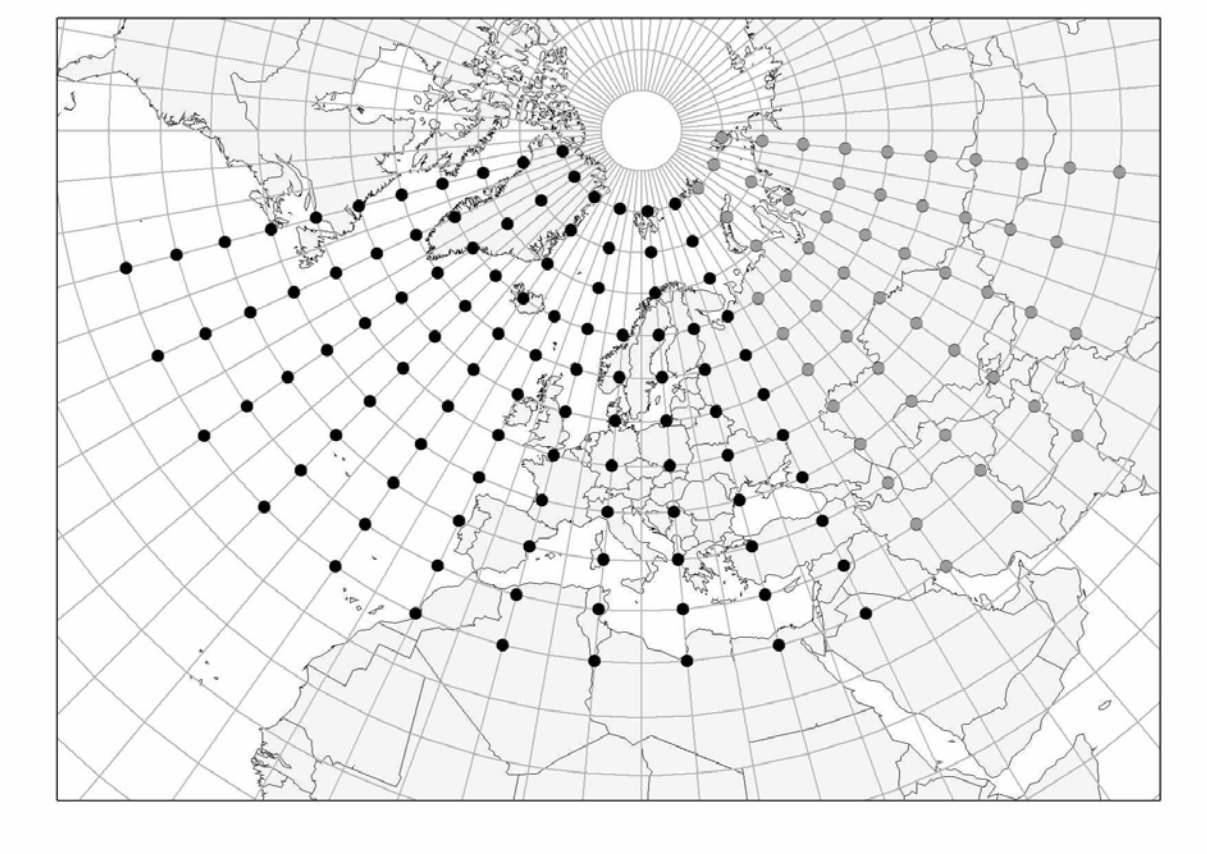

Figure 8.1. Pressure dataset grid-points used. Black points describes domain 1, while all the points (grey and black) describes domain 2.

The principal components are mathematically derived functions, describing the variance of the data set in an efficient way. The results of a principal component analysis of a geographical data set is two functions; the spatial and temporal components. Both the spatial and temporal components are uncorrelated (orthogonal). In a PCA of air pressure the spatial components describe circulation patterns, while the connected temporal components will represent circulation indices (the intensity of the patterns).

Table 8.1 Proportion of variance (in %) of the principal components of domain 1 1901-2000.

	PC1	PC2	PC3	PC4	PC5	PC6	PC7	PC8	PC9	PC10
Spring	38.6	17.2	11.8	9.7	5.6	3.2	2.6	2.1	1.9	1.0
Summer	36.6	16.6	11.3	8.1	5.3	3.7	2.8	2.7	1.7	1.5
Autumn	27.8	21.7	16.8	8.2	5.6	3.6	3.0	2.4	1.9	1.1
Winter	47.7	16.5	13.5	7.6	3.3	2.1	1.7	1.4	1.2	0.9

Table 8.2 Cumulative variance (in %) of the principal components of domain 1 1901-2000.

	PC1	PC2	PC3	PC4	PC5	PC6	PC7	PC8	PC9	PC10
Spring	38.6	55.8	67.6	77.3	82.9	86.2	88.8	90.9	92.7	93.7
Summer	36.6	53.1	64.5	72.6	77.9	81.6	84.4	87.1	88.8	90.4
Autumn	27.8	49.5	66.3	74.5	80.0	83.6	86.6	89.1	91.0	92.1
Winter	47.7	64.2	77.7	85.3	88.6	90.7	92.4	93.8	95.0	95.9

The proportion of variance explained by the components is shown in Tables 8.1 and 8.2. The components show seasonal variations in the explanation of the pressure variations. In the winter season the first component is very strong, explaining almost half the variance, and almost three times as much as the second component. This indicates that the pattern of the first component is very stable and dominant from year to year. To the contrary autumn shows little difference in explanation between the first three components, implying that all these patterns are almost equally significant. This means that these patterns might vary to be the most dominant from year to year.

The principal components for autumn are shown in Fig. 8.2. PC1 describes a westerly flow pattern, which in principle is the same feature as described by the North-Atlantic oscillation index (NAOI). The second component shows a pressure anomaly over Fennoscandia, with an opposite anomaly in the North-Atlantic. This pattern is often referred to as the Scandinavian pattern. It reflects the often persistent high pressure centre that occurs regularly over Eastern Fennoscandia, a typical blocking situation. The third component describes a pressure anomaly over the British Isles. Fig. 8.3 shows the temporal variations of these components, which is a measure of the intensity of the circulations they represent.

Table 8.3 and Fig. 8.4 shows the correlations between the regional runoff index series and the autumn principal components. In autumn river runoff generally depends solely upon precipitation activity, and it is therefore suited to study the relation between atmospheric circulation and runoff. The first three PCs show high correlations to runoff in different region. PC1 gives high correlations along the western coast. Also the south-eastern coastal region (region 2) has correlation coefficients higher than 0.5, and the southern region (region 4) is just below 0.5. The reason that also these regions have high correlation is the location of the negative pressure anomaly, in the Norwegian Sea, which will cause south-westerly to southerly winds in this area. Correlations in the northern regions are low. The second component shows lower correlation values. The highest correlation is found for region 10, (r^2 = -0.35), indicating that the runoff variations in this region depends on the intensity of the pressure anomaly over Russia. Component three however is highly correlated with the northern regions (9, 10 and 11).This is the British Isles anomaly, which in positive phase cause westerly winds towards northern Norway. This component is also strongly negative correlated with the south-eastern regions. This means that when this anomaly is in negative phase, south-eastern Norway gets it share of precipitation. This was the situation in November and December 2000, when this pattern was blocked for almost two months, giving very high amounts of precipitation in south-eastern Norway, and consequently high runoff values. In Fig. 8.4 it can be seen the lowest value of PC3 is found for just the 2000 season.

8.2 Prediction of regional runoff series by atmospheric circulation.

One of the aims of this study has been to use the relations between atmospheric circulation and regional runoff series to develop a model for describing variation of runoff using the atmospheric circulation indices as predictors. The circulation indices developed in this analysis are based on a principal component analysis, and the predictors will consequently be the temporal components of this analysis. A regression analysis is carried out in order to establish seasonal models for each region. Since the components have different influence on

the different regions, a stepwise regression algorithm was applied to establish the linear models.

In this chapter models based on the components of domain 1 are emphasized. Figs. 8.5-8.8 show the observed and modelled runoff for three runoff regions (regions 1, 5 and 10) for all the seasons. These regions are selected because they besides covering different areas of the country also represent different climatic regimes.

Table 8.4 shows the coefficients of determination for the regressions models established. For the spring and autumn seasons high values are obtained in several regions. These seasons are characterized by a direct link between weather and runoff, and not by large delays in runoff. In spring the runoff in many regions are heavily influenced by snow melt, and thereby also a delayed result of winter precipitation. This condition is not accounted for in the present model. In autumn most of the runoff is a product of precipitation, and the runoff response is usually quite fast. Therefore most of the regions show high coefficients of determination. One exception is region 12. This region is a continental region, and most of the drainage areas are in northern Finland and in Russia. Snow cover is usually established during this season, and the runoff is therefore not so directly influenced of precipitation. This region also show low correlations with the pressure components of domain 1, and is probably more circulations over Eastern Europe, Russia and Siberia. The low R-value in summer is also an indication of this.

For the summer and winter seasons water storage (soil water, snow storage) in the catchments complicates the direct link between atmospheric circulation. In addition evapotranspiration is also a major effect in summer, especially the southern parts of the country. In summer the precipitation conditions are different, with a higher frequency of scattered rain showers instead of precipitation due to large frontal systems. This is probably one reason why it is not possible to establish a model for region 2 in summer.

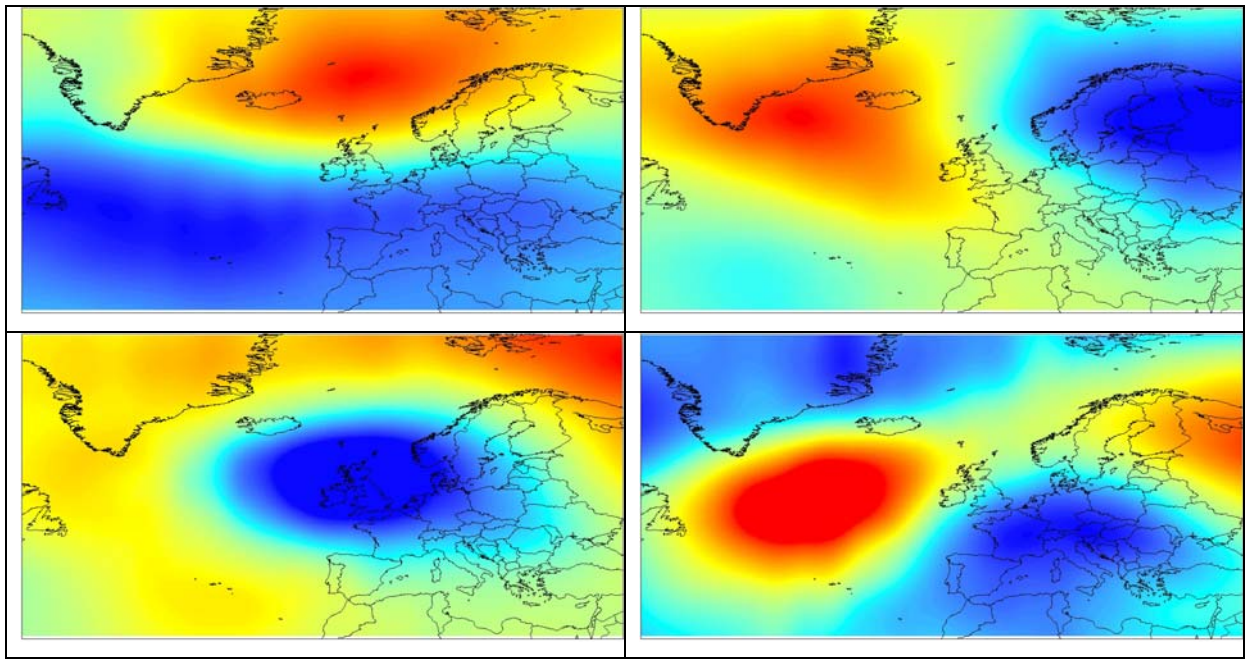

Figure 8.2 Principal component patterns of domain 1, 1901-2000, autumn.

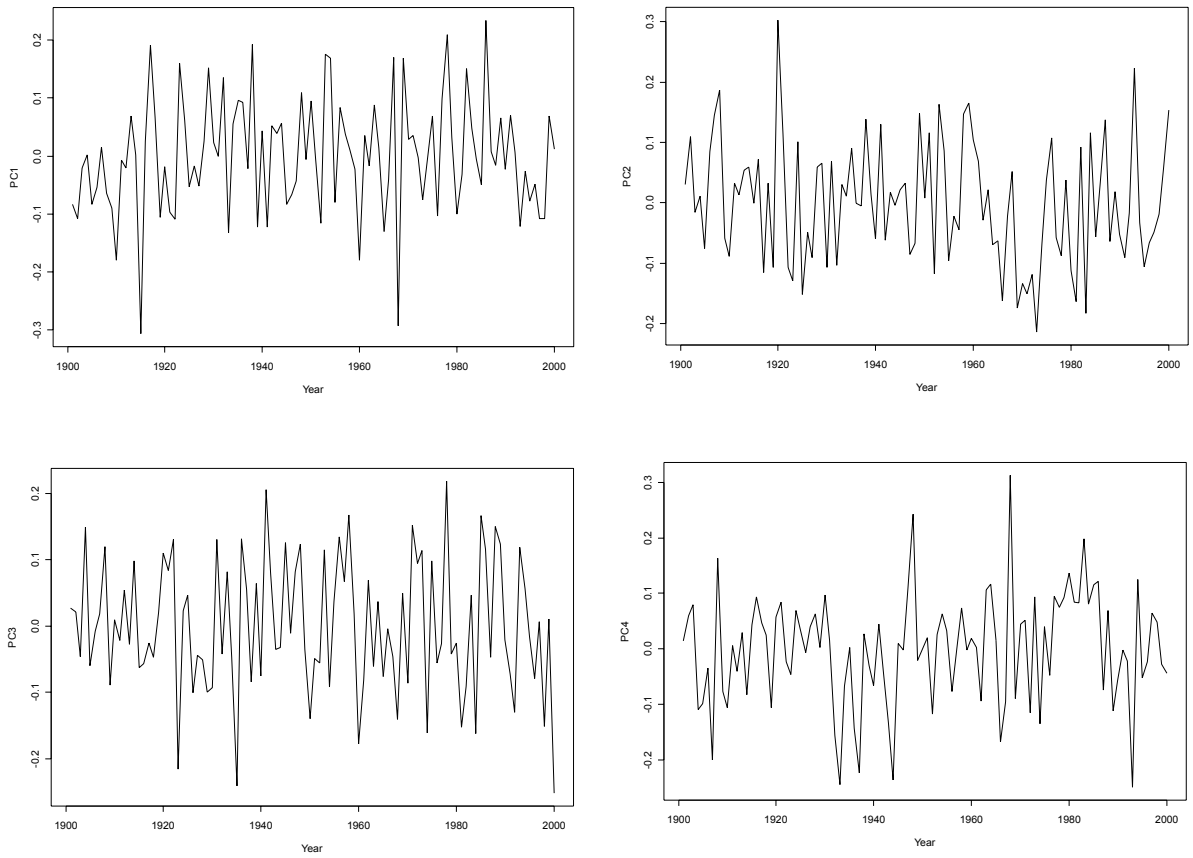

Figure 8.3 Temporal variations domain 1 autumn, 1901-2000.

Table 8.3 Correlations between regional runoff and principal components (domain 1 1901-2000) in autumn.

Region	PC1	PC2	PC3	PC4	PC5	PC6	PC7	PC8	PC9	PC10
1	0.374	0.209	-0.423	-0.014	-0.085	-0.095	-0.052	-0.032	-0.106	0.021
2	0.541	0.078	-0.144	0.247	-0.199	-0.137	0.020	-0.073	-0.104	0.074
3	0.338	0.283	-0.541	0.013	-0.141	-0.165	-0.066	0.013	-0.127	-0.062
4	0.499	0.196	-0.512	0.078	-0.110	-0.043	-0.096	0.060	-0.033	0.001
5	0.716	-0.192	-0.204	0.266	-0.120	-0.102	-0.036	-0.044	0.061	0.101
6	0.666	-0.197	0.105	0.297	-0.105	-0.044	0.037	-0.114	0.007	0.109
7	0.506	-0.121	0.283	0.320	-0.124	-0.060	0.145	-0.137	-0.026	0.093
8	0.398	-0.311	0.432	0.211	0.104	0.013	0.135	-0.054	-0.040	0.056
9	0.251	-0.313	0.526	0.185	0.045	0.054	0.119	-0.053	-0.117	0.059
10	0.287	-0.351	0.514	0.194	-0.094	0.024	0.096	-0.023	-0.140	0.104
11	0.195	-0.069	0.577	0.156	-0.298	0.120	0.117	-0.025	-0.140	0.050
12	0.289	-0.054	-0.050	0.076	-0.072	-0.013	0.156	0.066	-0.121	0.147

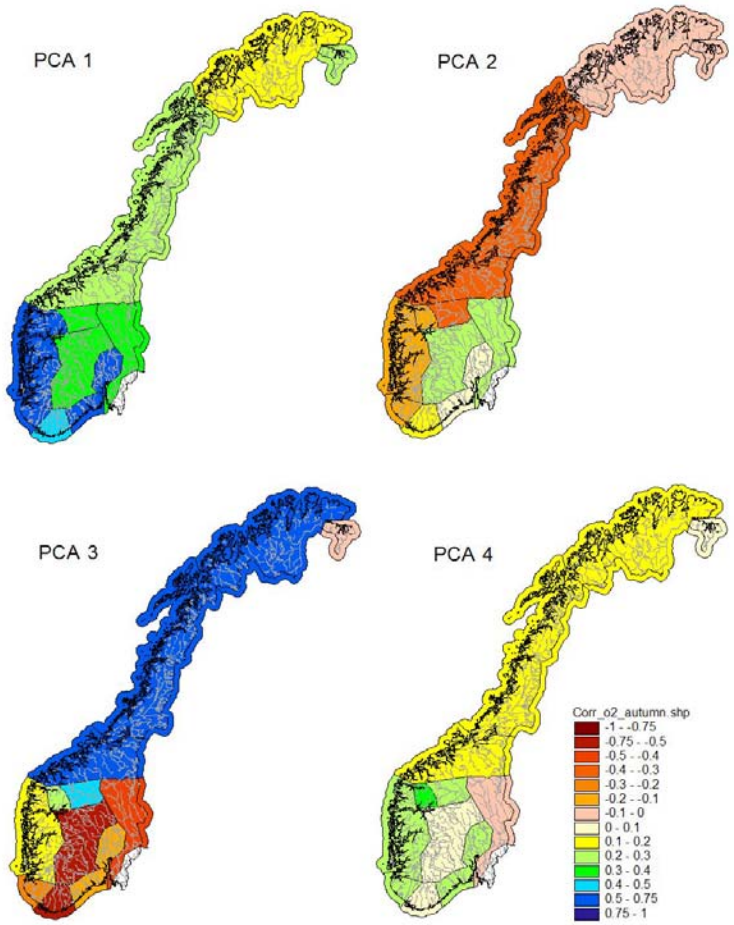

Figure 8.4 Correlations between regional runoff and the four most prominent domain 1 circulation patterns (PCs) in autumn 1901-2000.

Table 8.4 Coefficient of determination for the models of regional runoff based on circulation components.

REGION	SPRING	SUMMER	AUTUMN	WINTER
1	0.525	0.577	0.602	0.246
2	0.613	-[1]	0.627	0.570
3	0.504	0.651	0.731	0.344
4	0.662	0.646	0.741	0.721
5	0.826	0.529	0.823	0.819
6	0.773	0.429	0.755	0.835
7	0.719	0.534	0.663	0.822
8	0.742	0.509	0.697	0.725
9	0.680	0.526	0.687	0.673
10	0.748	0.623	0.711	0.790
11	0.631	0.642	0.698	0.805
12	0.519	0.365	0.289	0.566

[1]) No model was established.

In continental parts of the country snow cover is stable in most winters. The performance of the regression models will therefore be low, since runoff variations in these areas mostly are results of snowmelt associated with occasional “warm spells”. In the coastal regions the climate is mild and winter runoff common. Mild and wet periods are associated with certain circulation types, and the performance of the models is higher in these regions. This can clearly be seen from Fig. 8.8 where the modelled runoff of region 1 shows low variability compared to the observed runoff. This indicates that runoff variations in winter for this region not can be explained by the large scale circulation represented by the first ten principal components. The only component used in the regression model is PC 1, which covers 48% of the variance of the MSLP in domain 1. This component represents the intensity of the zonal airflow in the domain 1 area. However only very large scale variations are representative and the regional variability are not accounted. The circulation anomalies that might explain these variations are either found in the lower ranked components, or the runoff variations are caused by weather events that are not reflected by the seasonal pressure fields.

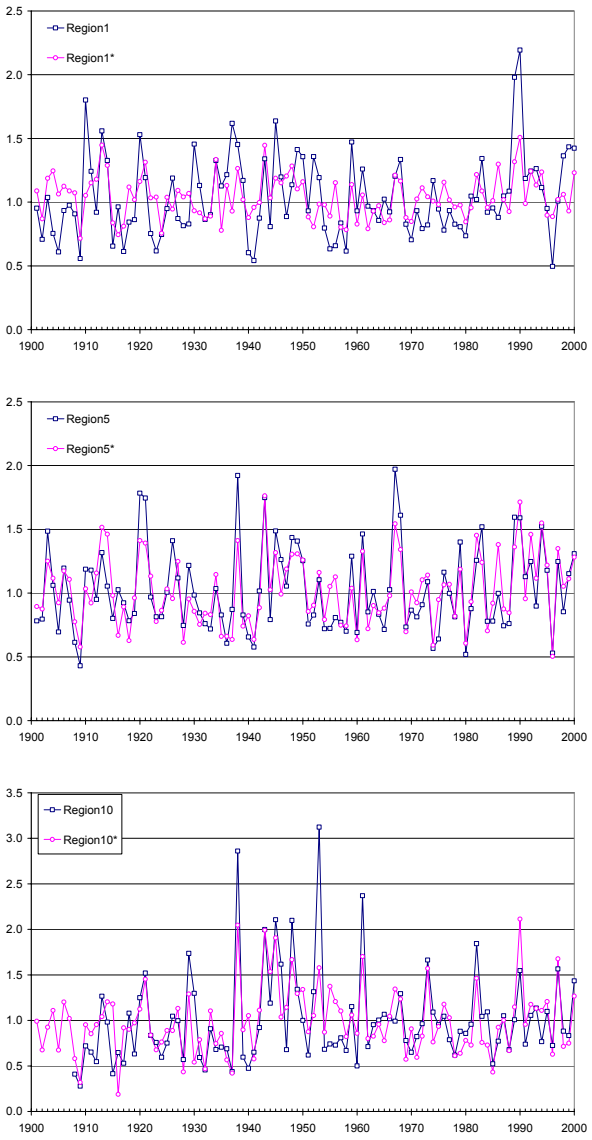

Figure 8.5 Observed and modelled regional spring runoff for regions 1, 5 and 10.

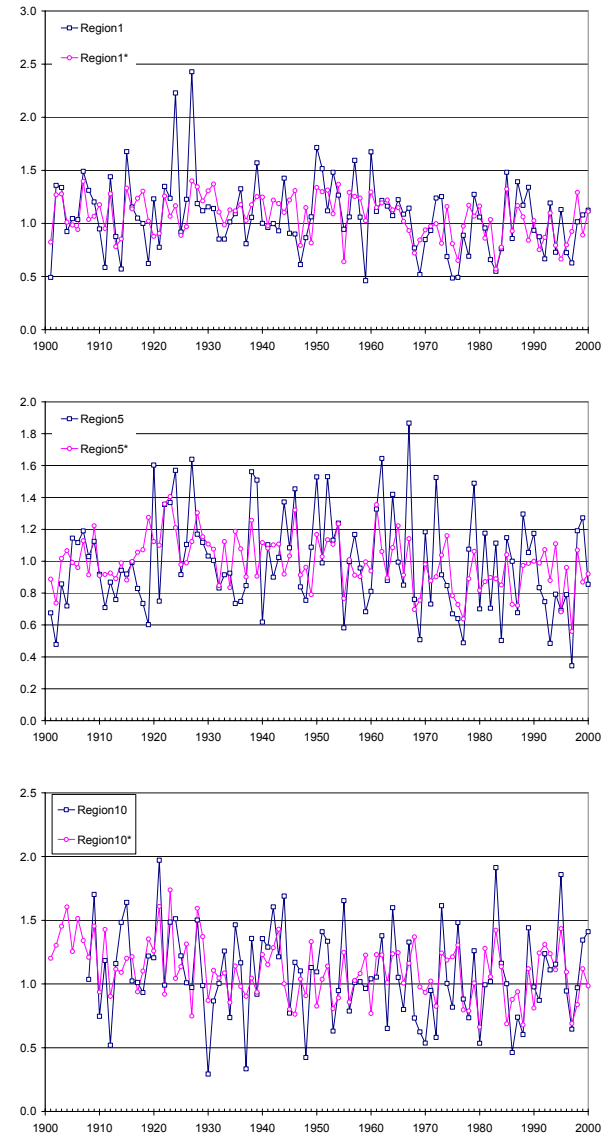

Figure 8.6 Observed and modelled regional summer runoff for regions 1, 5 and 10.

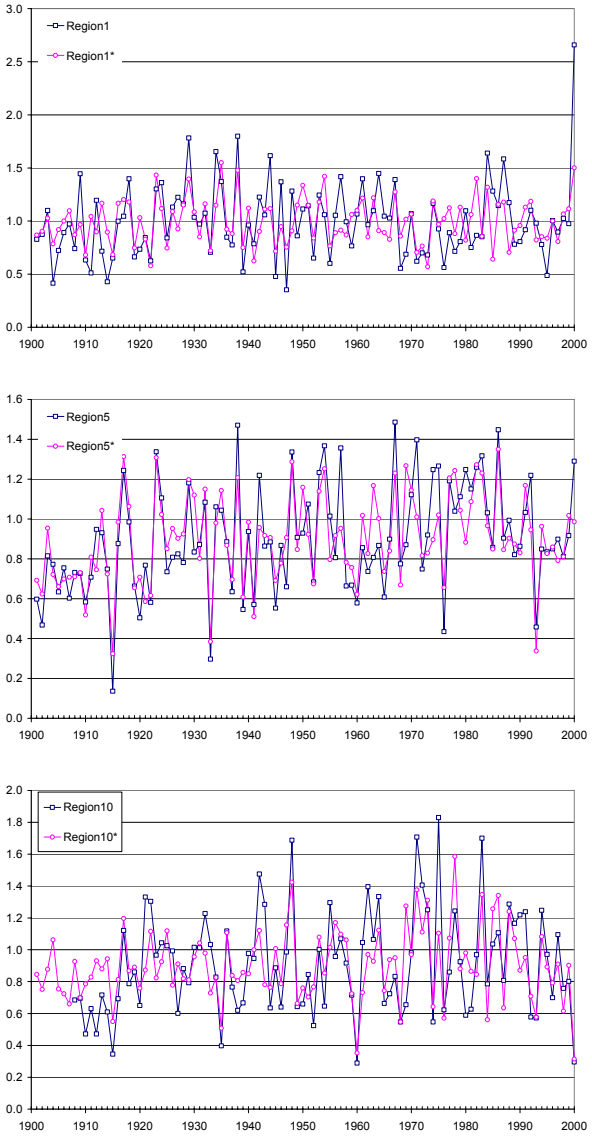

Figure 8.7 Observed and modelled regional autumn runoff for regions 1, 5 and 10.

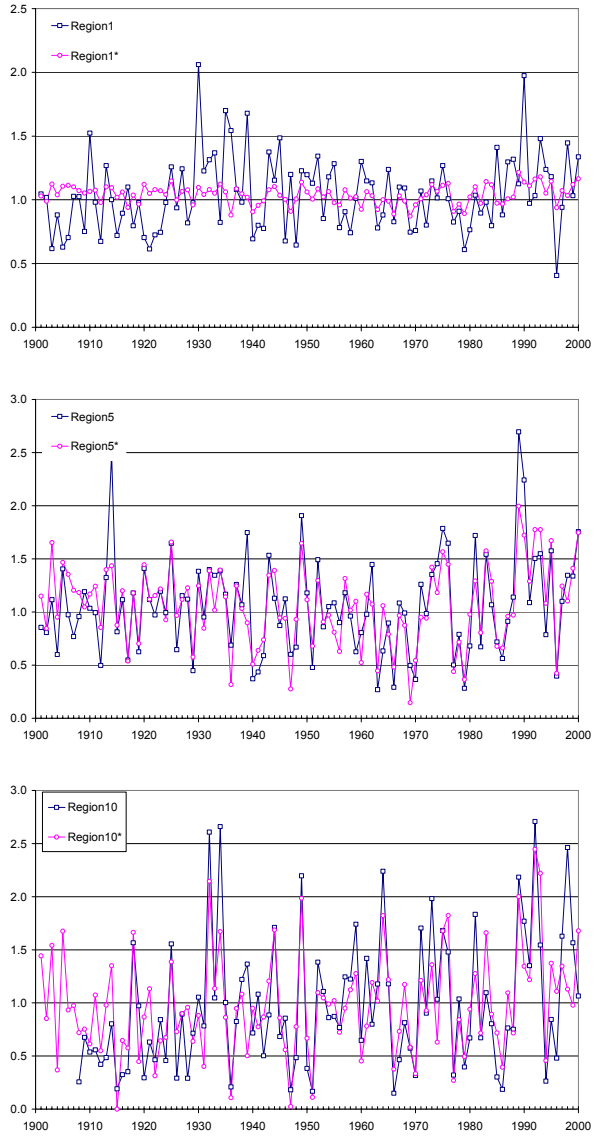

Figure 8.8 Observed and modelled regional winter runoff for regions 1, 5 and 10.

9. SUMMARY

The present report summarizes the main results from the project "Climate change and energy production potential" funded by EBL-Kompetanse AS (Project number M1.1.01_01).

The local climate scenarios for Norway are based on dynamical downscaling of three global climate model simulations: ECHAM4/OPYC3-IS92a with emission scenario IS92a for the period 2030-2049 and HadAm3-A2 & HadAm3-B2 with emission scenarios A2 resp. B2 for the period 2071-2100. A2 has a higher emission scenario for CO_2 than B2, and the projected global temperature increase up to 2100 for A2 is ca. 3.5ºC and for B2 ca. 2.5ºC.

A method for adjusting dynamically downscaled climate scenarios (daily time series of temperature and precipitation) has been developed to make the scenarios representative for

specific sites. By comparing results from control runs with observations the adjusted values were found to be satisfactorily tailored to the local climate conditions.

The adjusted scenarios from three simulations indicate similar qualitative changes in mean seasonal temperature; the largest temperature increase is projected in northern and south-eastern regions during autumn and winter. HadAm3-A2 is giving the largest temperature increase. The smallest temperature increase for all three simulations is found during summer. The projected seasonal precipitation change show a more different pattern for the three simulations: ECHAM4/OPYC3-IS92a projects increased precipitation in Western Norway during summer and autumn and a reduction in south-eastern parts during spring and summer. Both HadAm3-A2 and HadAm3-B2 project a decrease in mean summer precipitation in southern regions and an increase in northern regions. The largest increase for HadAm3-A2 is found in winter in south-eastern regions, while the largest increase for HadAm3-B2 is found in autumn all over the country.

During winter in southern areas, an increase is projected in both mean temperature, total precipitation amount and extreme daily precipitation. However, in south-eastern regions HadAm3-A2 and HadAm3-B2 project a decrease in total summer precipitation, but still an increase is projected in extreme daily precipitation during this season; i.e. less but more intense rainfall.

Different features contribute to uncertainties in local climate scenarios: 1). Unpredictable internal variations in the climate-system (”Natural variability”). 2). Uncertainties concerning changes in ”climate forcings”; (Both natural forcings (sun radiation, volcano-activity), anthropogenic release of greenhouse gases and aerosols, and changes in land-use). 3). Model deficiencies (Imperfect knowledge and treatment of processes, poor spatial resolution in global models and weaknesses in techniques for downscaling from global to regional/local climate).

A potential for improving the evaporation calculations both in regional climate models (HIRHAM) and water-balance models (GWB) is outlined. The different process parameterisation of the two models leads to significantly different evaporation estimates both for the present climate and for climate change scenarios. Both models overestimate the average annual evaporation compared to observations. HIRHAM overestimates winter evaporation whereas the GWB overestimates spring and autumn evaporation, and underestimates winter-evaporation. Furthermore, the HIRHAM model overestimates the evaporation especially in mountain regions. The differences in estimated evaporation between the two models are larger than the differences between HadAm3-A2 and B2. Both models indicate that the largest increase in evaporation will be during spring and autumn. The summer evaporation might decrease at many locations. The GWB indicates a much higher increase in average annual evaporation than the HIRHAM model. This difference is mainly explained by how the models parameterize evaporation from snow cover

The streamflow scenarios for the period 2030-2049 based on ECHAM4/OPYC3-IS92a indicate increase in the mean annual values in most of Norway, but a decrease in some catchments in the southernmost and southeastern parts and in Finnmark. The winter streamflow will increase everywhere. The spring streamflow will decrease in the southernmost part of Norway, but will increase elsewhere. The summer streamflow will decrease almost everywhere, while the autumn streamflow will increase in almost all catchments.

The streamflow scenarios for the period 2071-2100 based on the HadAm3-model show different development depending on the emission scenario used. The HadAm3-B2 results in moderately increased streamflow in most of the catchments. The HadAm3-A2 results in lower

streamflow than HadAm3-B2 in most catchments. For HadAm3-A2 the annual streamflow is projected to increase most in the southwest, but decrease in most of southeastern and southern Norway, in mid Norway and in the northernmost part of Norway. Both HadAm3-A2 and B2 indicate that the winter streamflow will increase. For the spring seasons, the simulations indicate reduced streamflow in the south and increased streamflow in the mountains and in most catchments in the west and north. Simulations for summer indicate a large reduction in streamflow, and simulations for the autumn indicate reduced streamflow in a region in most of southern Norway for the HadAm3-A2 and in the eastern and southern part of Southern Norway for the HadAm3-B2. Both HadAm3-A2 and B2 indicate an increase in Northern Norway.

The ECHAM4/OPYC3-IS92a scenarios, which are used in the study of heating season for the period 2021-2050, project substantially higher winter temperatures than observed in the 20th century. This leads to a reduction in heating-degree days of around 20% in large parts of Fennoscandia, indicating that the energy consumption for heating buildings will be substantially reduced during the next 50 years.

It is found that variations in atmospheric circulation can describe runoff variations on a seasonal scale. For some regions in some seasons however the relations are weak. One problem dealing with seasonal values is that the atmospheric circulation indices as well the runoff anomalies are smoothed, and thereby hide the direct links between certain atmospheric conditions and weather and runoff response. Especially will this be the case when trying to relate atmospheric circulation to extreme events. These results can though be used to address the effects of future trends and changes in the atmospheric circulation regime on runoff. Especially could effects caused by shifts in the significance of the circulation patterns be addressed.

References

Alexandersson, H.: 1986. A homogeneity test applied to precipitation data. Journal of Climatology, 6, 661-675.

Beldring, S., Roald, L.A., Voksø A.: 2002, Avrenningskart for Norge. Årsmiddelverdier for avrenning 1961-1990. (In Norwegian). (Map of annual runoff for Norway for the period 1961-1990.) Norwegian Water Resources and Energy Directorate, Document no. 2/2002, 49 pp.

Beldring, S., Engeland, K., Roald, L.A., Sælthun, N.R., Voksø, A.: 2003, Estimation of parameters in a distributed precipitation-runoff model for Norway. Hydrology and Earth System Sciences 7, 304-316.

Benestad, R.E,: 2004, Tentative probabilistic temperature scenarios for northern Europe Tellus 56A, 89-101

Benestad, R.E.: 2003, What can present climate models tell us about climate change? Climatic Change Vol 59, 311-332.

Benestad, R.E.: 2002, Empirically downscaled multi-model ensemble temperature and precipitation scenarios for Norway, Journal of Climate Vol 15, 3008-3027.

Benestad, R.E.: 2001a, A comparison between two empirical downscaling strategies, Int. J. Climatology,Vol 21, Issue 13, pp.1645-1668. [DOI 10.1002/joc.703]

Benestad, R.E.: 2001b, The cause of warming over Norway in the ECHAM4/OPYC3 GHG integration, Int. J. Clim. 15 March Vol 21 371-387.

Benestad, R.E.: 2000, Future Climate Scenarios for Norway based on empirical Downscaling and inferred directly from AOGCM results, DNMI Klima, 23/00, pp.127

Bergström, S.: 1995, The HBV model. In: Singh, V.P. (Ed.), Computer Models of Watershed Hydrology. Water Resources Publications, Highlands Ranch, 443-476.

Bjørge D., Haugen, J.E., and Nordeng, T.E.: 2000, Future climate in Norway, Research Report No. 103, Norwegian Meteorological Institute, Oslo

Bronstert, A: 2004, Rainfall-runoff modelling for assessing impacts of climate and land-use change, Hydrol. Process.18:567-570

Charles S., Bates, B.C., Whetton, P.H., and Hughes, J.P.: 1999, Validation of downscaling models for changed climate conditions: case study of southwestern Australia, Clim Res 12:1-14

Christensen, J.H., Cristensen, O.B., Lopez, P., Meijgaard, E. and Botzet, M., 1996: The HIRHAM Regional Atmospheric Climate Model. DMI Scientific report 96-4, Copenhagen, Denmark.

Cubash, U, Meehl, G.A., Boer, GJ, Stouffer, RJ and 5 others: 2001, `Projections of future climate change´. In: Houghton JT, Ding Y., Griggs DJ, Noguer M, van der Linden PJ, Dai X, Maskell K, Johnson CA (eds) Climate change 2001: the scientific basis. Contribution of Working Group I to the Third Assessment Report of International Panel on Climate Change. Cambridge University Press, Cambridge, p 583-638.

Daly, C., Neilson. R.P. and Phillips, D.L.: 1994, A statistical-topographic model for mapping precipitation over mountainous terrain. Journal of Applied Meteorology, 33, 140-158.

Doherty, J., Brebber, L. and Whyte, P.: 1998. PEST. Model independent parameter estimation. Watermark Computing, 185 pp.

Engeland, K., Engen-Skaugen, T., Haugen,J.E., Beldring, E., Førland, E.,: 2004, Comparison of evaporation estimated by the HIRHAM and GWB models for present and climate change scenarios. Research Report No. 17/2004, Norwegian Meteorological Institute, Oslo.

Engen-Skaugen, T.: 2004, refinement of dynamically downscaled precipitation and temperature scenarios, Research Report no. 15/04, Meteorological Institute.

Frei, C., J.H. Christensen, M. Déqué, D. Jacob, R.G. Jones and P.L. Vidale,: 2003, Daily Precipitation Statistics in Regional Climate Models: Evaluation and Intercomparison for the European Alps, J. Geophys. Res., 108, 10.1029/2002JD002287

Førland, E.J., Engen-Skaugen,T., Benestad, R.E., Hanssen-Bauer, I. & Tveito, O.E.,: 2004, Variations in Thermal Growing, Heating and Freezing Indices in the Nordic Arctic, 1900-2050. Arctic, Antarctic and Alpine Review (in press)

Førland, E.J., L. Roald, O. E. Tveito and Hanssen-Bauer,I..: 2000, Past and future variations in climate and runoff in Norway, DNMI Report 19/00 Klima

Førland, E.J., Allerup, P., Dahlström, B., Elomaa, E., Jónsson, T., Madsen, H., Perälä, J., Rissanen, P., Vedin, H. and Vejen, F.: 1996, Manual for operational correction of Nordic precipitation data. Norwegian Meteorological Institute DNMI Klima Report 24/96, 66 pp.

Giorgi F., Hewitson, B., Christensen J.H., Hulme, M and 5 others: 2001, `Regional climate information – evaluation and projections´. In: Houghton JT, Ding Y., Griggs DJ, Noguer M, van der Linden PJ, Dai X, Maskell K, Johnson CA (eds) Climate change 2001: the scientific basis. Contribution of Working Group I to the Third Assessment Report of International Panel on Climate Change. Cambridge University Press, Cambridge, p 525-582

Gordon, C., Cooper, C., Senior, C.A., Banks, H.,Gregory, J.M.,Johns,T.C., Mitchell,J.B.F. and Wood, R.A.: 2000, The simulation of SST, sea ice extensts and ocean heat transport in a version of the Hadley Centre coupled model without flux adjustments, Clim.Dyn., 16,147-168.

Gottschalk, L., Jensen, J.L., Lundquist, D., Solantie, R., Tolland, A.,: 1979, Hydrologic regions in the Nordic countries. Nordic hydrology, Vol. 10: 273-286.

Gottschalk, L., Beldring, S., Engeland, K., Tallaksen, L., Sælthun, N.R., Kolberg, S. and Motovilov, Y.: 2001. Regional/macroscale hydrological modelling: a Scandinavian experience. Hydrological Sciences Journal, 46, 963–982.

Groisman, P.Ya., Sun, B., Vose, R. S., Lawrimore, J. H., Whitfield, P. H., Førland, E. J., Hanssen-Bauer, I., Serreze, M. C., Razuvaev, V. N., and Alekseev, G. V:. 2003, Contemporary climate changes in high latitudes of the Northern Hemisphere: Daily time resolution. WMO/TD - 1172, [WMO Proc. of the International Symposium on Climate Change, Beijing, China ,31 March-3 April, 2003], World Meteorol. Organ. Publ. # 1172: 51-55.

Guttman, N. B., and Lehman, R. L.: 1992, Estimation of daily degree-days. Journal of Applied Meteorology. 31: 797-810.

Hanssen-Bauer, I, E.J. Førland and O.E. Tveito: 2003, Temperature and precipitation scenarios for Norway: comparison of results from dynamical and empirical downscaling. Clim Res 25:15-27.

Hanssen-Bauer, I. and Førland,E.J.: 2000, Temperature and precipitation variations in Norway 1900-1994 and their links to atmospheric circulation", International Journal of Climatology 20, pp. 1693-1708

Hanssen-Bauer, I. and Nordli, P.Ø.: 1998, Annual and seasonal precipitation variations in Norway 1896-1997. DNMI-Report No 27/98 KLIMA, 37 pp.

Haugen, J.E. and V. Ødegaard,: 2003, Evaluation of MPI and Hadley simulations with HIRHAM and sensitivity to integration domains, RegClim Phase III-General Technical Report No. 7 p: 19-29.

Hisdal, H., Holmqvist, E., Kuusisto, E., Lindström, G. and Roald, L.A.: 2004, Has streamflow changed in the Nordic Countries? In: A. Järvet (ed): 2004, Selected articles from the XXIII Nordic Hydrological Conference, Tallin, Estonia 8-12 August 2004. NHP Report No. 48.

Jones, P.D., 1987: The early twentieth century Arctic High - fact or fiction? Climate Dynamics 1, 63-75.

Lettenmaier, D.P., Wood, A.W., Palmer, R.N., Wood,E.F. and Stakhiv, E.Z.: 1999,Water resources implications of global warming: A U.S. regional perspective, Climatic Change 43:537-579.

Middelkoop, H., Daamen,K., Gellens,D.,Grabs,W., Kwadijk, J.C.J., Lang, H., Parmet, B.W.A.H., Schädler, B., Schulla, J. and Wilke, K: 2001, Impact of climate change on hydrological regimes and water resourches management in the Rhine basin, Climatic Change 49:105-128

Onof, C.: 2000, A precipitation and temperature generator for the Nordic climate. Norwegian water resources and energy directorate, report, Oslo.

Onof, C., and Weather, H.S.: 1993, Modelling of British rainfall using a random parameter Bartlett-Lewis Rectangular Pulse Model. J.Hydrol.149,67-95, Amsterdam

Pettitt, A.N.: 1979, A non-parametric approach to the change-point problem. Applied Statistics, 28, 126-135.

Quayle, R.G., and Diaz, H. F.: 1980, Heating degree-day data applied to residential heating energy consumption. Journal of Applied Meteorology, 19(3): 241-246.

Reynard, N.S., Prudhomme, C. and Crooks, S.M.: 2001, The flood characteristics of large U.K.Rivers: Potential effects of changing climate and land use. Climatic change 48:343-359.

Roald,L.A., Beldring, S., Engen-Skaugen,T., Førland, E.J.: 2005, Climate change impacts on stramflow in selected catchments in Norway, Norwegian Water Resources and Energy Directorate report, In prep.

Roald, L.A., Skaugen, T.E., Beldring, S., Væringstad, T., Engeset, R., and Førland, E.J.: 2003. Scenarios of annual and seasonal runoff for Norway base don climate scenarios for 2030-49'. Norwegian Water Resources and Energy Directorate Oppdragsrapport A No 10-2002 and Norwegian Meteorological Institute met.no Report 19/02, 56 pp.

Roeckner E, Bengtsson L., Feichter J, Lelieveld J. and Rodhe H.: 1999, Transient climate change si mulations with a coupled atmosphere-ocean GCM including the tropospheric sulphur cycle. J.Clim 12:3004-3032

Rummukainen, M, Bergström, S., Persson, G., Rodhe, J., Tjernstrröm, M.: 2004. The Swedish regional climate modelling programme, SWECLIM: A review. Ambio. Vol. XXXIII, Nos. 4-5. pp. 176-182.

Skaugen, T., Astrup, M., Roald,L.A. and Førland, E.J.: 2003, Scenarios of extreme daily precipitation for Norway under climate change. Nord. Hydrol. 35, (1)

Skaugen, T.E., and Tveito, O. E.: 2002, Heating degree-days – Present conditions and scenario for the period 2021-2050. DNMI Report 01/02 KLIMA, Norwegian Meteorological Institute, Oslo, 13 pp.

Sælthun, N.R.: 1996. The Nordic HBV model. Norwegian Water Resources and Energy Administration Publication 7, Oslo, 26 pp.

Sælthun, N.R., Aittonemi, P., Bergstrøm, S., Einarsson, K., Jòhannesson, T., Lindström, G., Ohlsson, P-E., Thomsen, T., Vehviläinen, B., and Aamodt, K.O.: 1998, Climate change impacts on runoff and hydropower in the Nordic countries. Final report from the project "Climate Change and Energy Production". TemaNord 1998:552. ISBN 92-893-0212-7. ISSN 0908-6692. Copenhagen. 170 p.

Taylor, B.L.: 1981, Population-weighted heating degree-days for Canada. Atmosphere-Ocean, Toronto, Canada, 19(3): 261-268.

Tveito, O.E. and Roald, L.A.: 2005, Relations between long-term variations in seasonal runoff and large scale atmospheric circulation patterns, met.no Report Climatology, in prep.

Tveito, O.E.: 2002, An objective comparison of observed and forecasted 24-hour precipitation, a spatial analysis, met.no Report 10/02 Klima

Tveito O.E., Førland, E.J., Heino, R., Hanssen-Bauer, I., Alexandersson, H., Dahlström, Drebs, A., Kern-Hansen,C., Jónsson, T., Vaarby Laursen, E., Westman, T.: 2000, Nordic temperature maps, Klima Report no. 09/00, Norwegian Meteorological Institute, Oslo

Tveito O.E., Førland, E.J., Dahlström, B., Elomaa, E., Hanssen-Bauer, I., Jónsson, T., Madsen, H., Perälä, J., Rissanen, P., Vedin, H.: 1997, `Nordic precipitation maps´, Klima Report no. 22/97, Norwegian Meteorological Institute, Oslo

Tveito, O. E. and Hisdal, H.: 1995, Disaggregation of large scale climatological information. NVE Rapport 9/1995.

Venäläinen, A., Tammelin, B., Tuomenvirta, H., Jylhä, K., Koskela, J., Turunen, M.A., Vehviläinen, B., Forsius, J., and Järvinen, P.: 2004, The influence of climate change on energy production & heating energy demand in Finland. Energy & Environment, 15, 93-109.

Węglarczyk, S.: 1998, The interdependence and applicability of some statistical quality measures for hydrological models. Journal of Hydrology, 206, 98-103.

Wood, A.W., Leung, L.R., Sridhar, V. and Lettenmaier, D.P.: 2004, Hydrologic implications of dynamical and statistical approaches to downscaling climate model outputs. Clim. Change 62: 189-216.

APPENDIX

Appendix 1

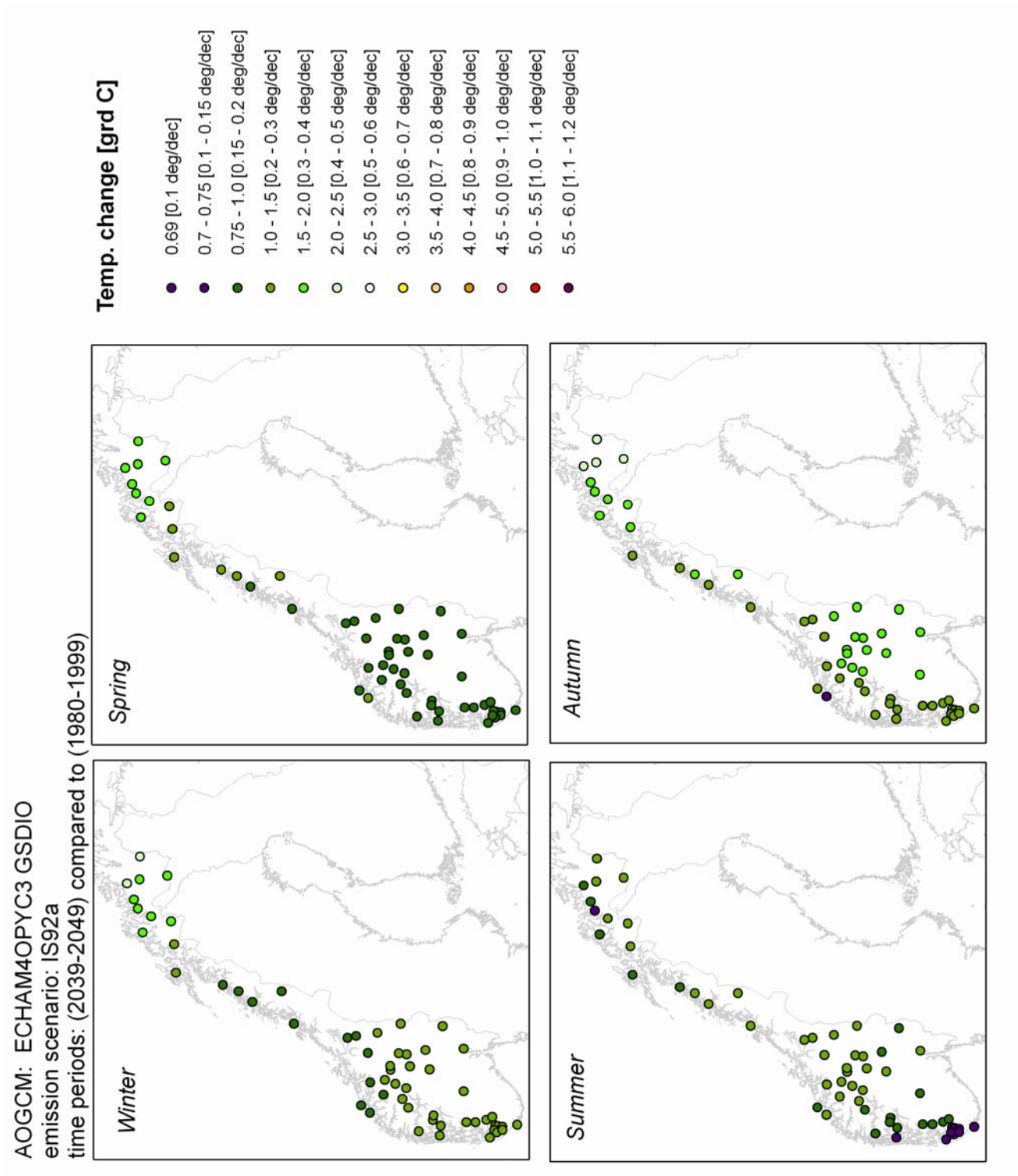
AOGCM: ECHAM4OPYC3 GSDIO
emission scenario: IS92a
time periods: (2039-2049) compared to (1980-1999)
Temp. change [grd C]
0.69 [0.1 deg/dec]
0.7 - 0.75 [0.1 - 0.15 deg/dec]
0.75 - 1.0 [0.15 - 0.2 deg/dec]
1.0 - 1.5 [0.2 - 0.3 deg/dec]
1.5 - 2.0 [0.3 - 0.4 deg/dec]
2.0 - 2.5 [0.4 - 0.5 deg/dec]
2.5 - 3.0 [0.5 - 0.6 deg/dec]
3.0 - 3.5 [0.6 - 0.7 deg/dec]
3.5 - 4.0 [0.7 - 0.8 deg/dec]
4.0 - 4.5 [0.8 - 0.9 deg/dec]
4.5 - 5.0 [0.9 - 1.0 deg/dec]
5.0 - 5.5 [1.0 - 1.1 deg/dec]
5.5 - 6.0 [1.1 - 1.2 deg/dec]
Winter
Spring
Summer
Autumn

Appendix 2

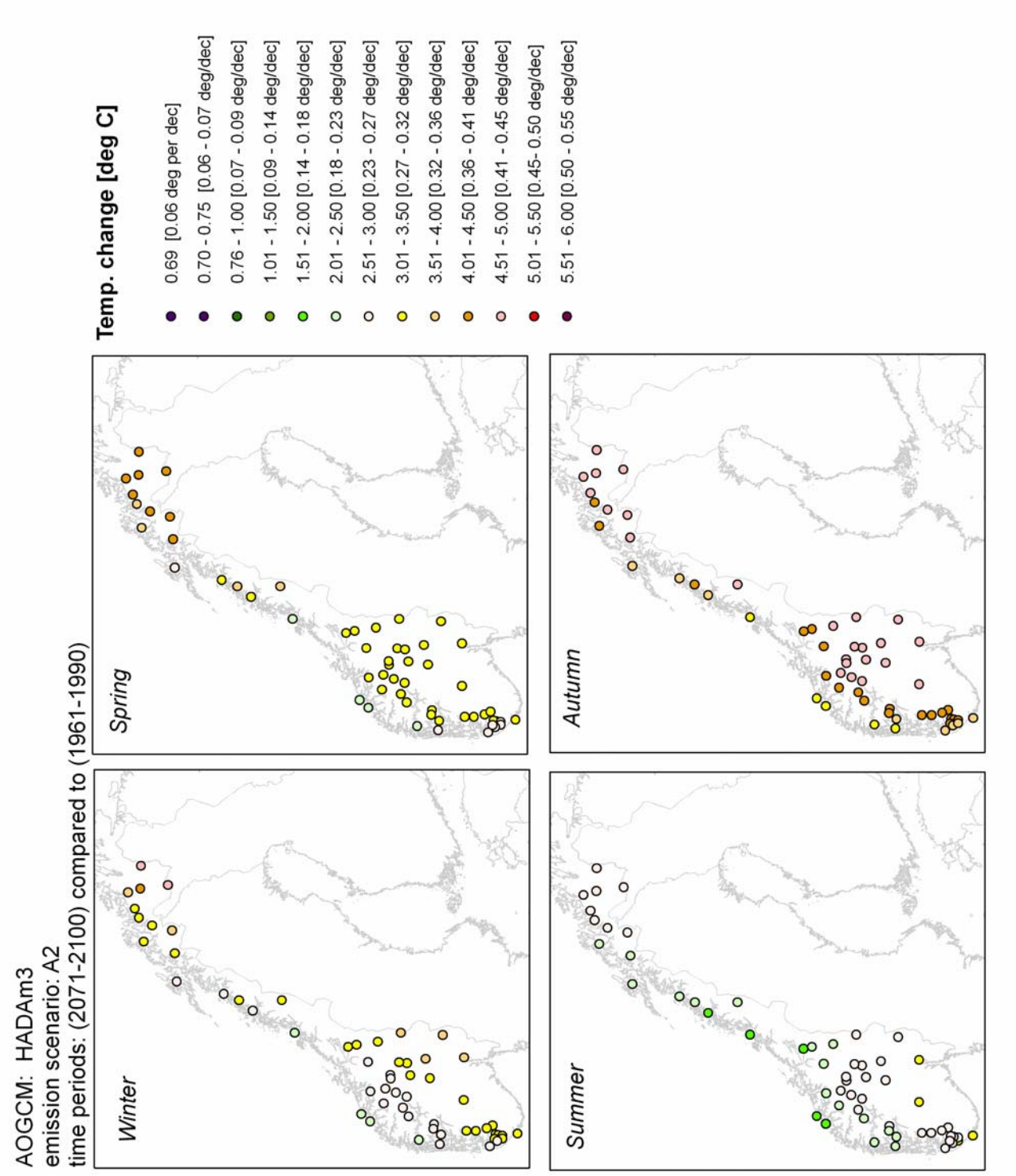
AOGCM: HADAm3
emission scenario: A2
time periods: (2071-2100) compared to (1961-1990)
Winter
Spring
Summer
Autumn
Temp. change [deg C]
0.69 [0.06 deg per dec]
0.70 - 0.75 [0.06 - 0.07 deg/dec]
0.76 - 1.00 [0.07 - 0.09 deg/dec]
1.01 - 1.50 [0.09 - 0.14 deg/dec]
1.51 - 2.00 [0.14 - 0.18 deg/dec]
2.01 - 2.50 [0.18 - 0.23 deg/dec]
2.51 - 3.00 [0.23 - 0.27 deg/dec]
3.01 - 3.50 [0.27 - 0.32 deg/dec]
3.51 - 4.00 [0.32 - 0.36 deg/dec]
4.01 - 4.50 [0.36 - 0.41 deg/dec]
4.51 - 5.00 [0.41 - 0.45 deg/dec]
5.01 - 5.50 [0.45- 0.50 deg/dec]
5.51 - 6.00 [0.50 - 0.55 deg/dec]

Appendix 3

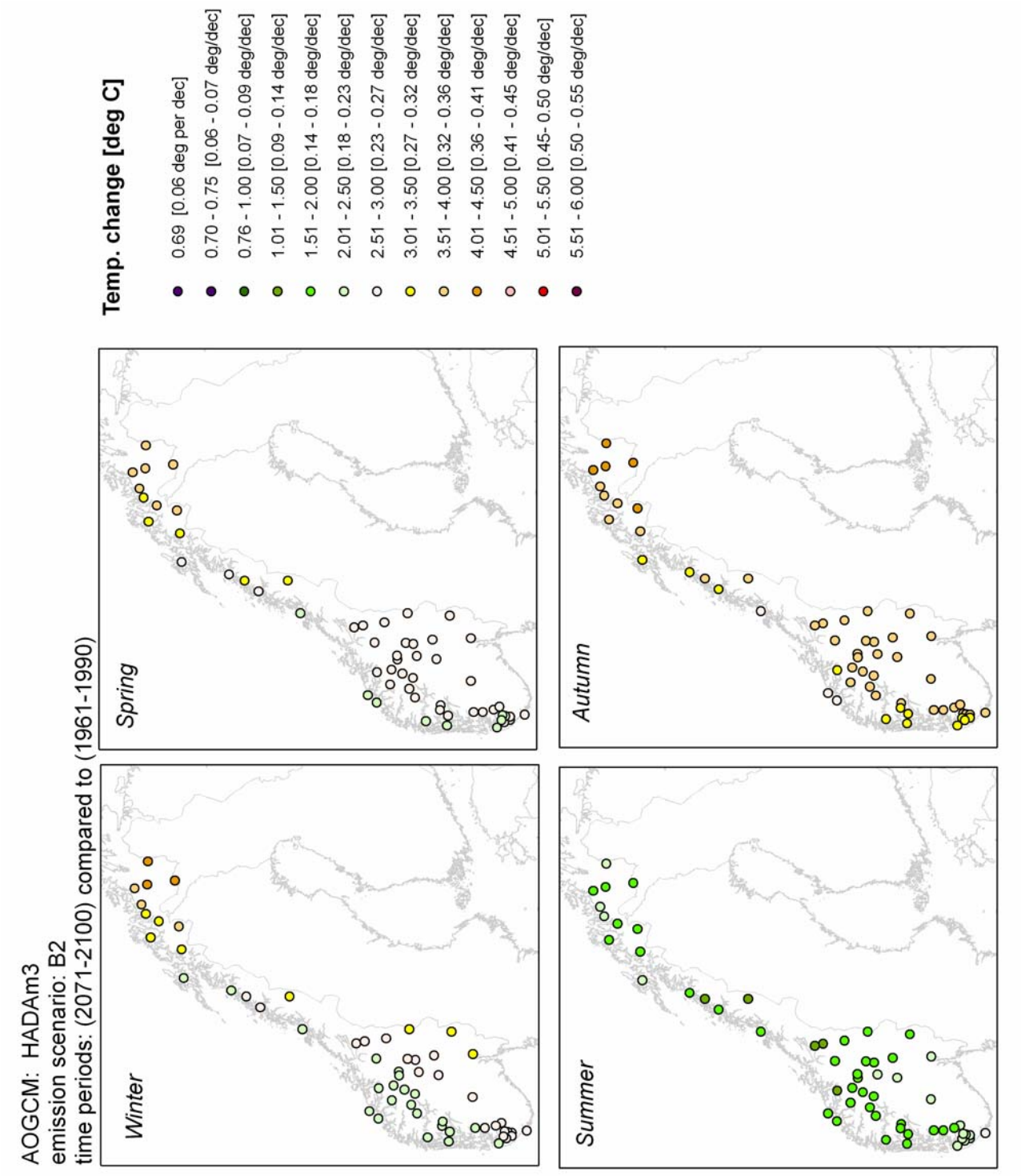
AOGCM: HADAm3
emission scenario: B2
time periods: (2071-2100) compared to (1961-1990)
Winter
Spring
Summer
Autumn
Temp. change [deg C]
0.69 [0.06 deg per dec]
0.70 - 0.75 [0.06 - 0.07 deg/dec]
0.76 - 1.00 [0.07 - 0.09 deg/dec]
1.01 - 1.50 [0.09 - 0.14 deg/dec]
1.51 - 2.00 [0.14 - 0.18 deg/dec]
2.01 - 2.50 [0.18 - 0.23 deg/dec]
2.51 - 3.00 [0.23 - 0.27 deg/dec]
3.01 - 3.50 [0.27 - 0.32 deg/dec]
3.51 - 4.00 [0.32 - 0.36 deg/dec]
4.01 - 4.50 [0.36 - 0.41 deg/dec]
4.51 - 5.00 [0.41 - 0.45 deg/dec]
5.01 - 5.50 [0.45- 0.50 deg/dec]
5.51 - 6.00 [0.50 - 0.55 deg/dec]

Appendix 4

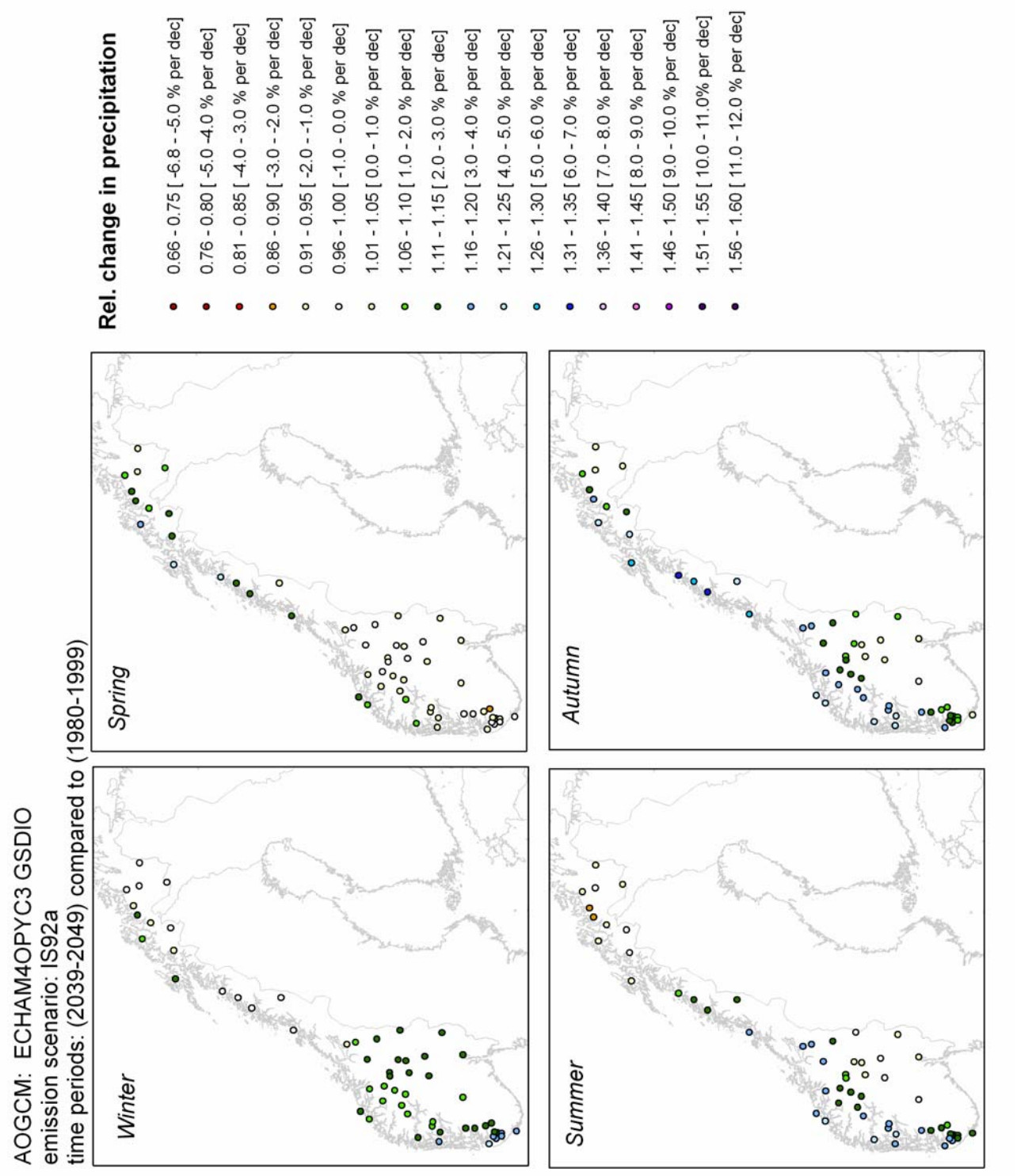
AOGCM: ECHAM4OPYC3 GSDIO
emission scenario: IS92a
time periods: (2039-2049) compared to (1980-1999)
Winter
Spring
Summer
Autumn
Rel. change in precipitation
0.66 - 0.75 [-6.8 - -5.0 % per dec]
0.76 - 0.80 [-5.0 -4.0 % per dec]
0.81 - 0.85 [-4.0 - 3.0 % per dec]
0.86 - 0.90 [-3.0 - -2.0 % per dec]
0.91 - 0.95 [-2.0 - -1.0 % per dec]
0.96 - 1.00 [-1.0 - 0.0 % per dec]
1.01 - 1.05 [0.0 - 1.0 % per dec]
1.06 - 1.10 [1.0 - 2.0 % per dec]
1.11 - 1.15 [2.0 - 3.0 % per dec]
1.16 - 1.20 [3.0 - 4.0 % per dec]
1.21 - 1.25 [4.0 - 5.0 % per dec]
1.26 - 1.30 [5.0 - 6.0 % per dec]
1.31 - 1.35 [6.0 - 7.0 % per dec]
1.36 - 1.40 [7.0 - 8.0 % per dec]
1.41 - 1.45 [8.0 - 9.0 % per dec]
1.46 - 1.50 [9.0 - 10.0 % per dec]
1.51 - 1.55 [10.0 - 11.0% per dec]
1.56 - 1.60 [11.0 - 12.0 % per dec]

Appendix 5

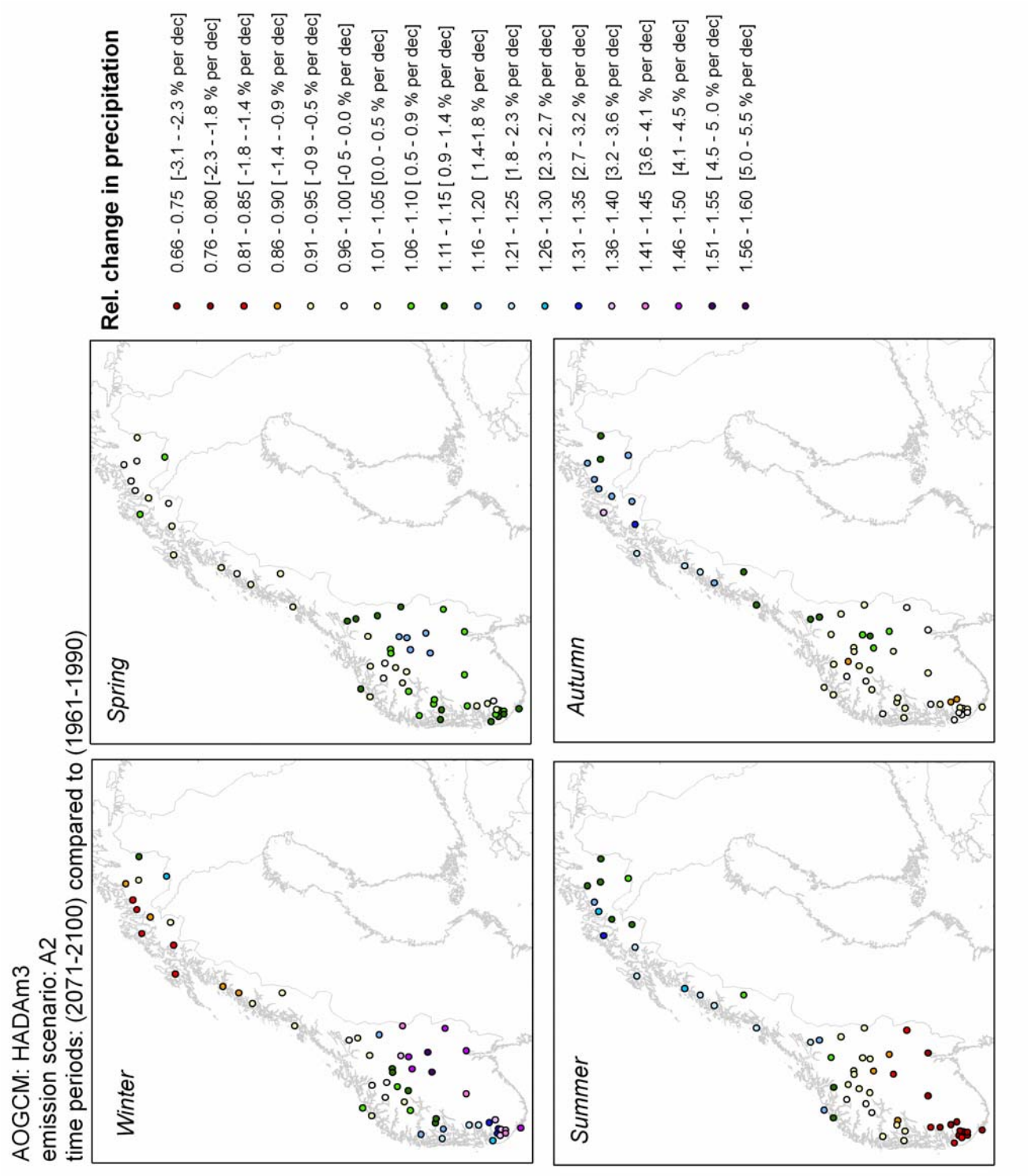
AOGCM: HADAm3
emission scenario: A2
time periods: (2071-2100) compared to (1961-1990)
Winter
Spring
Summer
Autumn
Rel. change in precipitation
0.66 - 0.75 [-3.1 - -2.3 % per dec]
0.76 - 0.80 [-2.3 - -1.8 % per dec]
0.81 - 0.85 [-1.8 - -1.4 % per dec]
0.86 - 0.90 [-1.4 - -0.9 % per dec]
0.91 - 0.95 [-0 9 - -0.5 % per dec]
0.96 - 1.00 [-0 5 - 0.0 % per dec]
1.01 - 1.05 [0.0 - 0.5 % per dec]
1.06 - 1.10 [0.5 - 0.9 % per dec]
1.11 - 1.15 [0.9 - 1.4 % per dec]
1.16 - 1.20 [1.4-1.8 % per dec]
1.21 - 1.25 [1.8 - 2.3 % per dec]
1.26 - 1.30 [2.3 - 2.7 % per dec]
1.31 - 1.35 [2.7 - 3.2 % per dec]
1.36 - 1.40 [3.2 - 3.6 % per dec]
1.41 - 1.45 [3.6 - 4.1 % per dec]
1.46 - 1.50 [4.1 - 4.5 % per dec]
1.51 - 1.55 [4.5 - 5 .0 % per dec]
1.56 - 1.60 [5.0 - 5.5 % per dec]

Appendix 6

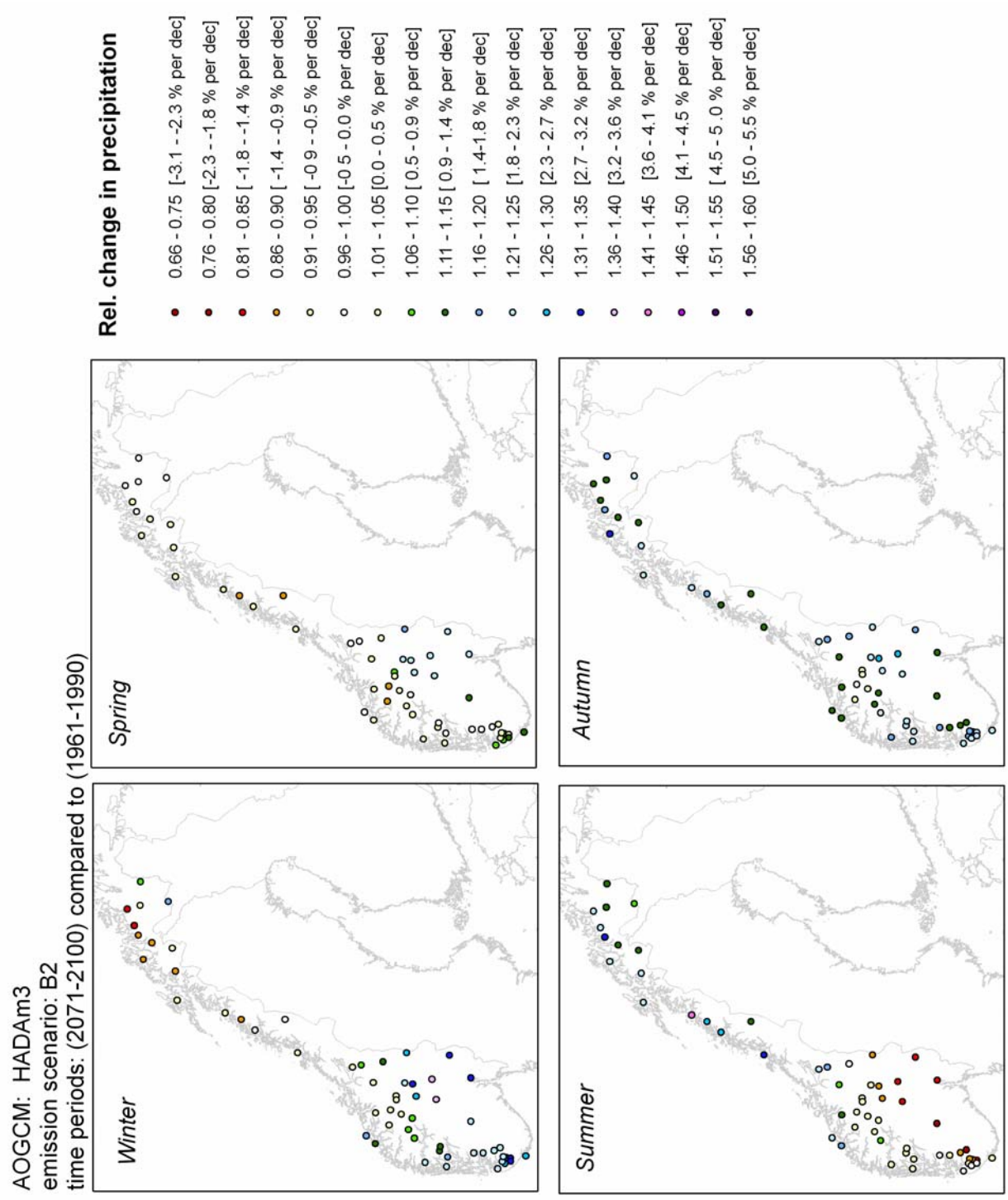
AOGCM: HADAm3
emission scenario: B2
time periods: (2071-2100) compared to (1961-1990)
Winter
Spring
Summer
Autumn
Rel. change in precipitation
0.66 - 0.75 [-3.1 - -2.3 % per dec]
0.76 - 0.80 [-2.3 - -1.8 % per dec]
0.81 - 0.85 [-1.8 - -1.4 % per dec]
0.86 - 0.90 [-1.4 - -0.9 % per dec]
0.91 - 0.95 [-0 9 - -0.5 % per dec]
0.96 - 1.00 [-0 5 - 0.0 % per dec]
1.01 - 1.05 [0.0 - 0.5 % per dec]
1.06 - 1.10 [0.5 - 0.9 % per dec]
1.11 - 1.15 [0.9 - 1.4 % per dec]
1.16 - 1.20 [1.4-1.8 % per dec]
1.21 - 1.25 [1.8 - 2.3 % per dec]
1.26 - 1.30 [2.3 - 2.7 % per dec]
1.31 - 1.35 [2.7 - 3.2 % per dec]
1.36 - 1.40 [3.2 - 3.6 % per dec]
1.41 - 1.45 [3.6 - 4.1 % per dec]
1.46 - 1.50 [4.1 - 4.5 % per dec]
1.51 - 1.55 [4.5 - 5 .0 % per dec]
1.56 - 1.60 [5.0 - 5.5 % per dec]

Appendix 7: Comparison between mean annual and seasonal streamflow of the control series and the observations for the period 1980-1999. The control series have been simulated by the ECHAM4/OPYC3-model with the IS92a emission scenario.

Station no.	Name	Annual mean		DJF mean		MAM mean		JJA mean		SON mean	
		Ctr.	Obs.	Ctr.	Obs.	Ctr.	Obs.	Ctr.	Obs.	Ctr.	Obs.
311.6	Nybergsund	73.6	67.3	34.7	26.9	85.0	79.2	102	97.2	76.8	64.5
2.13	Sjodalsvatn	19.1	19.2	2.58	2.44	7.42	8.96	54	49.1	15.8	15.6
18.10	Gjerstad	6.34	6.48	4.84	4.44	8.01	8.93	4.39	3.50	8.06	8.92
20.2	Austenå	10.6	9.78	8.11	5.70	15.3	15.4	6.74	9.48	9.95	11.6
26.20	Årdal	5.63	5.58	6.94	6.59	5.88	5.61	2.57	2.70	6.70	7.23
26.21	Sandvatn	1.82	1.83	2.32	2.16	1.86	1.93	0.82	0.84	2.15	2.32
27.26	Hetland	4.35	4.20	6.13	5.34	3.45	3.33	2.01	2.22	5.51	5.81
41.1	Stordalsvatn	13.6	13.7	8.69	11.5	14.0	11.9	15.5	14.7	16.2	16.3
48.5	Reinsnosvatn	9.54	9.64	2.83	2.51	7.20	6.87	17.8	20.0	11.4	9.02
50.1	Hølen	13.4	13.1	3.69	3.07	9.52	7.94	26.7	29.7	15.5	11.2
83.2	Viksvatn	45.9	45.1	19.5	22.5	39.1	36.0	76.0	71.5	53.6	49.2
104.23	Vistdal	3.92	3.88	1.93	1.76	4.72	4.52	4.98	5.56	4.24	3.59
107.3	Farstad	1.07	1.20	1.54	1.41	1.00	1.07	0.47	0.72	1.18	1.58
109.9	Risefoss	18.7	16.4	2.32	1.53	16.3	13.5	45.5	41.0	12.6	9.23
123.20	Rathe	99.9	103	53.0	32.0	126	140	127	147	102	91.0
123.31	Kjelstad	5.21	5.62	4.24	2.01	6.74	7.95	5.86	7.51	5.59	4.90
151.15	Nervoll	29.7	29.2	11.4	7.10	27.7	21.2	51.8	65.9	31.7	21.8
167.3	Kobbvatn	25.4	25.7	14.9	8.76	19.0	16.8	39.4	51.7	30.2	24.9
212.10	Masi	71.6	65.9	13.9	17.2	67.5	65.3	166	131	43.6	47.4

Appendix 8: Comparison between mean annual and seasonal standard deviations of streamflow of the control series and the observations for the period 1980-1999. The control series have been simulated by the ECHAM4/OPYC3-model with the IS92a emission scenario.

Station no.	Name	Annual std.		DJF std.		MAM std.		JJA std.		SON std.	
		Ctr.	Obs.	Ctr.	Obs.	Ctr.	Obs.	Ctr.	Obs.	Ctr.	Obs.
311.6	Nybergsund	8.26	11.3	8.43	6.34	15.2	17.6	21.4	21.2	27.2	21.9
2.13	Sjodalsvatn	2.28	2.43	0.40	0.67	3.64	4.25	7.65	6.40	5.03	4.11
18.10	Gjerstad	1.34	1.43	2.08	2.96	3.19	3.48	2.09	2.42	3.44	3.04
20.2	Austenå	1.86	1.81	3.73	2.92	4.47	4.05	3.22	3.10	3.73	3.56
26.20	Årdal	1.02	1.07	2.34	3.33	2.05	1.80	1.44	1.28	2.46	1.83
26.21	Sandvatn	0.32	0.36	0.76	1.10	0.65	0.63	0.45	0.47	0.79	0.60
27.26	Hetland	0.76	0.81	1.82	2.08	1.33	1.10	0.90	0.92	2.08	1.87
41.1	Stordalsvatn	2.52	2.76	2.18	6.04	3.50	3.70	4.94	3.36	6.24	4.89
48.5	Reinsnosvatn	1.63	2.05	1.07	1.29	1.99	2.30	4.78	5.19	4.39	2.68
50.1	Hølen	2.35	3.05	1.69	1.81	3.30	3.09	7.67	8.56	6.46	3.58
83.2	Viksvatn	8.54	8.86	6.97	12.4	10.1	15.0?	18.6	15.0?	22.2	14.0
104.23	Vistdal	0.96	0.66	1.24	1.20	1.25	1.08	1.65	1.08	2.02	1.56
107.3	Farstad	0.28	0.21	0.48	0.55	0.34	0.33	0.14	0.26	0.57	0.46
109.9	Risefoss	2.66	2.37	0.68	0.40	7.08	6.77	13.6	8.02	4.08	2.61
123.20	Rathe	17.3	16.5	27.4	18.0	31.7	27.1	39.6	44.7	44.5	36.8
123.31	Kjelstad	0.97	0.98	1.62	1.27	1.87	1.34	1.96	2.31	2.56	2.07
151.15	Nervoll	3.99	5.92	7.30	3.60	8.55	8.50	13.0	18.1	12.9	6.89
167.3	Kobbvatn	3.53	4.60	5.14	4.32	4.80	5.75	7.02	11.9	11.4	8.68
212.10	Masi	12.3	11.9	4.38	4.74	39.6	34.0	59.7	36.2	16.7	18.7

Appendix 9 A: Comparison between mean annual and seasonal streamflow of the control series (1961-1990) and the observations for the same period. The control series have been simulated by the HadAm3-model.

Station no.	Name			DJF mean		MAM mean		JJA mean		SON mean	
		Ctr.	Obs.	Ctr.	Obs.	Ctr.	Obs.	Ctr.	Obs.	Ctr.	Obs.
311.6	Nybergsund	70.4	68.0	36.8	26.5	83.4	78.9	99.9	99.9	70.8	71.6
20.2	Austenå	9.47	10.0	5.27	4.94	15.0	14.3	7.03	8.72	10.4	11.7
27.26	Hetland	4.05	4.03	5.33	4.78	3.27	3.10	2.16	2.26	5.49	5.66
41.1	Stordalsvatn	12.6	13.0	9.07	9.18	12.4	10.8	14.8	14.7	16.8	18.2
48.5	Reinsnosvatn	8.91	8.99	3.61	1.95	6.33	5.40	16.6	19.1	11.8	11.4
50.1	Hølen	12.4	12.1	4.52	2.58	8.45	6.60	24.0	27.6	16.2	13.7
83.2	Viksvatn	43.2	42.3	19.1	17.9	35.1	30.8	72.0	68.2	58.7	59.2
109.9	Risefoss	17.5	16.0	2.82	2.04	14.6	12.3	43.5	39.4	11.2	11.9
123.20	Rathe	97.9	95.2	44.9	29.2	134	105	123	102	108	96.7
167.3	Kobbvatn	24.8	24.8	12.7	7.84	18.4	16.0	41.6	49.6	32.1	27.4

Appendix 9 B: Comparison between the annual and seasonal standard deviations of the control series and the observations for the period 1961-1990. The control series have been simulated by the HadAm3-model.

Station no.	Name	Annual std.		DJF std.		MAM std.		JJA std.		SON std.	
		Ctr.	Obs.	Ctr.	Obs.	Ctr.	Obs.	Ctr.	Obs.	Ctr.	Obs.
311.6	Nybergsund	13.6	12.6	11.0	6.26	15.8	26.5	34.7	24.7	23.0	28.0
20.2	Austenå	2.00	1.93	2.31	2.44	3.78	3.43	2.89	4.45	4.94	4.97
27.26	Hetland	0.80	0.88	1.43	2.34	1.37	1.46	0.86	1.21	2.32	1.81
41.1	Stordalsvatn	2.24	2.76	2.47	5.87	3.45	3.64	4.36	3.89	6.33	4.57
48.5	Reinsnosvatn	1.56	1.88	1.23	1.38	1.98	2.05	4.64	4.88	4.56	2.88
50.1	Hølen	2.38	2.95	1.75	1.66	2.92	3.15	7.43	8.34	6.86	3.86
83.2	Viksvatn	7.84	8.96	5.93	11.7	10.4	8.60	16.7	16.2	25.4	13.2
109.9	Risefoss	3.04	2.33	0.84	1.10	5.37	7.91	14.7	9.44	4.45	3.35
123.20	Rathe	17.4	15.7	14.7	17.8	20.8	35.2	45.0	34.6	53.4	33.3
167.3	Kobbvatn	4.92	5.50	5.36	4.49	8.57	2.02	8.18	13.3	15.4	13.1

Appendix 10: Comparison of annual flood and low flow characteristics between the control run (1980-99) and observations from the same period. The control series have been simulated by the ECHAM4/OPYC3-model with emission scenarioIS92a.

Station no.	Name	Mean annual flood		Std.dev. annual flood		Mean annual low flow		Std.dev. annual low flow	
		Ctr.	Obs.	Ctr.	Obs.	Ctr.	Obs.	Ctr.	Obs.
311.6	Nybergsund	324	322	92.6	127	18.1	19.3	3.00	2.77
2.13	Sjodalsvatn	127	167	32.4	67.0	2.84	1.35	0.51	0.37
15.79	Orsjoren	216	204	74.3	56.4	4.12	3.86	1.05	1.21
18.10	Gjerstad	53.2	90.1	12.2	29.4	0.38	0.14	0.19	0.11
20.2	Austenå	52.8	67.7	10.6	17.6	1.52	0.68	0.36	0.50
26.20	Årdal	29.5	46.8	4.31	13.3	0.52	0.35	0.14	0.14
26.21	Sandvatn	9.52	13.3	1.42	3.96	0.17	0.14	0.043	0.055
27.26	Hetland	23.6	27.4	4.52	6.79	0.44	0.29	0.11	0.18
41.1	Stordalsvatn	57.2	66.8	9.41	17.3	1.43	1.38	0.33	0.51
48.5	Reinsnosvatn	43.2	54.8	5.76	10.5	0.87	0.56	0.20	0.27
50.1	Hølen	70.1	80.9	8.76	19.8	1.18	0.54	0.27	0.30
83.2	Viksvatn	206	187	40.8	34.1	4.80	4.12	1.35	1.70
104.23	Vistdal	20.3	35.8	7.34	11.1	0.40	0.45	0.067	0.17
107.3	Farstad	5.88	7.56	2.38	1.41	0.14	0.22	0.026	0.093
109.9	Risefoss	180	177	35.6	60.0	1.02	0.83	0.21	0.20
123.20	Rathe	512	412	139	194	15.72	*	2.46	*
123.31	Kjelstad	27.8	48.1	8.19	9.45	0.69	0.47	0.11	0.16
151.15	Nervoll	182	201	28.5	40.0	2.25	2.42	0.44	0.76
167.3	Kobbvatn	121	113	28.7	27.8	3.95	2.69	0.78	0.86
212.10	Masi	808	607	200	197	6.60	12.77	1.78	3.11

* The correction for ice results in the erronious value of 0 in the ”observed” series.

Appendix 11 A. Comparison between the annual and seasonal mean flood of the control series and the observations for the period 1961-1990. The control series have been simulated by the HadleyAM3 model.

Station no.	Name			DJF mean flood		MAM mean flood		JJA mean flood		SON mean flood	
		Ctr.	Obs.	Ctr.	Obs.	Ctr.	Obs.	Ctr.	Obs.	Ctr.	Obs.
311.6	Nybergsund	349	318	50.0	39.6	342	309	219	309	102	228
20.2	Austenå	55.3	69.9	23.8	18.4	51.1	55.7	23.8	40.1	38.6	53.2
27.26	Hetland	22.6	34.4	17.7	23.4	12.6	19.9	9.53	18.5	19.7	29.6
41.1	Stordalsvatn	60.0	76.4	33.8	39.9	35.8	40.0	38.6	47.8	53.1	67.1
48.5	Reinsnosvatn	44.6	53.8	10.8	8.62	29.6	33.2	39.2	50.2	36.1	37.0
50.1	Hølen	69.6	75.9	14.2	11.0	46.6	44.2	63.4	72.0	51.3	46.1
83.2	Viksvatn	194	181	63.4	64.8	124	113	156	145	173	158
109.9	Risefoss	161	218	3.35	6.42	112	136	146	190	35.0	33.9
123.20	Rathe	535	700	156	158	472	625	399	526	324	415
167.3	Kobbvatn	113	155	41.8	47.4	68.7	76.4	90.0	115	102	116

Appendix 11 B. Comparison of the standard deviations of the annual and seasonal flood for the control series and the observations for the period 1961-1990. The control series have been simulated by the HadleyAM3 model.

Station no.	Name	Annual std.		DJF std.		MAM std.		JJA std.		SON std.	
		Ctr.	Obs.	Ctr.	Obs.	Ctr.	Obs.	Ctr.	Obs.	Ctr.	Obs.
311.6	Nybergsund	153	107	17.0	14.0	150	110	126	96	34.2	95.5
20.2	Austenå	14.3	18.4	13.2	16.4	14.8	18.0	13.8	19.8	16.0	24.2
27.26	Hetland	4.74	11.8	5.65	11.7	5.09	10.3	5.76	11.8	5.94	11.2
41.1	Stordalsvatn	11.9	20.5	14.8	25.8	8.46	14.8	14.9	14.9	15.0	22.8
48.5	Reinsnosvatn	9.60	10.6	9.04	8.34	7.68	14.7	11.6	11.6	10.2	10.4
50.1	Hølen	14.5	19.4	14.2	8.46	15.4	21.6	18.1	19.3	15.9	16.2
83.2	Viksvatn	46.4	31.9	40.8	46.4	26.6	42.8	35.7	35.3	57.6	39.6
109.9	Risefoss	40.9	101	0.63	9.07	52.4	86.8	53.4	103	24.0	19.4
123.20	Rathe	132	147	106	110	135	172	135	177	158	171
167.3	Kobbvatn	28.6	53.9	29.2	57.6	18.3	31.6	15.4	25.1	37.4	68.6

Appendix 12. Relative runoff values for the scenario of annual and seasonal mean 2030-2049 based on the ECHAM4/OPYC3-model compared to the means of the control period 1980-1999 for emission scenario IS92a. The model was run in a transient mode 1980-2049.

Station no.	Name	Annual mean ratio	DJF-mean ratio	MAM-mean ratio	JJA-mean ratio	SON-mean ratio
		Sce./Ctr.	Sce/Ctr.	Sce./Ctr.	Sce./Ctr.	Sce./Ctr.
311.6	Nybergsund	1.037	1.156	1.090	0.941	1.002
2.13	Sjodalsvatn	1.106	1.243	1.635	1.020	1.161
15.79	Orsjoren	0.952	1.080	1.495	0.736	0.764
18.10	Gjerstad	0.948	1.440	0.896	0.960	1.068
20.2	Austenå	0.989	1.263	0.992	0.941	1.058
26.20	Årdal	1.076	1.239	0.799	0.973	1.140
26.21	Sandvatn	1.060	1.222	0.806	0.988	1.102
27.26	Hetland	1.108	1.150	0.893	1.149	1.178
257.257	Lyse	1.063	1.532	1.181	0.682	1.144
41.1	Stordalsvatn	1.106	1.473	1.031	0.786	1.205
48.5	Reinsnosvatn	1.058	1.772	1.365	0.787	1.226
50.1	Hølen	1.125	1.758	1.496	0.779	1.240
83.2	Viksvatn	1.157	1.528	1.269	0.879	1.268
104.23	Vistdal	1.122	1.775	1.138	0.936	1.174
107.3	Farstad	1.140	1.169	1.000	1.213	1.347
109.9	Risefoss	1.064	1.130	1.443	0.927	1.033
123.20	Rathe	1.112	1.156	1.049	1.058	1.239
123.31	Kjelstad	1.113	1.625	1.001	0.914	1.236
151.15	Nervoll	1.122	1.163	1.343	0.818	1.501
167.3	Kobbvatn	1.165	1.299	1.400	0.809	1.457
212.10	Masi	0.970	1.370	1.549	0.638	1.266

Appendix 13. Relative runoff values for the scenario of annual and seasonal mean 2071-2100 based on the HadAm3-model compared to the means of the control period 1961-1990 for emission scenario A2 and B2.

Station no.	Name	Annual mean ratio		DJF-mean ratio		MAM-mean ratio		JJA-mean ratio		SON-mean ratio	
		A2/Ctr.	B2/Ctr.	A2/Ctr.	B2/Ctr.	A2/Ctr.	B2/Ctr.	A2/Ctr.	B2/Ctr.	A2/Ctr.	B2/Ctr.
311.6	Nybergsund	0.958	1.008	1.173	1.264	1.173	1.178	0.747	0.791	0.824	0.944
2.13	Sjodalsvatn	1.061	1.098	1.271	1.283	2.910	2.468	0.703	0.791	1.304	1.499
15.79	Orsjoren	0.840	0.918	1.274	1.340	2.407	2.190	0.395	0.505	0.457	0.705
18.10	Gjerstad	0.942	1.014	2.009	2.022	0.853	0.842	0.606	0.623	0.668	0.962
20.2	Austenå	0.902	0.992	2.082	2.170	0.849	0.811	0.377	0.438	0.486	0.800
26.20	Årdal	0.970	1.082	1.622	1.594	0.763	0.757	0.542	0.737	0.660	0.979
26.21	Sandvatn	0.957	1.067	1.575	1.527	0.763	0.775	0.571	0.750	0.640	0.962
27.26	Hetland	0.998	1.114	1.331	1.292	0.887	0.893	0.685	0.926	0.723	1.044
257.257	Lyse	0.969	1.062	2.449	2.562	1.333	1.247	0.341	0.428	0.722	0.957
41.1	Stordalsvatn	1.000	1.092	1.896	1.836	1.144	1.063	0.467	0.581	0.810	1.025
48.5	Reinsnosvatn	1.010	1.105	2.240	2.334	1.858	1.693	0.464	0.594	0.862	1.068
50.1	Hølen	0.995	1.094	1.897	1.992	2.059	1.895	0.430	0.571	0.905	1.108
83.2	Viksvatn	1.040	1.112	1.751	1.858	1.507	1.374	0.578	0.688	0.978	1.138
104.23	Vistdal	1.033	1.008	1.537	1.589	1.092	1.074	0.601	0.650	0.936	1.042
107.3	Farstad	1.031	1.030	1.027	1.165	0.856	0.778	1.044	1.111	0.923	0.992
109.9	Risefoss	0.895	0.929	1.330	1.333	1.962	1.832	0.471	0.543	0.970	1.124
123.20	Rathe	0.997	1.028	1.488	1.607	0.981	0.935	0.759	0.804	1.008	1.137
123.31	Kjelstad	1.012	1.037	1.583	1.714	0.867	0.826	0.868	0.886	1.013	1.131
151.15	Nervoll	0.996	1.009	1.770	1.911	1.714	0.985	0.437	0.551	1.081	1.137
167.3	Kobbvatn	1.058	1.072	1.505	1.660	1.354	1.293	0.573	0.644	1.248	1.265
210.10	Masi	0.900	0.943	1.267	1.251	1.824	1.694	0.384	0.515	1.222	1.267

Appendix 14. Relative runoff values for the scenario of annual and seasonal standard deviation 2030-2049 based on the ECHAM4/OPYC3-model compared to the standard deviations of the control period 1980-1999 for emission scenario IS92a.

Station no.	Name	Annual std.dev. ratio	DJF-std.dev. ratio	MAM-std.dev. ratio	JJA-std.dev. ratio	SON-std.dev ratio
		Sce./Ctr.	Sce/Ctr.	Sce./Ctr.	Sce./Ctr.	Sce./Ctr.
311.6	Nybergsund	1.557	1.657	1.649	1.311	0.773
2.13	Sjodalsvatn	1.482	1.537	1.734	1.593	1.099
15.79	Orsjoren	1.170	1.298	1.488	0.926	0.815
18.10	Gjerstad	1.078	1.311	1.216	0.849	0.746
20.2	Austenå	1.198	1.528	0.940	0.551	0.990
26.20	Årdal	1.225	1.790	0.717	0.708	1.085
26.21	Sandvatn	1.219	1.548	0.723	0.733	1.013
27.26	Hetland	1.316	1.872	0.880	1.011	1.106
257.257	Lyse	1.335	2.049	1.416	0.738	1.049
41.1	Stordalsvatn	1.182	2.056	1.823	0.808	0.965
48.5	Reinsnosvatn	1.190	1.618	1.538	0.958	0.957
50.1	Hølen	1.183	1.085	1.448	1.043	0.913
83.2	Viksvatn	1.116	0.977	1.440	0.992	0.910
104.23	Vistdal	0.771	3.052	1.056	1.139	0.871
107.3	Farstad	0.893	2.083	1.029	1.428	1.035
109.9	Risefoss	1.470	0.813	1.460	1.352	1.105
123.20	Rathe	1.083	0.624	1.117	1.139	0.781
123.31	Kjelstad	1.031	2.814	1.032	1.079	0.746
151.15	Nervoll	1.674	1.152	1.966	1.646	1.614
167.3	Kobbvatn	1.535	1.143	2.179	1.449	1.413
212.10	Masi	1.446	1.824	0.865	0.964	1.182

Appendix 15. Relative runoff values for the scenario of annual and seasonal standard deviations 2071-2100 based on the HadAm3-model compared to the standard deviations of the control period 1961-1990 for emission scenario A2 and B2.

Station no.	Name	Annual std.dev. ratio		DJF-std.dev. ratio		MAM-std.dev. ratio		JJA-std.dev. ratio		SON-std.dev. ratio	
		A2/Ctr.	B2/Ctr.	A2/Ctr.	B2/Ctr.	A2/Ctr.	B2/Ctr.	A2/Ctr.	B2/Ctr.	A2/Ctr.	B2/Ctr.
311.6	Nybergsund	0.888	0.961	1.701	1.417	0.826	0.855	0.662	0.651	0.847	0.937
2.13	Sjodalsvatn	0.754	1.130	3.084	2.451	1.420	1.365	1.189	0.850	0.870	1.518
15.79	Orsjoren	0.754	0.830	2.293	2.094	0.921	1.111	0.579	0.647	0.610	0.976
18.10	Gjerstad	0.848	0.803	1.388	1.305	1.238	1.302	1.103	0.670	0.836	1.196
20.2	Austenå	0.943	0.869	1.931	1.908	0.995	0.847	0.497	0.409	1.093	1.739
26.20	Årdal	1.107	0.980	1.442	1.129	0.809	0.668	0.878	0.908	0.608	1.172
26.21	Sandvatn	1.091	0.970	1.348	1.077	0.790	0.661	0.968	0.935	0.592	1.143
27.26	Hetland	1.175	1.050	1.295	0.999	0.829	0.685	0.919	1.023	0.526	1.254
257.257	Lyse	1.103	0.976	2.738	2.230	1.148	0.933	0.602	0.398	0.556	1.125
41.1	Stordalsvatn	1.170	1.107	2.022	1.615	1.118	0.928	0.729	0.624	0.668	1.208
48.5	Reinsnosvatn	1.070	1.205	2.948	2.498	1.424	1.127	0.735	0.672	0.684	1.138
50.1	Hølen	0.933	1.133	2.381	2.226	1.349	1.213	0.662	0.682	0.708	1.057
83.2	Viksvatn	1.046	1.134	1.910	1.928	1.630	1.360	0.919	0.811	0.793	0.959
104.23	Vistdal	1.045	1.045	1.355	1.485	1.103	0.887	0.678	0.637	0.902	0.916
107.3	Farstad	1.000	0.750	2.190	2.484	1.161	0.742	1.059	1.118	0.913	0.725
109.9	Risefoss	1.039	1.023	3.498	3.197	0.826	0.832	0.694	0.595	0.955	1.249
123.20	Rathe	0.894	1.091	1.738	1.961	1.095	0.816	0.653	0.706	0.802	0.925
123.31	Kjelstad	0.945	1.110	1.555	1.798	1.134	0.886	0.722	0.775	0.797	0.898
151.15	Nervoll	0.808	0.908	1.460	1.896	1.021	0.987	0.463	0.874	0.726	0.911
167.3	Kobbvatn	0.864	1.010	1.534	1.576	1.147	1.040	0.814	1.200	0.786	0.899
210.10	Masi	0.918	1.342	2.139	2.117	0.647	0.688	0.454	1.945	1.092	1.640

Appendix 16. Trends in the annual streamflow for the transient run of the MPI-ECHAM4 model 1980-2049 based on the Mann-Kendall test. +/- significant on .99 level, +/- significant on .95 level, (+)/(-) not significant, but direction is shown, 0 no trend at all.

Station Number	Name	River	Annual and seasonal trends 1980-2049				
			Annual	DJF	MAM	JJA	SON
311.6	Nybergsund	Klara	(+)	+	(+)	(-)	(+)
2.13	Sjodalsvatn	Sjoa	+	(+)	+	(+)	(+)
15.79	Orsjoren	Numedalslågen	(-)	+	-	-	(-)
18.10	Gjerstad	Gjerstadelv	(-)	(+)	(-)	(-)	0
20.2	Austenå	Tovdalselv	(-)	+	(-)	-	(+)
26.20	Årdal	Sira	(+)	0	-	(-)	(+)
26.21	Sandvatn	Sira	(+)	+	-	(-)	(+)
27.26	Hetland	Bjerkreimselv	(+)	(+)	(-)	(+)	(+)
257.257	Lyse	Lyseelv	(+)	+	+	-	+
41.1	Stordalsvatn	Etneelv	(+)	+	(+)	-	+
48.5	Reinsnosvatn	Opo	+	+	+	-	+
50.1	Hølen	Kinso	+	+	+	-	+
83.2	Viksvatn	Gaular	+	+	+	-	+
104.23	Vistdal	Visa	+	+	+	(-)	+
107.3	Farstad	Farstadselv	(+)	(+)	0	+	+
109.9	Risefoss	Driva	(+)	+	+	(-)	(+)
123.20	Rathe	Nidelva	(+)	(+)	(+)	0	+
123.31	Kjelstad	Nidelva	(+)	(+)	(+)	(+)	+
151.15	Nervoll	Vefsna	(+)	(+)	+	-	+
167.3	Kobbvatn	Kobbelv	+	(+)	+	-	+
212.10	Masi	Alta	(-)	(+)	+	-	+

Appendix 17 A: Simulated annual and seasonal streamflow for 83.2 Viksvatn based on the ECHAM4/OPYC3-model for the period 1980-2049

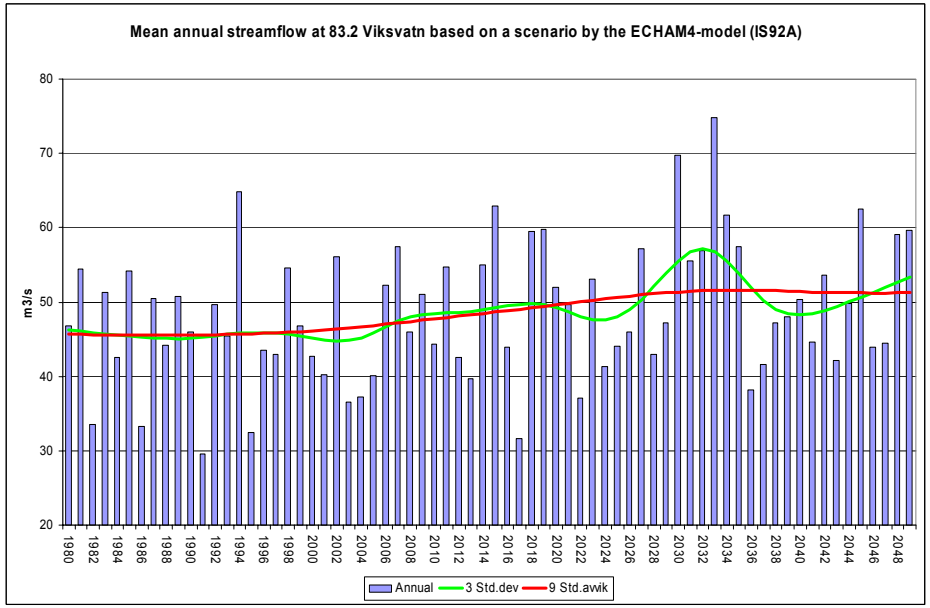

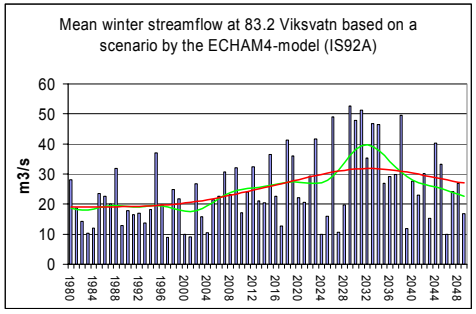

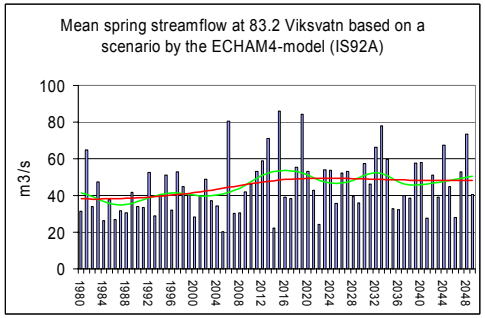

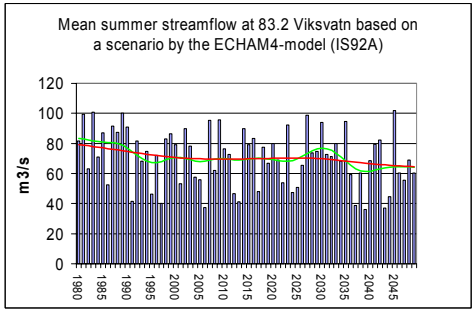

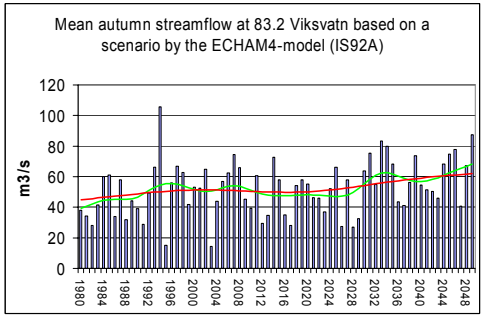

Appendix 17 B: Simulated annual and seasonal streamflow for 83.2 Viksvatn based on the HadleyAM3-model for the control and scenario period for emission scenario A2 and B2.